1278

SYNCHRONIZED CYCLIC CAPILLARY ELECTROPHORESIS

Norbert Burggraf

Ciba-Geigy Ltd. Basle
Corporate Analytical Research

Université de Neuchâtel
Institute de Microtechnique

Synchronized Cyclic Capillary Electrophoresis

Ph. D. Thesis
by
Norbert Burggraf

Basle 1995

Dissertation Director:
Prof. Dr. Nico F. de Rooij, Institute de Microtechnique, Université de Neuchâtel, Switzerland

Examination Committee:
Prof. Dr. N.F. de Rooij, Institute de Microtechnique, Université de Neuchâtel, Switzerland
Dr. A. Manz, Corporate Analytical Research, Ciba-Geigy Ltd., Basle, Switzerland
Prof. Dr. R. Deschenaux, Institute de Chimie, Université de Neuchâtel, Switzerland

Πάντα ῥεῖ

(panta rhei)

Heraklit

(6th to 5th century B.C.)

Outline

Chapter 1

Introduction

Chapter 2

Device and Layout

Chapter 3

Theory

Chapter 4

Experimental

Chapter 5

Results and discussion

Chapter 6

Chapter 1 Introduction

1.1 Capillary Electrophoresis

This thesis deals with an important modification of the well known and important analytical technique of capillary electrophoresis (CE). Therefore, a brief introduction of the principles and general aspects of CE will be given.

1.1.1 General aspects of capillary electrophoresis

The pioneering work in the field of capillary electrophoresis (CE) was done by Everaerts et al. in 1979 [MIK 79] and Jorgenson et al. in 1981 [JOR 81]. Today CE is a modern separation technique which allows the separation of differently charged molecules in narrow-bore (5-200 μm i.d.) capillaries. It is a commonly used analytical method in the identification and quantification of biopolymers and widely used in the field of analytical research. The basic instrumental configuration for CE is both relatively simple. It requires a glass capillary (usually the capillaries are fused silica because near UV light is used for detection), two electrolyte reservoirs, two electrodes, a high voltage power supply and a detector. Appropriate combination of these components results in the basic configuration used for CE, as shown in Fig. 1.1.

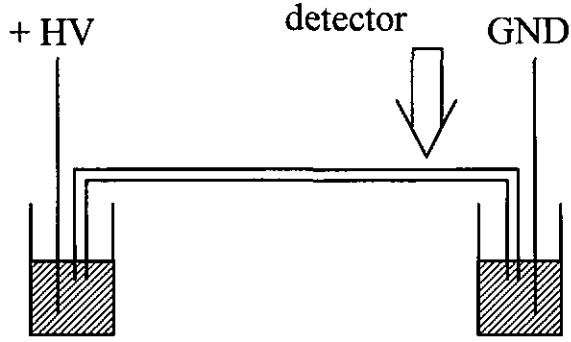

Figure 1.1 Illustration of a basic setup for capillary electrophoresis.

In principle, an analysis by CE consists of three steps: injection, separation and detection. The injection of a sample into the separation capillary can be either performed by applying pressure or electrokinetically, using an electric field to cause

migration of ions and flow of the bulk solvent. In both cases it is necessary to insert one end of the capillary into a vessel filled with sample, and apply a pressure or a voltage for a certain time along the capillary to move sample solution into the capillary. The separation starts by applying a potential along the capillary. The main detection schemes used in CE are absorbance, laser-induced fluorescence or electrochemical detection.

The physical phenomenon underlying CE is the migration of charged particles in an electrical field. The velocity v (m/s) of a particle i finding itself in an applied electric field of strength E (V m^{-1}) is described by

$$\vec{v}_i = \mu_i \cdot \vec{E} \tag{1.1}$$

where μ_i (m^2 V^{-1} s^{-1}) is the apparent effective mobility of particle i. In CE, one has to distinguish between the electrophoretic mobility (μ_{ep}), which is the mobility of an ion, and the electroosmotic mobility (μ_{eo}) which is the mobility of the electrolyte in the capillary, due to electrophoresis and electroosmosis, respectively. These two effects require the definition of two different velocities. Both effects will be explained below. The effective mobility, μ_i, of eq. (1.1) is therefore the sum of μ_{eo} and μ_{ep}.

1.1.2 Electrophoresis

The term electrophoresis consists of two parts, *electro-* and *phoresis*. A direct translation from the Greek language for *phoresis* is a transport phenomena which uses external help. The whole word can then be defined as the transport of particles using an electrical field. The term ""particle" or "charged particle" is used in this work as a general term which stands also for the terms "ion" or "charged molecule".
If a charged particle is moved through a viscous medium by an applied electrical potential, an equilibrium between two main forces will occur after the particle has reached its specific velocity. These two forces are:
1) The electrical force, which depends on the charge, q, of the particle in an electrical field [JAC 83a]

$$\vec{F}_e = q \cdot \vec{E} \tag{1.2}$$

where $q = z \cdot e$, with z the ion charge and e (As) the elementary charge.
2) The frictional force, which results when a particle is moved through a viscous medium. This force is calculated using the Stokes equation [REI 85]:

$$\vec{F}_f = 6\pi\eta\, r\, \vec{v} \tag{1.3}$$

where η (kg m^{-1} s^{-1}) is the dynamic viscosity of the media, and r_i (m) the radius of the moving particle. The Stokes equation can be used under the assumption that the ions are spherical and have small velocities, which is generally the case in CE. The friction coefficient f_i is defined as

$$f_i = 6\pi\eta\, r_i \tag{1.4}.$$

In the steady state, $\vec{F}_e = \vec{F}_f$, which, when combined with eq. 1.1, yields the electrophoretic mobility of a charged particle:

$$\mu_{ep,i} = \frac{z_i \cdot e}{f_i} \tag{1.5}$$

where z_i is the ion charge of the particle i.

Equation 1.5 is fundamental because it indicates that the mobility is governed by the specific physical property of charge/size ratio. For small ions, the separation is mainly determined by ionic charge. Besides the dynamic viscosity, η, of the surrounding solution, ion qualities, as well as the hydration layer of the ions and ion pairing determine the mobility of the particle. The mobility is totally independent of the applied electrical field. It should be stated that eq. 1.3 is only valid for small Reynolds numbers, which in this case is equal to the condition that the moving particle is spherical and small in comparison to the channel. In all cases in this thesis this condition can be assumed to be fulfilled.

Assuming only electrophoretic effects in a basic CE system, only cations or anions can be separated, due to the fact that the only driving force is an electrical force (eq. 1.2). This means that only cations or anions will be moved through the capillary and separated, depending on the polarity of the applied voltage.

A more complete description of the electrophoretic mobility of an ion in a real electrolyte solution has to deal with two further effects. One is caused by the hydrated counterions of the electrolyte, which move as well in an applied electrical field [KOR 66a]. This motion causes a counterflow which lowers the overall mobility of the sample. A second force arises through the deformation of the cloud of counterions around the sample molecules in an electrical field. This asymmetric deformation results in a local electrical field gradient which is directed opposite to the applied electrical field, and which therefore lowers the velocity of the sample molecule [KOR 66b]. That means that for a given sample concentration, the electrophoretic

mobility is not only given by eq. (1.5), but is also affected by several complex parameters like the radius of the charged cloud of counterions and their mobility, and the value of the local field gradient caused by the asymmetric deformation of the charged cloud. For a more detailed discussion of these effects, the reader is referred to ref. [KOR 66a], [WED 82].

Therefore, some fundamental equations for capillary electrophoresis in general are given in Eqs. (1.6) - (1.8) [WEI 93]:

$$v_{ep} = \frac{L_d}{t_m} \tag{1.6}$$

$$v_{ep} = \mu_{ep} \cdot E \tag{1.7}$$

$$\mu_{ep} = \frac{L_d / t_m}{V / L_t} \tag{1.8}$$

$$\Leftrightarrow \quad t_m = \frac{L_d \cdot L_t}{V \cdot \mu_{ep}} \tag{1.8a}$$

where μ_{ep} ($m^2 V^{-1} s^{-1}$) is the electrophoretic mobility of particle i, L_d length of the capillary from the injection side to the detector, L_t is the total length of the capillary, V the applied voltage, and t_m the migration time. The field strength is then simply the voltage divided by the total capillary length L_t. The difference in mobilities of two components (μ_1, μ_2) leads to a difference in migration time and therefore in a separation.

$$\frac{\mu_1}{\mu_2} = \frac{z_1 \cdot r_2}{z_2 \cdot r_1} = \frac{t_{m_2}}{t_{m_1}} \tag{1.8b}$$

The equations 1.6 to 1.8a demonstrate that reducing the length L_t or L_d leads to a reduced migration time. Higher voltages also allow for faster separations (eq 1.8a), since the migration time is inversely proportional to the applied voltage. Very short migration times can be achieved in this way.

Under certain circumstances, electroosmotic flow of the bulk solvent can be suppressed. This is true in the case of capillary gel electrophoresis (CGE) where entangled polymers are used to enhance separation. Use of micellar solutions with ion-pairing agents can also result in reduced electroosmotic effects

1.1.3 Electroosmosis

Electroosmotic flow is induced by applying an electrical field along a buffer-filled capillary tube. The surface of a fused silica capillary is usually negatively charged, due to the pI value of 1.5 of the silanol groups [BEC 91]. The pI value of a molecule is defined as the pH at which equal concentrations of the cationic and anionic forms of the molecule exist [GLO 77]. The capillary surface charge attracts oppositely charged ions (cationic counterions) to compensate the negative charge, thus forming an adjacent double layer. The characteristics of the double layer, as well as the historical evolution of its understanding, are described below.

The electrical field component parallel to the surface will cause an electrical force to be experienced by the counterions (eq. 1.1). When the electrolyte velocity at the capillary wall suddenly changes, viscous forces accelerate the bulk of the electrolyte, dragging the bulk solution inside the capillary towards the cathode. Numerical simulations have shown that the velocity gradient inside the capillary approaches zero on a time scale between 100 µs and 1 ms [DOS 93].

The velocity of the electroosmotic flow (EOF) as defined by Smoluchowski in 1903 (originally in the CGS unit system) is given by [SMO 03]

$$\vec{v}_{eo} = \frac{\varepsilon \varepsilon_0 \zeta}{\eta} \vec{E} \tag{1.9}$$

where E is the applied electric field strength, η is the dynamic viscosity, ζ is the zeta potential, ε is the dielectric constant of the medium and ε_0 is the dielectric constant for vacuum. The zeta potential depends on the concentration, the pH and the ionic strength of the electrolyte used. It can be influenced by surfactants adsorbing to the capillary wall or by other organic modifiers. The value for ζ is in the order of mV [SCH 91]. Equation (1.9) implies that ε and η have the same values in the double layer as in solution.

It is important to point out that eq. (1.9) is expressed in the SI unit-system (système international d'unités). This will be adhered to for all equations used in this work. Unfortunately, it is not always clearly distinguished in the literature if the SI or the Gaussian CGS unit system is being used. This can cause problems for those who are not familiar with the conversion rules. Ref. [WEI 93], for example, uses the SI unit-system, whereas Ref. [LI 92] uses the CGS unit-system. A table to convert equations and symbols between the two different unit systems is given in Appendix A1.

Equations 1.6-1.8 for electrophoresis can also be used for electroosmosis. To distinguish between the effects, it is necessary to distinguish between the subscript

"ep" for electrophoresis and "eo" for electroosmosis. Variables which are the summation of both effects will have the index "tot" (which stands for total) in this work. Therefore, equations 1.6-1.8 can be written for the total mobility or velocity as well.

To understand the effect of electroosmosis, it is necessary to have a closer look at the interface between the capillary surface and the liquid. For this, the theory describing the interface between an electrode and the surrounding electrolyte, also known as electrical double layer theory, can be used. The description for this behavior has been extrapolated to the interface at capillary surfaces and buffer solutions. A brief historical summary about the electrical double layer theory is given by Bergethon and Simons [BER 90]. The first description of the double layer model was given independently by Helmholtz [HEL 79] and by Perrin. This model was based on the description of a parallel plate capacitor and is the historical derivation of the term "double layer". Helmholtz and Perrin found a linear decrease of potential over distance for the closest layer of ions bound at the surface.
The work done by Gouy (1910) and Chapman (1913) [GOU 17], [CHA 13] suggested the replacement of the capacitor plate-like arrangement of counterions by a diffuse cloud of charge that was more concentrated near the electrode surface and extended out into the bulk solution. In this model, the decay of potential from the electrode as a function of distance into the bulk electrolyte depends on the charge and on the ionic strength of the solution. Only electrostatic interactions are considered in this model. The effects of closest approach of ions to the surface, as well as ion size or water interactions are neglected; ions are treated as point charges. The decrease of potential over distance from the surface is found to be an exponential decay.
In 1924 Stern combined the two earlier models into what is called the "Stern model" [STE 24]. This model considers the effect of ion size and adsorption to the surface. By exchanging point charges with ions of distinct size, the distance between the counter charge and the surface becomes larger. Due to adsorption forces, the layer closest to the surface will be altered when compared to that predicted by a model in which only electrostatic interactions are considered. The number of ions populating the innermost layer where adsorption is important, and the distance of closest approach of this layer to the surface, are both finite. Therefore, there is a limit to the distance of the nearest approach of this layer to the surface, resulting in a region of linear potential decay with respect to distance. This layer can be also described as an ion cloud. This inner region is similar to that described by Helmholtz and Perrin and is called the Stern layer. The remainder of charge needed to neutralize the surface charge is arranged like the Gouy/Chapman diffuse layer.

The modern model is a further extension of the Stern model. Essentially, the surface is viewed as hydrated and the orientation of the solvent dipoles are dependent upon the surface charge. By using a theory which is based on the Debye-Hückel theory, which describes ions as charged spheres, it is possible to define a distance δ' from the capillary wall where no charge is found but aligned solvent molecules are attached to the wall (Fig. 1.2). This layer is defined by $0 < x < \delta'$ and called the inner Helmholtz layer. Therefore, δ' defines the minimum distance between ions and the wall. The next layer of unhydrated ions forms a layer of adsorbed species comprising the plane of closest approach, as in the Helmholtz/Perrin model. In the case of a glass surface, this layer has a substantial cationic character. This layer of ions closest to the capillary wall is tightly bound and therefore immobile, even under the influence of an electrical field [WEI 93].

The next region consists of hydrated counterions, which can be moved upon application of an external electrical field as described above. This region is part of the outer Helmholtz layer which is defined by $0 < x < \delta$. The distance δ is assigned assuming that all other forces besides coulombic-forces can be neglected for x-values larger than δ. For these x-values, the potential follows an exponential decay behavior. This region, following the outer Helmholtz layer, is known as the diffuse outer layer or Gouy-Chapman layer (Fig. 1.2).

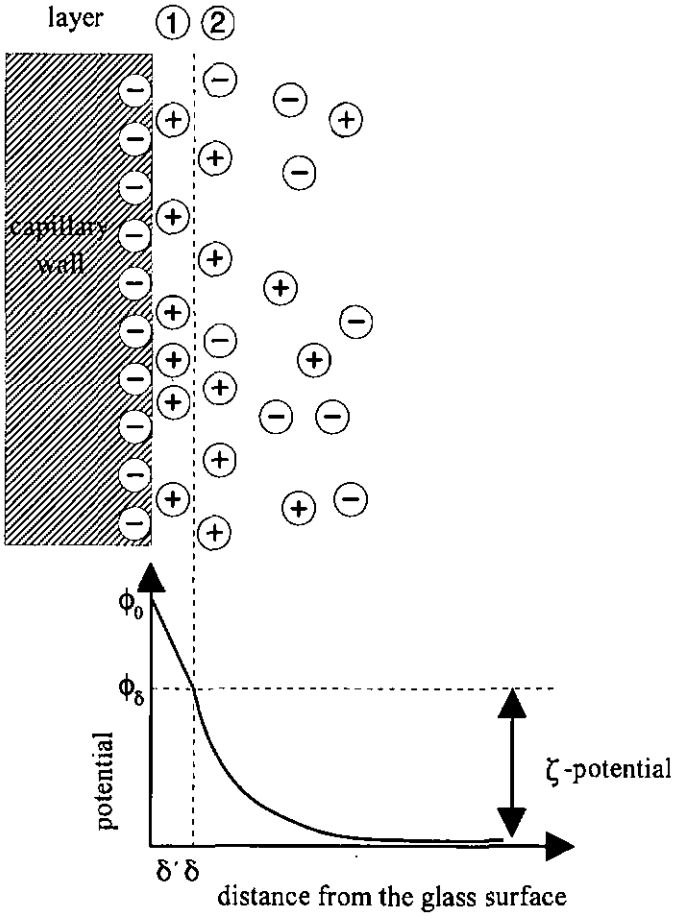

Figure 1.2 Schematic drawing of the interface between capillary and solution. The graph shows the dependence of the potential versus distance from the capillary wall.

The potential difference between δ and the middle of the capillary is called the zeta potential (ζ-potential). V.P. Andreev and E.E. Lisin [AND 93] calculated the value of

the zeta-potential for a wide range of concentrations C_0=(10^{-5} - 10^{-1}) M of KCl solution and an inner diameter (i.d.) of (2 - 240) µm. For a field strength of 100 V/cm to 150 V/cm the zeta potential varied from -6 mV to -100 mV.
While the electric double layer at metal electrodes is well understood, this is not the case for more complex surfaces such as silicon dioxide surfaces. Other models, like the "porous surface" model or the "surface complex" model, employ a triple-layer model to describe the solution/surface interface. Further references regarding these approaches are given in [SCH 91].[BOU 86] [BOU 91].

Electroosmosis and electrophoresis are independent of each other and can be treated as a superimposition of two velocities. Electroosmosis dictates an additional constant mobility value for all components. To get the total mobility, this constant mobility must be added to the electrophoretic mobility. Electroosmosis makes no direct contribution to the separation. In the case of a glass surface and for pH ranging from neutral to basic values, the direction of electrophoretic movement of negatively charged species is opposite to the direction of the electroosmotic flow. However, in general the absolute value of the electroosmotic velocity (eq. 1.9) is higher than that of the electrophoretic velocity. Therefore, all species within the capillary tend to move in one direction. The total velocity of this movement depends on the different charge and size of the molecules (eq. 1.5). Typical values for μ_{eo} and μ_{ep} are in the order of 1 to 10 * 10^{-4} $cm^2V^{-1}s^{-1}$, where for anions the sign of the electrophoretic mobility is negative. Some of the various possibilities to control the electroosmotic flow are given in Appendix A2.

Due to the effect of the double-layer, as described above, the electroosmotic effect causes a piston-type flow profile, which is shown in Fig 1.3. This is in contrast to a parabolic flow profile, which arises in pressure-driven or Poiseuille flow systems. Electroosmotic flow leads to uniformity of the velocity distribution, except close to the capillary walls. This layer of non-uniformity is usually small in comparison to the channel width and can therefore be neglected. The flat flow profile is beneficial, because it does not directly contribute to the dispersion of the sample zones. Therefore, separation efficiency is increased in comparison to pressure-driven flow systems. The flow rate and the flow profile are generally independent of the capillary diameter. The profile will be disrupted , however, if the capillary internal diameter is too wide (≥ 200 to 300 µm) [NEI 92a]. A very detailed theoretical description about the electrokinetic flow in narrow cylindrical capillaries is given by R. Whitehead and C.L. Rice [RIC 65].

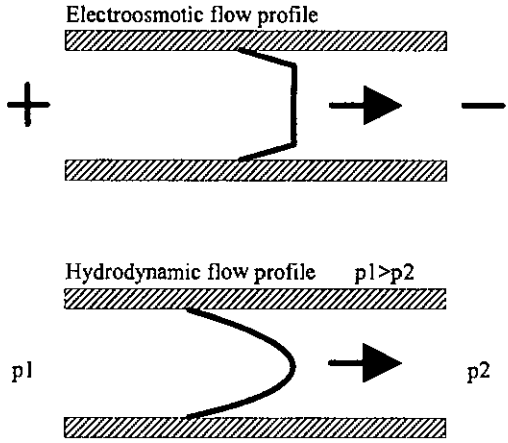

Figure 1.3 Electroosmotic flow profile and parabolic-shaped hydrodynamic flow profile. The arrow indicates the direction of movement.

1.1.4 Separation efficiency

In separation techniques, the parameter used to describe the separation efficiency is the *number of theoretical plates, N*. The concept of theoretical plates evolved from studies of extraction, distillation and countercurrent distribution, where distinct stages in a separation exist [GID 91]. It is also widely used in all chromatographic techniques. There, a single plate (number of theoretical plates, N=1) is equal to the separation efficiency of a single distillation or a two phase extraction equilibrium. For a separation system with continuous zonal systems like CE, the number of distinct stages can be taken as infinite, leading to a Gaussian concentration distribution. N is defined by:

$$N = \frac{L_d^2}{\sigma_{tot}^2} \tag{1.10}$$

where σ_{tot}^2 (in terms of length) is the total variance of a measured Gaussian peak and includes all contributions to band broadening. The main sources of band broadening generally considered result from axial diffusion (σ_{diff}), the injection (σ_{inj}) and detection process (σ_{det}), temperature effects due to Joule heating (σ_{temp}), and adsorption effects at the capillary walls (σ_{ads}). It should be mentioned that σ_{det} can be divided into two different contributions. One comes from the detection volume; the

other is determined by the contribution from the time constant of the detector, which depends on the electronics. The total variance can then be expressed as:

$$\sigma^2_{tot} = \sigma^2_{diff} + \sigma^2_{inj} + \sigma^2_{det} + \sigma^2_{temp} + \sigma^2_{ads} + \sigma^2_{others} \qquad (1.11).$$

σ^2_{others} includes effects like nonuniformity of the double layer or other influences from the apparatus. It is possible to reduce the contribution of all other bandbroadening effects besides axial diffusion. This can be done by optimizing the injection process, the detection volume and system, and by avoiding other bandbroadening effects. Einstein's equation describes the band broadening due to axial diffusion in liquids:

$$\sigma^2_{diff} = 2Dt \qquad (1.12)$$

where D is the diffusion coefficient (cm^2s^{-1}) and t is time (s). D is ideally only temperature dependent, but because of ionic interactions in electrolyte solutions it can also be dependent on concentration [KOR 66c].
Assuming that axial diffusion is the only band broadening effect, we can substitute Einstein's equation into the equation for the number of theoretical plates yields:

$$N = \frac{\mu_{tot} V}{2D} \qquad (1.13).$$

This shows that the maximum number of theoretical plates obtainable using an optimized (ideal) system is linearly dependent on the applied voltage for a given system. As already mentioned, the overall mobility is given by $\mu_{tot} = \mu_{ep} + \mu_{eo}$.

Plate models, however, are often used in describing the continuous transport processes of chromatography, field-flow fractionation, electrophoresis, sedimentation, and related zonal methods.
Another parameter for the separation efficiency is derived from equation 1.12 by replacing t with L/v. This gives

$$\sigma^2 = \frac{2D}{v} \cdot L \qquad (1.14)$$

This equation clearly shows that σ^2 is directly proportional to the migration distance L if v is kept constant. The factor of proportionality is defined as

$$H = \frac{2D}{v} \qquad (1.15).$$

H is called the *height equivalent to a theoretical plate* and has the unit of length. Eq. 1.14 can then be expressed as

$$\sigma^2 = H \cdot L \tag{1.16}$$

The relation between the number of theoretical plates N and the height equivalent H is then given by

$$N = \frac{L}{H} \tag{1.17}$$

The most important parameter for the separation of two specific components is given by the resolution R_S. The resolution gives a value for the overlap of two zones with specific components. In general, R_S is given for two Gaussian peaks by

$$R_s = \frac{L_2 - L_1}{2(\sigma_1 + \sigma_2)} \tag{1.18}$$

where L_1 and L_2 are the locations of the zones. The two sigmas, σ_1 and σ_2, can be expressed by an average sigma σ with $\sigma_1 + \sigma_2 = 2\sigma$. Eq. 1.18 can then be written as

$$R_s = \frac{\Delta L}{4\sigma} \tag{1.19}$$

Substituting σ into eq. 1.15 yields

$$R_s = \frac{\Delta L}{4\sqrt{H \cdot L}} \tag{1.20}$$

The difference in location, ΔL, for two different electrophoretic mobilities, μ_{ep}, at a time, t, is given by

$$\Delta L = \Delta\mu_{ep} \cdot E \cdot t = \frac{\Delta\mu_{ep}}{\bar{\mu}_{ep}} \bar{L} \tag{1.21}$$

with t being equal to the mean distance over mean velocity

$$t = \frac{\bar{L}}{E \cdot \bar{\mu}_{ep}} \tag{1.22}$$

For the resolution, R_S, we then get

$$R_s = \frac{\Delta\mu_{ep}}{\bar{\mu}_{ep}} \cdot \frac{\bar{L}}{4\sqrt{H \cdot \bar{L}}} \tag{1.23}$$

and finally with eq. 1.17

$$R_s = \frac{1}{4} \frac{\Delta\mu_{ep}}{\bar{\mu}_{ep}} \sqrt{N} \tag{1.24}.$$

It is important to stress that the resolution is proportional to the square root of the number of theoretical plates. Substituting for N in eq. 1.24 using eq. 1.10 shows the linear dependency of the resolution on the migration length of the sample. This is an important relation and will be discussed in more detail in the chapter 1.3 and 3.1. Another important dependence of the achievable resolution becomes apparent by substituting N in eq. 1.24 by eq. 1.13. This yields:

$$R_s = \frac{1}{4} \frac{\Delta\mu_{ep}}{\bar{\mu}_{ep}} \sqrt{\frac{\bar{\mu}_{ep} V}{2D}} \tag{1.25}$$

Besides the technical limitations of applying high voltages (larger than 30 kV), eq. 1.25 indicates that the resolution does not have a linear dependency to the voltage. Therefore, increasing the voltage is a limited means of improving the resolution. For what is called "baseline" - resolution, R_S has to be larger than 1.5. "Unit"-resolution is gained at R_S =1, and two distinct maxima can be found for $R_S > 0.5$. For more detailed information on capillary electrophoresis, the reader is referred to references [WEI 93], [BEC 91], [LI 92], [NEI 92], [GID 91], [MOS 92], [FOR 89].

1.2. The μ-TAS concept

1.2.1 Analytical chemistry

The goals of analytical chemistry are to devise means for the identification, the quantification and the structural elucidation of chemical samples. This is necessary in various fields of production within chemical industry. The main fields of analytical chemistry are quality control, clinical chemistry, process monitoring and process control, as well as solving existing problems in environmental and safety matters. Thus, analytical chemistry has grown to become one of the most dynamic scientific disciplines in the last forty years [WID 93]. During this period, the efficiency of analytical methods has improved by a factor of ten per decade. The improvement in efficiency refers to the time required to perform a chemical analysis, as well as to the progress which has been made in lowering the detection limits. The size of the analytical equipment and the cost incurred to solve a chemical problem by analytical means have been reduced by the same magnitude. Parallel to the increase in efficiency, there has been a trend from the application of analytical chemistry as a *retrospective* approach into a *diagnostic* or even a *prognostic* science. This development is the result of the need to replace quality control of the end product into an active chemistry-driven process-integrated quality control. In order to demonstrate the different development levels, we distinguish between off-line, at-line, on-line, in-line, in-situ, and non invasive modes, allowing different degrees of end-point, feed-forward and feed-back control [WID 93].

It is possible to divide the steps necessary to perform a chemical analysis into three main groups. The first group involves all steps related to the sample, while the second group is comprised of detection schemes. Finally, the third step encompasses all electronic steps. Listed below are the various categories encountered in each of the groups described above.

1) *sample related steps*
sampling
sample transport
sample pretreatment like filtering, dissolving, extraction
sample preparation like derivatisation steps, masking of interferents
enrichment of trace components
separation
fraction collection

2) *detection*
qualitative determination
quantitative determination
structural and compositional elucidation of compounds

3) *electronic related steps*
data acquisition
signal processing
instrument control
data handling and storage
documentation and interpretation of the results

1.2.2 The integrated total analysis system (TAS)

The idea of an integrated total analysis system (TAS) was first published in 1983 [WID 83]. The concept of a TAS can be described as an integrated analytical system combining all above listed steps necessary to perform a chemical analysis. This can be done by combining all sampling handling steps with measurement steps into a complex system, in which the different modules are interconnected by wires and tubes. Therefore the "total" stands for the linkage of *all* (total) necessary steps into one instrument. This is clearly described in ref. [WID 83], where the system is called *integrated total analysis system*. In combination with a modular-based setup, a TAS can provide faster and more complete chemical analyses than a "naked" sensor. The TAS concept has many potential applications in fields such as biotechnology [LUE 90], [FIL 91], process control [TSC 87], [GRA 90], and the environmental [GUI 83], [EDM 85], and medical sciences [SHA 89], [STI 85], fields in which continuous monitoring has become increasingly important [BUR 94].

1.2.3 The µ- TAS concept

The concept of a miniaturized total analysis system, or µ-TAS, was first presented at the Transducers '89 conference (June 25-30, 1989, Montreux) [MAN 90a]. "Miniaturized" in this case does not necessarily mean a reduction of the overall outer dimensions of the system. The main goal of this concept is to increase the speed and efficiency of a chemical analysis. In the case of liquid chromatography or capillary electrophoresis, it can be shown that smaller capillary inner diameter and shorter capillary length can increase the resolution of a separation and can give a higher separation speed [MAN 93a]. Another advantage obtained from the size reduction is

the reduced consumption of reagents and carrier solution. These benefits can be obtained by using miniaturized flow manifolds, which minimize the distances between sampling and detection point. Thus, the μ-TAS concept is the further development of the TAS concept.

The analytical device described in this work is embedded in the μ-TAS concept developed at the Corporate Analytical Research at Ciba-Geigy. Within this above described concept, there exist already devices for sample preparation, separation and detection, and for fluid handling. Examples of different components which can be used as modules for a μ-TAS system are given in chapter 1.2.6.

1.2.4 Reasons for miniaturizing a CE system and integrating it onto a planar microstructure

There are several reasons for the miniaturization of a CE system and integrating it onto a microstructure. Table 1.1 gives a quick overview of the main advantages:

Table 1.1

	relations	benefit	remarks
migration time	$t \propto L^2$	migration time decreased when length decreased	for N, V const. eq. (1.8a)
separation efficiency	$N_{max} \propto \frac{L}{d}$	efficiency increased when inner diameter decreased	d is the inner diameter of the channel, L length of the channel power dissipation is limited to 1 W/m
injection-volume	$N \propto \frac{1}{(\sigma_{inj}^2 + \sigma_{bb}^2)}$	efficiency increased when bandbroadening decreased	(eqs. 1.10 and 1.11) σ_{bb} stands for all other contributions to the band broadening
sample consumption	$Volume \propto L \cdot d^2$	sample consumption decreased when diameter decreased	d is the inner diameter of the channel L is the length of the channel

Benefits gained by the miniaturisation and integration of a CE system into a microstructure.

Assuming that L_d, the length of the capillary from the injection side to the detector, and L_t, the total length of the capillary, are in the same order of magnitude, equation (1.8a) shows that the migration time is proportional to the square of the length used, L. This clearly shows that the migration time in an electro-driven separation system can be strongly lowered using short capillaries.

A critical and limiting factor in electro-driven separation techniques is the generation of heat. The generation of heat per unit length Q (Wm^{-1}) in a capillary of cross section A (m^2) is proportional to the square of the voltage applied:

$$Q = A \cdot \gamma \cdot E^2 \tag{1.26}$$

where γ is the electrical conductivity. Decreasing the tube diameter gives an increased ratio of surface to volume. This results into a better heat dissipation through the surface. Decreasing the tube diameter has thus far been the main way to avoid excessive temperature increases [JAN 89]. The cross-section of a 50 μm i.d. fused silica capillary, for example, is five times larger than the micro channels used for this work. For a given cross section, heat dissipation is more efficient in rectangular columns than in cylindrical capillaries [JAN 89]. Integration of capillaries onto planar microstructures using micromachining techniques produces channels with relatively rectangular cross sections. Micromachining refers to the manufacturing of three-dimensional structures in silicon, glass, and other planar substrates using techniques developed for the production of integrated circuits in the microelectronics industry. The manufacturing technique will be described in more detail in chapter 2. Due to the better power dissipation capability of the micromachined channels, the application of higher electrical field strength in contrast to conventional CE is possible, which results in much shorter separation times and in better separation efficiency (eqs. 1.8a and 1.25). Miniaturization therefore leads to a more efficient and faster separation. In terms of separation efficiency, N_{max}, the maximum achievable number of theoretical plates is limited by the maximum voltage which can be applied to the system. This in turn is limited by the restriction that the relation between current and voltage fulfill Ohms law.

Another reason for miniaturizing a CE system is also a result of micromachining technologies, which allow the fabrication of complex flow manifolds. With these techniques, it is possible to manufacture small but well defined volumes down to femtoliters. Some examples will be described in chapter 1.2.6. Therefore, it is possible to produce channels in a planar surface and use them for CE. Using well-defined injection schemes with small volumes, the contribution to the bandbroadening in terms of σ_{inj} can be reduced and therefore the separation efficiency increased.

Finally, it should be mentioned that solvent and sample consumption are lowered through miniaturization. This results mainly from the well defined channel geometry, as well as from the reduction of dead volumes. By reducing all three dimensions of a flow system by a factor of c the volume of that system decreases by a factor of c^3. This is a benefit which is common to all capillary-based methods, of course, and is independent of how the capillaries are actually manufactured.

1.2.5 Similarity considerations

In hydrodynamics as well as in aerodynamics it is often necessary to extrapolate physical properties of a liquid (or gas) stream to another system of different dimensions. This is also relevant for the miniaturization of a system for liquid handling. Within this topic we can describe a miniaturized CE system as a system for liquid handling. In this context, all physical rules for extrapolating properties like velocity, geometric size, pressure drop and flow characteristics are of special interest. The conditions which must be fulfilled to compare two systems are called the similarity conditions. They are basically the following [BOH 91], [MAN 86], [BIR 60]:

a) The two systems being compared must be similar in their geometry. This refers to their length, area and volume dimensions as well as to their surface roughness. Generally, two systems of different geometrical dimensions are not similar in their hydrodynamic properties because of their surface roughness. This is because it is much easier to scale the length, the area, or the volume dimensions of a system down than it is to scale down the surface roughness. Usually macroscopic systems already have a very smooth surface, which makes it often impossible to get the same surface roughness/length relationship in a miniaturized system. Pipelines for the transport of oil, for example, have a smooth inner surface, and it is technically not possible to scale the surface roughness of such a system down to a miniaturized model system. This has to be considered when using models to evaluate physical properties. Table 1.1 summarizes the geometric conditions for the similarity of two systems:

Table 1.2

system 1	system 2
length L_1	length L_2
area A_1	area A_2
volume V_1	volume V_2
average surface roughness k_1	average surface roughness k_2
conditions: $\frac{A_1}{A_2} = \frac{L_1^2}{L_2^2}$ $\frac{V_1}{V_2} = \frac{L_1^3}{L_2^3}$ $\frac{k_1}{L_1} = \frac{k_2}{L_2}$	

Geometric conditions for the similarity of two systems [BOH 91].

b) The two systems being compared must be similar in their physical properties. This includes velocities, accelerations, forces and also the physical properties of the liquid (or gas) used . Finally, both systems must be similar in their thermodynamic behavior in terms of temperature, heat capacity, heat conductivity among other parameters.

Table 1.3

system 1	system 2
velocity v_1	velocity v_2
acceleration a_1	acceleration a_2
mass m_1	mass m_2
time t_1	time t_2
force F_1	*force* F_2
density ρ_1	density ρ_2
dynamic viscosity η_1	dynamic viscosity η_2
kinematic viscosity ν_1	kinematic viscosity ν_2
conditions: $\frac{a_1}{a_2} = \frac{v_1 \cdot t_2}{v_2 \cdot t_1}$ $\frac{m_1}{m_2} = \frac{\rho_1 \cdot L_1^3}{\rho_2 \cdot L_2^3}$	

Physical conditions for the similarity of two systems [BOH 91].

A combination of the geometric and physical properties can be obtained by using dimensionless variables such as the Reynolds number. This number is of special interest for distinguishing between laminar and turbulent flow.

$Re < Re_{crit}$: laminar

$Re > Re_{crit}$: turbulent

The Reynolds number describes the relation between inertial force and viscous force affecting a particle in the liquid stream. It is defined as:

$$Re = \frac{v \cdot L \cdot \rho}{\eta} = \frac{v \cdot L}{\nu} \tag{1.27}$$

with the kinematic viscosity ν ($m^2\ s^{-1}$), density ρ ($kg\ m^{-3}$), and liquid velocity v (m/s). Because the Reynolds number is a stability criteria it is very sensitive for small disturbances. Therefore, the critical Reynolds number for the sudden change from laminar to turbulent can be given as between 1000 and 1200 for a smooth round shaped tube [BOH 91], [KNE 90], [BER 75].

For further discussion about other dimensionless parameters dealing with similarity considerations the reader is kindly referred to the References [MAN 93a], [BOH 91], [KNE 90], [BER 75].

1.2.6 Examples of components for the μ-TAS concept

Various components and the investigations being carried out to develop a μ-TAS will be briefly described. For further information about single components, the reader is kindly referred to the references given in the text.

free flow electrophoresis

For continuous micro sample preparation, a miniaturized free-flow electrophoresis (FFE) system was developed. FFE in its macro form is one of the very few continuos separation methods for high molecular weight compounds. An FFE system was miniaturized and integrated onto a silicon micro structure at ICSensors, Milpitas,CA, USA. All dimensions were reduced by a factor of 10 with respect to the conventional FFE case. With this system it was possible to achieve a continuous separation of small ions according to their charge by using 50 V with a response time of 2 to 5 minutes [RAY 94a]. Further investigations into the separation of biomolecules and biological cells are still going on [RAY 94b].

flow-injection analysis

A flow injection analysis (FIA) system usually requires several pumps and tubing for controlling solution flows, making it relatively complex both in terms of system construction and maintenance. An added limitation is that the volume of a tubing-based system is generally in the mL range, and cannot be reduced by the several orders of magnitude necessary to achieve the μL and sub-μL volumes relevant for μ-TAS. An alternative 3D approach to flow manifold assembly, based on a concept of stacked planar micro fluidic elements has been developed at Ciba-Geigy. The individual elements are fabricated photolithographically to yield features such as holes and channels having μL volumes. Realization of such systems has been possible in cooperation with the Institute of Microtechnology (IMT), University of Neuchâtel, Switzerland, who have provided silicon-based micro membrane pumps for evaluation in stacked format. Larger batches of pumps and fluidic chips have been produced at the Centre Suisse d'Electronique et de Microtechnique (CSEM) SA in Neuchâtel, based on processes developed at IMT. First experiments with the stacked system concept saw incorporation of ion selective field effect transistors (ISFETs) together with micropumps to measure potassium and pH in aqueous solutions [SCH 92], [SCH 93a], [SCH 93b], [SCH 93c], [BER 94], [VER 94a], [SCH 95]. Wet chemical analysis of phosphate has also been demonstrated, with dramatic reduction in reagent consumption [VER 93], [VER 94b]. Together, these studies have shown that the reduction in system volume achieved with this approach can lead to the implementation of flow system configurations which are impractical in larger

systems. In addition, the modularity of the system allows easy adaptation to analyses based on different modes of detection, such as electrochemical sensors or small volume optical detection. Projects in progress include efforts to develop stacked flow manifolds for on-line monitoring of biotechnological processes, as well as for real-time *in vivo* monitoring of lactate in a hospital environment. The latter project involves combination of microdialysis as sampling technique with a micro fluidic/sensor system [VER 94c], [HOG 94].

liquid chromatography on a chip

Miniaturization in the field of high pressure liquid chromatography (HPLC) was first realized through the use of particles of micrometer dimensions as column packing to achieve improved separation efficiency. As column manufacturing technologies improved, use of both open and microparticle-packed columns which themselves have diameters of 1 mm or less has become more common. In theory, open tubular LC has the advantage that a given performance can be achieved in shorter analysis times and lower pressures than with packed LC columns. However, column diameters need to be less than 10 µm if a reasonable performance is to be achieved in one minute [MAN 90b]. Micromachining techniques would thus be of obvious advantage in the fabrication of small diameter open columns. Two examples of devices for open tubular LC exist in the literature, one in silicon [MAN 90b], the other in glass [COW 95]. Another advantage that planar devices have is that system components can all be incorporated into one channel network with virtually no intermediate dead volumes. This was exploited in an HPLC device designed at Ciba-Geigy for packed column applications, and fabricated at ICSensors in Milpitas, California. Preliminary results indicated that these HPLC chip could be operated at pressures up to 120 atm, with the limiting factor not the chip itself, but the interface with the peripheral system. It was possible to pack the capillary column on the assembled chip, and a separation of two components was obtained [OCV 94].

fast capillary electrophoresis on a glass chip

The first results using capillaries manufactured into a glass chip and used for CE were presented in June 1991 at the HPCE'91 conference in Basel, Switzerland [MAN 92a] and at the Transducers'91 conference in San Francisco, USA [MAN 91b], [HAR 91]. Another generation of micromachined CE systems was designed and used by C.S. Effenhauser in the Corporate Analytical Research department, Ciba-Geigy, Basel, Switzerland. An injection scheme integrated onto the chip allowed volume-defined electrokinetic sample injection without sample biasing [EFF 93]. Optimized experiments yielded separation times ranging from a few seconds to a few tens of

seconds. Plate heights down to 0.3 µm have been obtained using a separation length of 24 mm and an electric field of 1 kV/cm [EFF 93]. Automated repetitive sample injection and separation is also described in [EFF 93]. Also reported are experiments performed with chips filled with noncrosslinked 10 % polyacrylamide gel [EFF 94]. A synthetic mixture of fluorescent phosphorothioate oligonucleotides ranging from 10 to 25 bases in length were separated in less than 45 s with the application of 2300 V/cm [EFF 94]. Plate height up to 0.2 µm were obtained.

Recently, J.M. Ramsey and coworkers at Oak Ridge National Laboratory, Oak Ridge, TN, USA, showed high speed separations of rhodamine B and fluorescein in less than a second [JAC 94a]. Plate heights down to 0.7 µm were achieved using an electric field strength of 1.5 kV/cm. A postcolumn reactor was presented to conduct postseparation derivatisation using o-phthaldialdehyde (OPA) as a fluorescent tag [JAC 94b]. Separation of two postseparation labeled amino acids were shown. An open channel electrochromatography on a microchip represents another application of micromachined chemical analysis devices. Electroosmotic flow was used to move the sample into the microchip and to pump the mobile phase through the chip. First results obtained with this device were presented recently [JAC 94c].

D.J. Harrison at the University of Alberta, Edmonton, AL, Canada, is one of the pioneers in the field of CE on micromachined glass chips [MAN 92a], [HAR 92a]. He and his coworkers have done some fundamental investigations of electroosmotic pumping and valveless control of fluid flow within a manifold of capillaries on a glass chip [HAR 93a], [SEI 94a]. Therefore, the technique of capillary electrophoresis on a glass chip is now well described and open to many other applications. Besides glass, a variety of other materials can be used for the manufacturing of microstructures onto a chip. As one example, the work done by B. Ekström and coworkers at Pharmacia AB, Uppsala, Sweden should be mentioned. They manufactured channels for CE in polymer substrates [EKS 90], [MAN 93b]. Ceramic was used as a material in the work done by D. Petersohn and coworkers [KNA 90].

Further information about the use of planar glass structures for CE are given in: [BUR 93a], [BUR 93b], [BUR 93c], [EFF 94b], [EFF 95], [FAN 94], [HAR 92b], [HAR 93b], [HAR 93c], [JAC 94e], [JAC 94d], [MAN 91d], [MAN 91e], [MAN 93c], [SEI 93], [SEI 94b], [WOO 94].

The realization of the µ- TAS concept requires the combination of microstructuring techniques well known from the electronics industry with a knowledge of analytical techniques. At the University of Twente, The Netherlands, a workshop entitled "Micro Total Analysis Systems" was held for the first time (21 - 22 November 1994). The proceedings of this workshop (ref. [BER 95]) give a good overview on the state of the art in this field.

1.3 SCCE - idea and concept

1.3.1 The idea of synchronized cyclic capillary electrophoresis (SCCE)

Underlying every scientific work is a concept. The idea behind the synchronized cyclic CE (SCCE) system was first developed and patented by A. Manz at the Corporate Analytical Research at Ciba-Geigy Ltd. Basel, Switzerland [MAN 91c]. Before describing the concept and idea of SCCE in more detail, the reasons for modifying standard CE instruments will be explained. Since commercial instruments have only been available for the past five years, a brief overview of the available instruments can be found in ref. [ODA 94]. A closer examination of the results obtained using commercial CE instruments shows a limitation in separation efficiency. As indicated earlier, the maximum achievable number of theoretical plates is limited by the maximum voltage which can be applied to a given system. Historically, voltage differentials of 30 kV are readily and economically available, due to the prevalent use of 30 kV power supplies in the television industry. The already well developed technology for production and use of these power supplies, along with the associated cables, plugs and relais, was transferred to the field of instrumentation for analytical chemistry. The use of voltage differentials much above 30 kV incurs risk of arcing, because at 30 kV the dielectric breakdown distance in air is approximately 1 cm [GER 82].

In commercially available CE instruments, a maximum voltage of 30 kV drops along a capillary of a given length and therefore defines a certain electric field strength. The sample experiences this field only once. Thus, if the separation does not occur within this length, then alternative approaches must be found. As described in eq. 1.10, the number of theoretical plates, and therefore the separation efficiency, is increased by increasing the length of the capillary. Increasing the length while keeping the applied voltage constant results in longer migration times. Migration times can be decreased by increasing the applied voltage, though this approach is limited technically by the lack of availability of high voltage power supplies above 30 kV. A similar limitation occurs in modern liquid chromatography (LC). In LC, the column length also dictates the achievable separation efficiency. As a way around of this problem, the technique of column switching was developed in LC. Column switching involves the selective transfer of a fraction of effluent from a primary column to a secondary column for further separation [RAM 88]. This results in much higher separation efficiencies, since it is possible to carry out the column switching as long as it is necessary to perform the separation.

A method for obtaining an "infinite" capillary length where a fraction of the sample mixture passes many times through the applied electric field is provided by using

micromachining techniques. These techniques enable the production of small channels in various shapes and lengths in different materials arranged in any number of different configurations. Fig. 1.4 shows schematically the idea of a capillary of infinite length. This system allows the sample to be moved around the channel as long it is necessary to separate the sample. In reality, this system as it is represented in fig 1.4 would not work using only two electrodes. To operate such a system, at least three electrodes would be necessary. This will be discussed in more detail in the chapter 2.2.1. The direction of the electrical field strength inside the channels can be changed by switching the electrodes to which the voltage is being applied. This is done in such a way that the section of the cyclic capillary in which the components of interest are to be found at a given time is kept at an appropriate electric field strength. Therefore, it is possible to move a sample around a cyclic capillary just by switching the applied voltage in the desired way. This scheme is the basis for understanding the idea which underlies synchronized cyclic CE.
Another advantage of such a system is the constant electrical field, which is independent of the length used to perform the separation. On its way around one cycle, the components are exposed to a voltage which corresponds to twice the voltage applied. That makes it possible to provide the system with a high electrical field strength over an "infinite" capillary by using finite voltages.

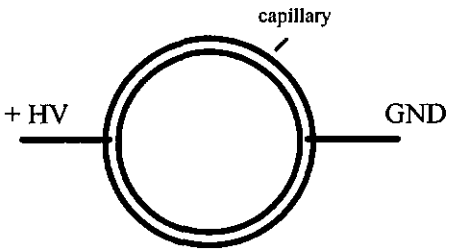

Figure 1.4 Schematic drawing of the idea behind the synchronized cyclic capillary electrophoresis (SCCE) system.

A different approach to increase the "effective" length of a capillary was reported by Culbertson and Jorgenson [CUL 94]. They used a system in which the sample is pushed backwards through the capillary by applying a pressure when the sample has reached the end of the capillary. After pushing the sample back, the separation can be started again. Repeating this procedure several times, they were able to demonstrate the separation of leucine and isoleucine within 8 hours and a separation efficiency of 17.3 million theoretical plates [CUL 94]. These amino acids possess very similar

mobilities and have proven difficult to separate using standard CE instruments. The disadvantages of this procedure are the contribution to the band broadening from the Poiseuille type flow profile while pushing the sample backwards, and the timescale involved.

There have been other approaches to focus on one single component during a CE separation. Modifying the electrolyte makes it possible to adjust the electroosmotic flow in a way that, for a certain component i, the electrophoretic mobility is adjusted to the same value as the electroosmotic mobility, but with the opposite sign ($\mu_{ep,i} = -\mu_{eo}$). This leads to a migration of all other components and the component of interest will remain at a certain position within the capillary. Another attempt deals with the control of zeta potential by applying a radial voltage to the capillary [WU 93]. This will influence the electroosmotic velocity, which can be adjusted to the electrophoretic mobility of a component of interest. Both of these methods depend on a stable surface chemistry within the capillary, a condition which is difficult to fulfill. Therefore, the application of these techniques is still limited.

1.3.2 Realization and principle of SCCE

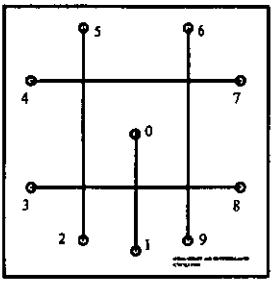

Figure 1.5 Schematic drawing of a channel layout usable for SCCE. Figure 1. Channel layout of a microstructure for use in cyclic capillary electrophoresis. The channels are fabricated photolithographically, whereas the holes are mechanically drilled. The square channel in the center is used for the separation. This channel is 10 μm deep and 40 μm wide. The other channels are serving as inlets and outlets. The numbers are reservoir numbers referred to in the text.

A structure for synchronized cyclic CE on a planar glass plate was realized by arranging four connecting capillaries in a square (Figure 1.5). At each corner of the square, two channels connect the loop to external reservoirs filled with electrolyte. These channels act as inlet and outlet channels, and as buffer reservoirs. The square channel is the actual separation channel. A second channel crosses the separation channel at the midpoint of one side. This channel is required for the injection of sample into the system. The ends of this channel are also connected to external reservoirs. The device has ten reservoirs in which electrodes are immersed to apply high voltage and cause electrokinetic flow through the channels. In the case shown in Fig. 1.6, nine of these reservoirs are filled with electrolyte solution, whereas the reservoir in the center of the device is filled with sample solution. The analysis process consists of three parts, the injection and separation processes, and detection. The injection process described here is only one of several different methods conceivable with this layout.

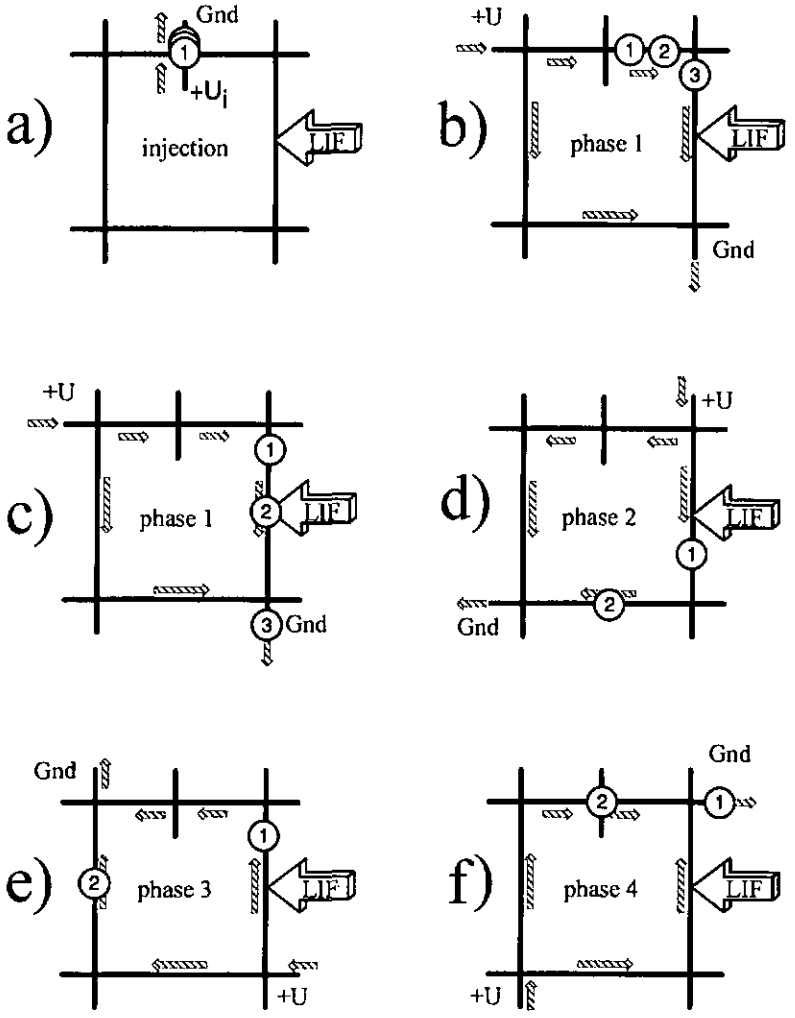

Figure 1.6 The principle of synchronized cyclic capillary electrophoresis in a channel system similar to the one shown in Fig. 1.5. Three sample components, labelled 1, 2 and 3, are symbolized by circled numbers. The large arrow on the right side indicates the location of the laser-induced fluorescence (LIF) detector. The direction of the liquid flow is shown by the hatched arrows. The voltage switching procedure is synchronized to component 2. (a) injection phase, (b) during phase 1, (c) at the end of phase 1, (d) and (e) phase 2 and 3, (f) end of the cycle.

A voltage U_i is applied to the electrodes in the reservoirs at the ends of the injection channel. This causes a flow of electrolyte through the injection channel, thereby filling the intersection zone between the separation channel and the injection channel. The flow of sample through the injection channel must last long enough to be sure that even the slowest component has reached the intersection. This guarantees an injection volume whose composition is truly representative of the sample. An electrical voltage is then applied between reservoirs 8 and 5 (see Fig. 1.5), causing the sample to be driven into the separation channel (see Fig 1.6 b). When the sample has entered the separation channel, it moves together with the flow of electrolyte in the direction indicated by the arrows shown in Figure 1.6 b. In the example given, the positions of three sample components are symbolized by the circled numbers 1, 2 and 3. The procedure is synchronized to the migration speed of component 2. The separation starts when a voltage U is applied to the electrodes in the electrolyte reservoirs across the diagonal of the square channel system (phase 1, see Fig. 1.6 b and c). An electrical current and the electrolyte both move symmetrically clockwise and counterclockwise through the channels. New carrier electrolyte enters at the upper left corner, whereas electrolyte containing sample components, which are moving more rapidly than the synchronized species, exits the system at the lower right corner (see component 3 in Fig. 1.6 c). When component 2 reaches the midpoint of the first side of the square, the potential applied to the electrodes is switched one position to the right to the next electrode set. This causes a situation which is similar to a rotation of the electric fields by 90 degrees. The channel segment containing component 2 remains at identical electric field strength, but the electric field in the segments adjacent to those containing the component of interest has changed its direction. Fig. 1.6 shows the corresponding changes in electrolyte flow (phase 2). At the end of phase 2, the slow moving component 1 has not passed the lower right corner. Shortly before component 2 reaches the midpoint of the next side, the voltages are switched to the next position. As can be seen in Fig. 1.6 e (phase 3), the slow moving component 1 now migrates in the opposite direction. One phase further (Fig. 1.6 f), component 1 is eliminated from the sample mixture. Only component 2 remains in the square channel system. One cycle has now been completed, and the next cycle starts with phase 1. A more complex sample mixture would need more cycles to be separated in the desired way.

Only a well defined window out of the complete electropherogram is seen by the detector this way. For monitoring purposes, this would certainly suffice, because normally interest is focused on one single component. The accompanying components only play a role in certifying the identification and quantification of the component of interest.

On its way around one cycle, component 2 is exposed to a voltage which corresponds to twice the voltage applied (see table 1.4). For n cycles, this value increases to 2n of the voltage applied. Thus, the possibility exists to increase the value of N/U (number of theoretical plates per volt) dramatically compared to standard fused silica capillaries [BUR 94].
Recently, a "cyclic" CE system was patented by Hewlett Packard (HP), in which the cycle was assembled out of standard fused silica capillaries [HEW 94].

Table 1.4

		corners / sides	time elapsed	migration distance	voltage accumulated	signal band-width	no. of theoretical plates
cycle 1	phase 1	1	17 s	2 cm	1 kV	93 ms	33,000
	phase 2	2	33 s	4 cm	1.9 kV	132 ms	63,000
	phase 3	3	50 s	6 cm	2.9 kV	161 ms	96,000
	phase 4	4	1:06 min	8 cm	3.8 kV	186 ms	130,000
cycle 2		8	2:15 min	16 cm	7.6 kV	264 ms	254,000
cycle 5		20	5:30 min	40 cm	19 kV	417 ms	638,000
cycle 10		40	11:10 min	80 cm	38 kV	589 ms	1,300,000
cycle 20		80	22:15 min	1.6 m	76 kV	833 ms	2,600,000

Parameter set of synchronized cyclic capillary electrophoresis. Calculation basis: a channel circumference of 8 cm, a voltage applied of 2 kV (where 1.9 kV drops on the separation capillary), an assumed corner effect of 50 µm length, a migration speed of 1.2 mm/s and a diffusion coefficient of $3.3 \cdot 10^{-10}\ m^2 s^{-1}$. Injection, detection volumes and any other bandbrodening effects are neglected [BUR 94].

Chapter 2 Device and Layout

2.1 Device fabrication and preparation

2.1.1 General aspects of micromachining

The production of the planar glass devices used for SCCE is based on micromachining technology. As already mentioned, micromachining refers to the manufacturing of three-dimensional structures in planar substrates using techniques originally developed for the production of integrated circuits in the microelectronics industry. The term micromachining includes a number of different techniques like film deposition, photolithography, etching processes and bonding processes. A typical process for manufacturing microstructures starts with the deposition of a layer of a specific material on the surface of the planar substrate. This film can be a light sensitive film like a photoresist, a metal layer, metal or silicon oxides or a polymer. To perform this coating, a variety of techniques are used, depending on the material deposited. The main techniques are spin coating for photoresists, physical vapor deposition (PVD), chemical vapor deposition (CVD) and sputtering for metallic and other layers. The Langmuir-Blodgett technique can be used for polymers and thermal oxidation for silicon oxides. With these techniques, film thicknesses between a few nanometers to a few micrometers can be obtained [BÜT 91], [MAN 93a].
Photolithography involves the transfer of a given 2-dimensional pattern to a layer of photoresist with subsequent transformation of the pattern into a 3-D structure in the substrate surface. The transfer is performed by imaging a mask which contains the geometric information of the microstructure onto the photoresist, using visible light, UV, X-ray or e-beam. The illumination step may involve methods such as contact-exposure, proximity-exposure or projection-exposure [BÜT 91]. The difference between these three methods is given by the distance between the mask and the substrate. For contact-exposure, there is no gap, whereas for proximity-exposure a distance called "proximity distance" (approx. 10 - 30 µm) is given to avoid mechanical destruction of the photoresist. The advantage of contact-exposure is given in the higher spatial resolution obtainable. Projection-exposure uses an imaging of the mask onto the substrate and therefore is characterized by a larger distance and the use of optical elements like lenses.
For the manufacturing of three dimensional structures, etching steps are necessary. Typical etching methods fall into two categories: wet etching (isotropic and anisotropic) and plasma or dry etching.
The predominant material used in the microelectronics industry remains silicon. Many of the structures fabricated in silicon for non-electronic purposes have moving parts,

as a consequence of its mechanical stability. Micromachining, however, lends itself well to the patterning of a number of different materials, allowing structures for many different applications to be fabricated. Thus, substrates such as fused silica [KOU 95], ceramics [EKS 90], plastics [STA 93], and glass [ALT 63] are becoming complementary materials to silicon. Glass is used as the material for the manufacturing of the SCCE devices because of its good electrical insulating property. Due to the micrometer dimensions required, it is not possible to manufacture these structures using precision machining techniques, and micromachining provides a good alternative. A brief description of the process for micromachining planar glass substrates for CE on chip will be discussed below.

2.1.2 Micromachining procedure for the fabrication of SCCE devices

Micromachined glass devices were fabricated at Baumer IMT, Greifensee, Switzerland, using their proprietary process. The various steps involved in the manufacturing of micro channels in glass are shown schematically in Fig. 2.1. Initially, a well cleaned glass substrate is covered with a metal layer such as chromium using a technique known as chemical vapor deposition (CVD). Afterwards, a layer of photoresist (positive or negative) is deposited on the metal layer by using the spin coating technique. A mask which contains the 2-dimensional geometry of the structure is positioned above the substrate. By illuminating the photoresist through the mask with a light source of a specific wavelength, the layout of the structure is imaged onto the surface of the covered device. The mask used for the production of the structures for this work was made out of ferric oxide. In the case described here, the technique of contact-exposure was chosen. The illumination changes the solubility of the irradiated photoresist. For negative resist, polymerization occurs and therefore only the unexposed areas can be dissolved, in a process known as development of the photoresist. Positive resist, however, becomes soluble after being exposed to the light source. In the fabrication described here, only positive resist is used. After developing the resist, the metal layer is removed by an etching process using an appropriate acid. Now the areas of the glass substrate defined by the mask are accessible for further treatments, which can be carried out after the removal of the photoresist layer.

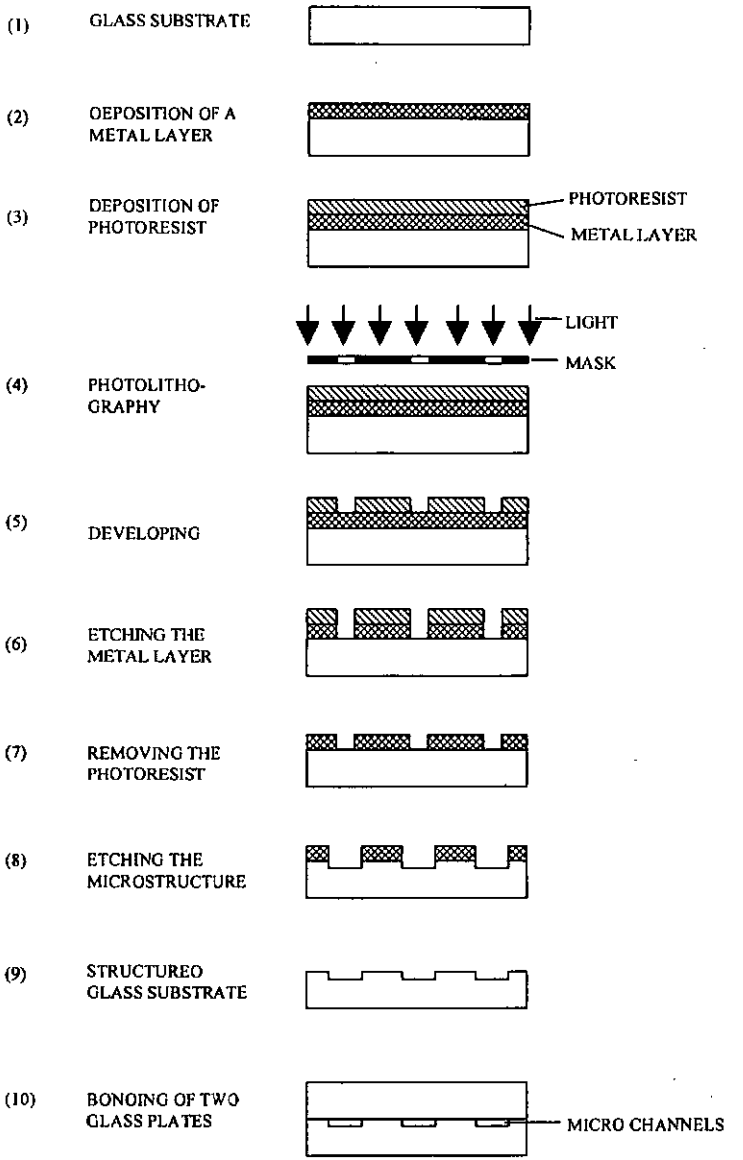

Figure 2.1 A cleaned glass substrate (1) is coated with a metal layer such as chromium (2) and a layer of photoresist (3). Then the device is illuminated through a mask, by a light source so that the micro structures are defined by exposure of the photoresist (4). The resist is developed (5) and oxide is etched (6). After removing the photoresist (7), the micro structures are formed by etching the glass substrate (8), (9). Finally, a second glass plate is thermally bonded on top to serve as a cover plate (10).

Dipping the device into a HF-glycerin solution initiates the etching process of the glass. This method of wet etching amorphous glass is an isotropic process, which means the possible aspect ratios achievable are limited because etching occurs at the same rate in all three directions. This results in the widths of channels being wider than defined by the mask, since the mask is underetched. Note that aspect ratio is defined as the ratio of depth to width of a micro structure. To obtain evenly etched structures, it is important to move the device during the etching process. This ensures that the etching products are removed from the surface, the unused etching solution is able to contact the channel surface, and that the local temperature and concentration gradients reach equilibrium [BÜT 91]. Etching times can vary from seconds to minutes, depending on the type of glass and the required etch depth of the structures. The structures used in this work were made by Baumer IMT, Greifensee, Switzerland. All structures were fabricated from HOYA 4012 SLW 5 glass, which is a type of soda lime glass. The number 40 stands for the size of 4 inch by 4 inch, the 12 stands for the thickness of 0.12 inch (3 mm), and the 5 stands for the planarity of the glass plates, which was chosen to be better than 5μm.
A second glass plate of the same type and smoothness was also provided by this company. These glass plates are used as cover-plates, and had several holes of 1/16" (± 0.1 mm) diameter drilled mechanically through the thickness of the chip.
The choice of glass is important for determination of etching parameters, as the composition of glass can vary significantly from one type to another. Preliminary etching experiments with another type of glass (HOYA SL), a white crown glass, gave roughly shaped structures of poorer quality. A change of the glass type from HOYA SL to HOYA SLW resulted in much better defined structures with much smoother surfaces. The chemical composition of both glass types is given in table 2.1. The choice of glass type was also determined by the detection scheme, which was laser induced fluorescence detection using an Ar^+- ion laser at 488 nm. Therefore, the glass type must be transparent for visible light. Background fluorescence emitted from the glass must be minimal.

Table 2.1

glass-type	SiO_2 %	Al_2O_3 %	CaO %	MgO %	Na_2O %	K_2O %
HOYA SL	72.0	2.0	6.0	3.0	7.0	10.0
HOYA SLW	72.0	2.0	6.0	3.0	16.0	1.0

Chemical composition in percent of two different glass types used for etching experiments. First etching experiments were performed with the HOYA SL type glass and resulted in rough and badly defined structures (see Fig. 2.2). The HOYA SLW was finally used as the material for the fabrication of the structures because of its better etching behavior.

In order to asses the quality of etching, SEM photographs were taken from structures manufactured out of both glass types.

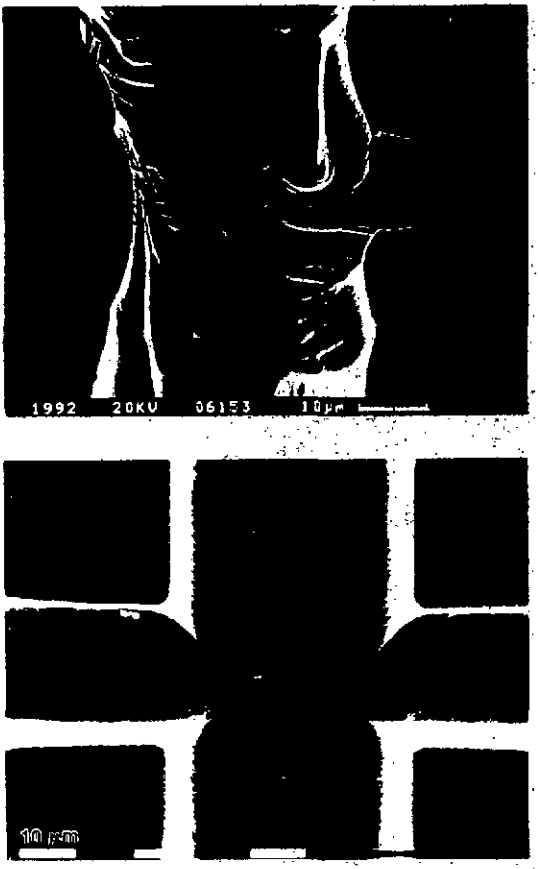

Figure 2.2 SEM photographs taken of the microstructures. Picture (a) shows a T-junction type channel geometry etched into HOYA SL glass type. The nominal dimensions of the main channel are 40 µm (± 4) in width and 10 µm (± 2) in depth. Picture (b) shows a four-way junction manufactured out of HOYA SLW glass. The given dimensions are the same for both structures.

It appears that differences in Na_2O and K_2O content strongly determine etching characteristics of HOYA SL and HOYA SLW glasses. However, this effect was not studied in detail.

2.1.3 Cleaning and bonding of the SCCE device

The final preparation and bonding of the SCCE devices is accomplished in a cleanroom (class 100)* at CIBA-GEIGY, Basel, Switzerland. Before bonding structured and cover glass plates together, they are cleaned using a standard cleaning procedure. This process consists of mechanical and chemical cleaning steps. During mechanical cleaning, the plates are rubbed with a circular motion on a paper tissue (cleanroom type tissues) imbued with cleaning solution. The cleaning solution used for this step was Texclean™ 100, (The Texclean Company, Upper Saddle River, N.J., USA). To remove organic impurities, the two glass plates are placed in acetone (Selectipur ©, particle class 0, E. MERCK, Darmstadt, Germany), and are ultrasonicated for a few minutes. After a rinsing step with ultra pure water and drying, the cover plate is placed on top of the plate containing the structures. Alignment of the holes of the cover plate over the ends of the channels is then performed under a microscope.

The bonding of the glass plates is done in an oven by heating them to the softening point of the glass. The temperature protocol is given in Fig. 2.3.

The softening point of glass is defined as the temperature at which glass sags under its own weight. The surface of the glass is then tacky enough to stick to other glass. For bonding two glass plates together, both glass plates have to be held at this temperature for several minutes. It is important to place the device in the oven such that the holes are not covered, in order to ensure success of the bonding process. This allows the equilibration of the air pressure inside and outside the channels during the heating and cooling processes.

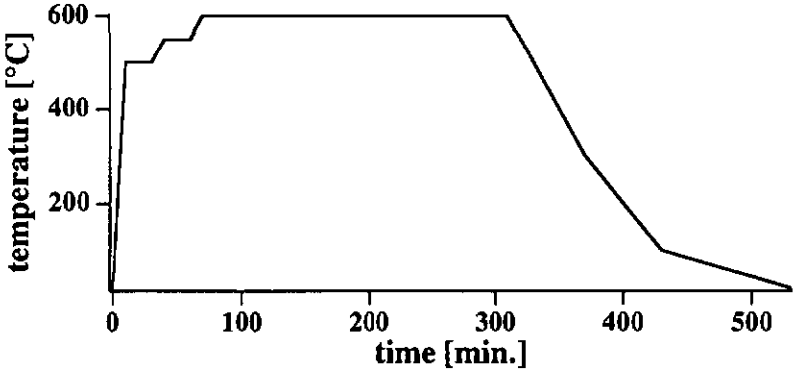

Figure 2.3 Graph of temperature as a function of time for the bonding process of two glass plates (HOYA SLW) used for SCCE.

* class 100 is defined as a maximum number of 100 particles smaller than 0.5 µm per cubic foot air (see also Appendix A3).

After allowing the device to cool down to room temperature overnight, the device is ready for further preparation. The procedure described above is very reliable and gives an overall success rate of more than 90 %. Insufficient bonding is usually due to dirt particles between the two glass plates. Sometimes, an additional bonding process can be performed to complete bonding if the first bonding process was not successful.

2.1.4 Final preparation of the device

The final preparation can be carried out outside the cleanroom in the laboratory. However, care must still be taken to avoid particles entering the channels, as they could subsequently plug them. To use the device for CE experiments, reservoirs for the electrolyte and the sample must be connected to the channels. In our approach, pipette tips, (Gilson pipette tips for Pipetteman ©, yellow, 200 µl), serve as the reservoirs and must be glued into the holes on the top of the device. An epoxy glue, Araldite rapid © (Ciba-Geigy Ltd.), is used, and the glue is allowed to cure overnight. Afterwards, the channels can be filled with electrolyte, gel or sample, for subsequent SCCE experiments.

It is important to arrange the reservoirs and the electrodes in a way that air bubbles generated by electrolysis will not enter the channels. This is done by inserting the electrodes into the open reservoirs from the top and by keeping a distance to the channel entrance.

2.2 Layouts of the structures used for SCCE

In order to build functional models for cyclic capillary electrophoresis, two different layouts for testing the principle of the technique were designed and fabricated. These two layouts are named CYCE2 and CYCE3. The term "CYCE" is used as an abbreviation for cyclic capillary electrophoresis. In the following, the expression "SCCE layouts" refers to these two layouts. Another layout for testing corner effects was designed and fabricated and is named CYCE1. All three different layouts will be described in the following sections.

2.2.1 CYCE1

The layout CYCE1 was originally designed to test the influence of the corner design on the profile of a plug moved around such a corner. Figure 2.4 shows a schematic picture of the layout. Seven different corner designs are manufactured onto one chip. The dimensions and the detailed drawing of the layout for CYCE1 is given in Appendix A6. Due to the fact that this layout was only produced in HOYA SL type glass, which resulted in structures of poor quality (see also section 2.1.2), no experiments were performed with this layout.

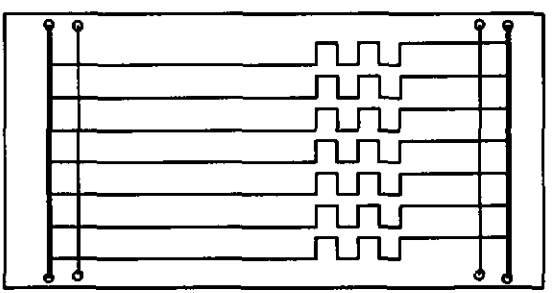

Figure 2.4 Schematic layout of CYCE1. The detailed layout and dimensions of the device are given in Appendix A6.

2.2.2 Geoeral remarks about layouts for SCCE (CYCE2 and CYCE3)

The main principle behind the design of the two SCCE layouts is to have a separation channel (main channel) and several channels serving as inlets and outlets for the electrolyte. The ends of these side channels are connected to solution reservoirs, in which electrodes are immersed for the voltage control. Figure 2.5 shows the schematic arrangement of the channels for both SCCE layouts.

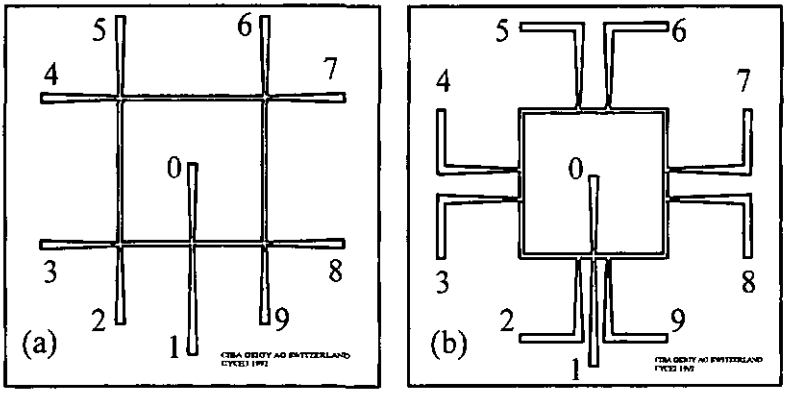

Figure 2.5 Schematic layout of CYCE2 (b) and CYCE3 (a). The main channel consists of four intersecting channels arranged in a square. The ten side channels connect the buffer reservoirs to the main channel. The detailed layout and dimensions of all devices used for this work are given in Appendix A6. The numbers are reservoir numbers referred to in the text.

The reason why a square shaped and not a circular separation channel is used for a "cyclic" CE system has to do with the manufacturing steps of such a device. As mentioned in section 2.1.2, it is necessary to produce a mask for the illumination step (see fig. 2.1 (d)). These masks are usually produced line by line using an X-Y stage. Therefore, it is much easier and more precise to manufacture structures out of rectangular shapes. In principle, it is possible to produce a circular separation capillary as well, however.

As mentioned, the goal of such a system is to move a sample around a cyclic channel system by applying an electrical field. Transport of solution can be achieved simply by switching the locations at which the voltage is applied. Basic considerations about the number of electrodes necessary to obtain cyclic flow leads to a minimum number of three electrodes. Fig. 2.6 shows the schemes for two to seven electrodes. The

arrangement of two electrodes is enclosed because of its use to describe the idea behind the system (see section 1.3.1, Fig. 1.4)

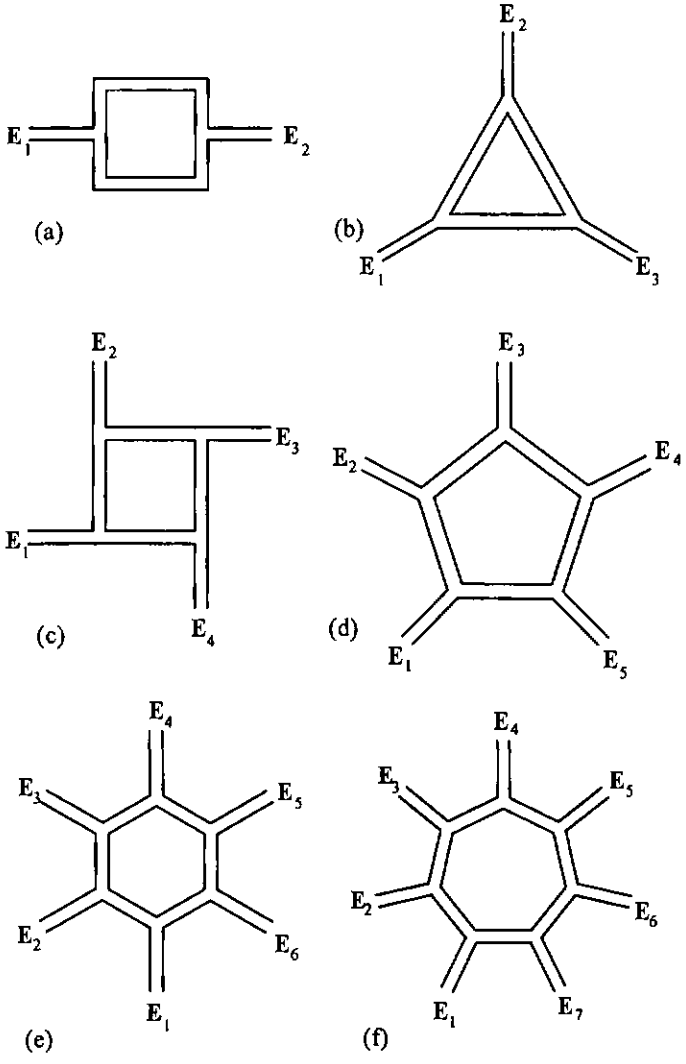

Figure 2.6 Schematic comparison of the number and arrangement of electrodes used for SCCE. The location of each electrode is indicated as capital E at the end of each side channel. The indices are electrode numbers referred to in table 2.4 and 2.5.

Using only two electrodes, it is possible to move the sample back and forth between the two electrodes, but not in a cyclic manner. The sample will always remain within one half of the system between two electrodes. The use of 3 electrodes, which divides the main channel into three parts of the same length, represents an asymmetric approach. This is schematically shown in Fig. 2.6 (b). Applying a voltage between two of the three electrodes will always cause asymmetric electrical fields, since one channel segment between the electrodes is shorter than the other. Different electrical field strengths within the channel will cause different liquid flow-rates in the two segments. To move a sample around the main channel, at least three switching steps are necessary with such a setup. Using five and seven electrode arrangements result in similar systems.

Table 2.2

number of electrodes	2	3	4	5	6	7
usable for SCCE	no	yes	yes	yes	yes	yes
symmetric electrical field possible	yes	no	yes	no	yes	no

Comparison of different numbers of electrodes used for SCCE. Only even numbers of electrodes allow the application of a symmetric electrical field.

Table 2.2 shows the comparison of different numbers of electrodes used for SCCE. This comparison shows that only even numbers of electrodes larger than two results in a symmetrical electric field in combination with the capability to move a sample around the main channel, assuming voltages are applied across the diagonal. The symmetry of the electrical field obtained by the fourfold symmetry leads to a symmetric flow in both halves of the circuit. Of course, the possibility to generate asymmetric electric fields also exists. These arguments holds for higher even numbers of electrodes too.

SCCE device with n side channels

There is a basic concept underlying all voltage switching examples used for SCCE. Assume a cyclic system with n electrodes (n side channels and therefore n T-junctions), where n > 2, and all electrodes (E_i with i=1 to n) can be connected individually to high voltage or ground or can be disconnected (floating). The first step towards achieving cyclic movement is the application of a voltage between two electrodes (E_k, E_m, with $m > k$ and $m, k < n$) in such a way, that there exists at least one electrode E_l with $m > l > k$. The cyclic system is then divided into a section with

$(m-k-1)$ side channels and a section with $(n-(m-k+1)$ side cbannels $(\{n,i,k,l,m,x,sw\} \in \mathrm{N}$, where N is the set of natural numbers $\{1, 2, 3, \ldots\})$. For the sake of simplicity, we assume that the sample of interest is placed between electrodes E_k and E_l, close to electrode E_k, and that the polarity is applied in such a way that the sample moves towards the electrode with the higher index. Applying a voltage between the two electrodes E_k and E_m, the sample will move towards electrode E_m, passing the electrode E_l (which is floating at this stage) and the corresponding side channel. After the sample has passed this intersection, a voltage can be applied between electrode E_l and electrode E_{m+x} where $x = l-k$ (with $x \geq 1$ for $l > k$). The number x determines the number of floating electrodes (side channels) located between the two "driving electrodes" - that is the number of side channels that the sample passes before the next voltage switch occurs. The number x should not change during one loop, which is equal to ensuring that there is always a constant electrical field for the channel section in which the sample is moved at a given time. This switching procedure must be continued until the sample has reached its starting point, completing one cycle.

The number of switching steps necessary to move a sample along a complete cycle can not be calculated in a definite manner. For a selection of given numbers n and x, the number of times the voltage is switched (sw), is given in table 2.3. The data in this table assume that the sample is always moved to a point where no intersection exist between the sample and electrode E, which is equal to the condition $m-l=1$.

Only for even values of n can sw be calculated (under certain conditions, see below) to be

$$sw = round(\frac{n}{x}) \tag{2.1}$$

where n is the number of electrodes (side channels) and x is the number of side channel between electrode E_k and electrode E_l. This equation is valid for all calculated numbers for sw larger than or equal to two. "round" stands in this case for the mathematical function of rounding to the next natural number. For odd numbers of electrodes the number of switches (sw) necessary to move along a complete cycle can not be calculated in a definite way.

Table 2.3

even number of electrodes			odd number of electrodes		
n	x	sw	n	x	sw
4	1	4	3	1	3
4	2	2	5	1	5
6	1	6	5	2	3
6	2	3	5	3	2
6	3	2	7	1	7
6	4	2	7	2	4
8	1	8	7	3	3
8	2	4	7	4	2
8	3	3	7	5	2
8	4	2			
8	5	2			
8	6	2			

Number of switching steps (*sw*) necessary to perform a complete cycle in dependency of the number of side channels (*x*) being between the two electrodes used for the application of the voltage (in the section where the sample is located).

A selection of switching sequences is listed in table 2.4, explaining how to move a sample around a closed loop.

Table 2.4

number of electrodes (n)	3		4		5		6		7	
symmetric switching (ss) asymmetric switching (as)	ss	as	ss	as	ss	as	ss	as	ss	as
switching steps (numbers refer to the indices of the electrodes used in Fig. 2.6)	--	1-3 2-1 3-2	1-3 2-4 3-1 4-2	1-4 3-2	--	1-5 4-3	1-4 3-6 5-2	1-5 4-2	--	1-4 5-7
current used for the separation (%)	--	33	50	25	--	20	50	33	--	43

Examples for the switching procedure for different numbers of electrodes. The numbers used to describe the switching steps refer to the numbers used in Fig. 2.6. The assumed starting point of the sample is always left of electrode E_1. The moving direction is assumed to be clockwise. The order of the electrode numbers refer to their polarity. For all examples the switching time is always the same which is equal to a constant electrical field.

If the switching is performed using five or more electrodes there will be a number of asymmetric swiching procedures possible to move the sample around the structure. Table 2.5 gives the four possible switching procedures for the case of five electrodes.

Table 2.5

number of procedure	(1)	(2)	(3)	(4)
value for x	x=3	x=3	x=2	x=1
switching procedure (electrodes to which the voltage is applied)	1-5 3-2	1-5 4-3	1-4 3-1 5-3	1-3 2-4 3-5 4-1 5-2

All possible switching procedures for the setup with five electrodes: condition: switching time is always the same which is equal to a constant electrical field. Numbers refer to the electrodes used in Fig. 2.6. In all four procedures, the switching time is the same, which is equal to a constant electrical field.

As a result of these considerations a system with n=4 and x=1 was chosen to do the feasibility studies of such a cyclic system. This leads to four switching steps to move a sample around one cycle (sw=4). Using a system with x=1 results in the maximum achievable electrical field for the part of the channel used for the separation. A four side channel system was chosen as this yields symmetric electrical fields, and is in addition easier to manufacture. In practice, eight side channels were used instead of four these side channels are serve as inlets and outlets which is explained below. The resulting pairs of T-junctions (see layout, Appendix A6) are close together and can therefore be treated as single side channels. Therefore, the systems still satisfy the criteria for a four side channel system.

As shown in Fig. 2.5, both SCCE layouts have eight side channels connected to the main channel, and an additional channel crossing the main channel perpendicularly at the midpoint of one side. This channel realizes a four way intersection with the main channel and is used for the injection process (see Fig. 1.6); it is therefore referred to as the injection channel. The dimension of this intersection is 40 by 40 µm in width and 10 µm in depth, resulting in a geometrically defined volume of 16 pL. The eight other channels are used as inlets and outlets to move electrolyte into the main channel as well as out of the channel (see Fig. 1.6). It is necessary to point out that it is important to distinguish between inlet and outlet channels. If a sample was moved out of the

main channel as shown for the components (1) and (3) in Fig. 1.6, it is important to make sure that these components will never enter the main channel again during the next cycles. Therefore, it is necessary to define four of the eight side channels as inlets, and the other four strictly as outlets. This was one of the basic considerations for the design of the two SCCE layouts.

Another consideration in the design was that most of the applied voltage drop should occur over the main channel, with a much smaller voltage drop over the side channels. This is because a higher electrical field strength gives a higher separation efficiency (see eq. 1.25). The electrical resistance of the channels is determined by the geometry of the channels. The dimensions of the side channels were defined to be much larger than the dimensions of the main channel, so that the electrical resistance of these channels was much smaller. Ohm's Law thus dictates a smaller voltage drop over the side channels. For the two SCCE layouts, the relation of the resistance of the side channels to the resistance of one side of the main channel (one quarter of the circumference) was chosen to be 9 for CYCE2 and 10.6 for CYCE3. The exact dimensions of the two SCCE layouts are given in Appendix A6.

The figures in Appendix A6 show a maximum width of 320 µm for the side channels. When specifying these dimensions, it was realized that these large channel widths could cause problems during the bonding process between the structured glass plate and the cover glass plate. As described already in section 2.1.3, the bonding is performed by a softening process of both glass plates. Therefore, there was a risk that the heating process would cause a sagging of the cover plate into the wider parts of the side channels. This would reduce channel dimensions and therefore increase the electrical resistance in an undefined way. To avoid any sagging effects, a vertical wall (out of glass) was left in the channel, designed for the support of the channel ceiling (see Appendix A6).

Due to the small dimensions of the channels, blocking caused by dirt entering the channels must be avoided. The design of the side channels was performed in a conical shape (see Appendix A6), so that both sharp corners and any dead volumes were reduced to a minimum. This results in a reduction of locations within the side channels where dirt or air bubbles could collect.

The layouts CYCE2 and CYCE3 were fabricated out of HOYA SLW type glass, whereas the layout CYCE1 was only fabricated out of HOYA SL type glass. The size of the glass wafer used was 4" * 4" (10.16 cm * 10.16 cm). Therefore, the outer dimensions of the two layouts CYCE2 and CYCE3 were chosen to be 2" * 2" (5.08 cm * 5.08 cm). This was done so that four layouts fit onto one substrate. Only one etching step was required for all four devices, since all channel depths are the same. Layout CYCE1 has the outer dimensions of 2" * 4", which allows the fabrication of

two structured glass plates per etching step. The thickness of a single glass plate was chosen to be 0.12" (3 mm). This results in a total thickness of the bonded device of 0.24" (6.1 mm). To make the cover glass plates interchangeable, the layouts of CYCE2 and CYCE3 were designed in such a way that the ends of the channels on both devices are superimposable. This makes it possible to use the cover plate with the ten holes for both SCCE layouts. Besides flexibility, the longer delivery time for the cover plates than for the etched glass plates was an additional reason for making them all the same. Because the holes were drilled mechanically, a lower output rate for the cover plates than for the etched glass plates was obtained. Design simplification was thus useful in avoiding long delays in the experimentation process.

2.2.3 CYCE2

CYCE2 has eight side channels connected to the main channel (two side channels to each side of the main channel), and an additional channel crossing the main channel perpendicularly at the midpoint of one side. Four high voltage power supplies are required to achieve cyclic transport of the sample. In contrast to the layout of CYCE3, the intersections between the side channels and the main channels were designed in the form of a T-junction. This was done to lower the loss of sample due to so-called "corner-loss". This "corner loss" will be described in more detail in chapter 5.1.4. The volume of the whole main channel can be calculated as 32 nl. One of the side channels has a volume of 21 nl The two injection channels are different in length. The one directed toward the center of the chip has a length of 10 mm. The outer injection channel is 2 mm longer. Their volumes are 13 nl and 19 nl, respectively.

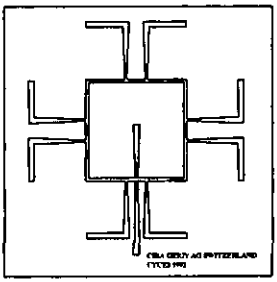

Figure 2.7 Schematic layout of CYCE2. The detailed layout and dimensions of all devices used for this work are given in Appendix A6.

2.2.4 CYCE3

The most obvious layout for a structure used for cyclic CE was realized in the design of CYCE3. Four channels arranged in a square result in a square shaped separation channel and eight side channels. As for the layout CYCE2, four high voltage power supplies are required to achieve cyclic motion of the sample too. The volume of the whole main channel can be calculated as 32 nl which is the same value as for CYCE2. Each side channel has a volume of 23 nl. The two injection channels have the same length and volumes as for CYCE2.

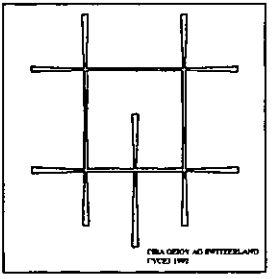

Figure 2.8 Schematic layout of CYCE3. The detailed layout and dimensions of all devices used for this work are given in Appendix A6.

The switching procedure for layout CYCE3 is different to that used for CYCE2. Both procedures are given in section 4.3.2. The side channels of CYCE3 combine to pairs of channels connecting the main channel at the corner. These pairs can be treated as one side channel since they intersect each other precisely at the location where each joins the main channel. Therefore, this layout should be considered as one with four side channels.

Chapter 3 Theory

3.1 Theoretical background of SCCE

3.1.1 General remarks about the theory behind SCCE

This section describes the theoretical considerations involved in SCCE, with some reference to the general theory of capillary electrophoresis (CE) already described in chapter 1. The theory behind the cyclic CE system can be divided into sections, some of which can be described as advantages of the system, some as disadvantages of the system. The general advantages for miniaturizing a CE system and integrating it onto a planar microstructure arise from the shorter migration time, the increase of separation efficiency, the precision of the injected sample volume and the reduction of sample consumption which can be achieved. These topics have already been described in section 1.2.4 and listed in table 1.1. The specific properties of the SCCE principle as an ideal separation system will be dealt with in the following sections.

3.1.2 The separation efficiency of SCCE

As already explained in section 1.1.4 the efficiency of a CE system depends on the achievable *number of theoretical plates, N*. This number in turn depends on the length of the capillary and the applied electrical field.

infinite capillary

As shown already in figure 1.6, the SCCE system makes possible the simulation of a capillary with an infinite length. Therefore, the sample can be moved as long as it is necessary to perform a separation of interest. This is an advantage in comparison to standard CE, where capillaries of a given effective length are used, resulting in a physical limitation for a separation (see also section 1.3.1, the idea of SCCE).

high number of theoretical plates

For a given electrical field, the number of theoretical plates obtainable in a standard CE system is directly proportional to the length of the capillary used. With Eq. 1.1 and 1.12, 1.10 can be transformed to 3.1:

$$\vec{v}_{tot} = \mu_{tot} \cdot \vec{E} \qquad (1.1)$$

$$\sigma^2_{diff} = 2Dt \tag{1.12}$$

$$N = \frac{L_d^2}{\sigma^2_{tot}} \tag{1.10}$$

$\Leftrightarrow$

$$N = \frac{\mu_{tot} \cdot E}{2D} \cdot L \tag{3.1}$$

With ($\mu_{tot} = \mu_{ep} + \mu_{eo}$) the total mobility, E the electric field, and D the diffusion constant, Equation 3.1 shows that the "infinite" capillary in combination with a constant electrical field makes it possible to achieve very high plate numbers. A calculated example is shown as a graph in Figure 3.1.

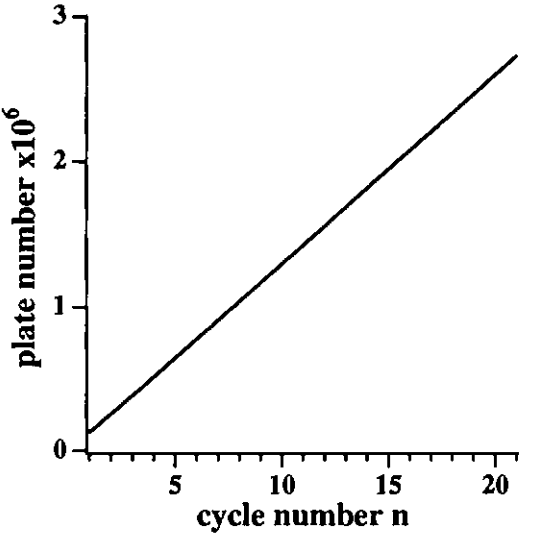

Figure 3.1 This graph shows the linear dependence of the number of theoretical plates N, on the length of the capillary, assuming a constant electric field. Values used for the calculation are: $D = 10^{-10}$ m²/Vs, $E = 1'000$ V/cm, $\mu_{tot} = 3.25 \cdot 10^{-4}$ m²/Vs. Only axial diffusion (in the direction of flow) is assumed in this case, and all constant contributions to the bandbroadening, such as injection, detection and others, (see section 1.1.4) are neglected.

voltage accumulation

On its way around one cycle, a component of interest is exposed to a voltage which corresponds to twice the voltage applied. For n cycles, this value rises to 2n of the voltage applied. Thus, the possibility exists to increase the value of N/U (number of theoretical plates per volt) dramatically compared to standard fused silica capillaries. A sample moved around ten times while 5'000 Volts are applied (which corresponds to an electric field strength of approximately 1'000 V/cm) can be theoretically compared to a sample moved along an 80 cm long standard capillary with 80'000 Volt applied.

3.2 Detection window

3.2.1 The focusing effect of SCCE

Moving a sample consisting of different components with different mobilities around the SCCE system makes it necessary to synchronize the switching frequency to the mobility of one of the components. All other components will be moved out of the system during the cycling (see section 1.3.2 Fig. 1.6 component 1 and 3) at some point, depending on their relative mobilities. The possibility to synchronize the switching frequency of the voltage applied to the different sets of electrodes (see section 1.3.2, realization and principle of SCCE) results in a "focusing effect" to a certain electrophoretic mobility. This focusing effect can be described in detail by defining a *given time window* (GTW), which answers the question of which sample components find themselves in a given section of the main channel together with the component of interest at a given time t. This time , t, is the time required for the component of interest to reach a certain point in the separation channel, and dictates when the voltage is switched. In other words, t is the synchronisation time.

3.2.2 General remarks

definitions and general remarks

Before going into a more detailed discussion about the given time window, it is necessary to define the terms used to describe the GTW.

$L_{synch.}$: the location in terms of length within the separation channel where the component to which the system is synchronized is located when a voltage switching occurs.

L_{max}: the location in terms of length within the separation channel which a faster sample component (to which the system is not synchronized) can move without moving out of the main channel (and out of the window).

L_{min}: the location in terms of length within the separation channel up to which a slower sample component (to which the system is not synchronized) must reach in order to remain within the section of interest.

$v_{synch.}$: the velocity of the component to which the system is synchronized.

v_{max}: the velocity of a component to reach L_{max}.

v_{min}: the velocity of a component to reach L_{min}.

$\mu_{synch.}$, μ_{max} and μ_{min}: mobilities corresponding to $v_{synch.}$, v_{max} and v_{min}.

$t_{synch.}$: the synchronisation time (or voltage switching time)

The GTW or detection window can be defined by using values for the relative mobilities. The "upper limit" is given by μ_{max} normalized by $\mu_{synch.}$, or $\mu_{max}/\mu_{synch.}$; similarly, the "lower limit" is given by $\mu_{min}/\mu_{synch.}$. Equation 3.3 shows that the relative mobilities can be calculated using the values for L_{max} and L_{min}. Starting with Equation. 1.1, and assuming a constant voltage, the following relations are valid:

$$\vec{v}_i = \mu_i \cdot \vec{E} \tag{1.1}$$

with

$$E = \frac{V}{L}$$

$$\frac{L_{max}}{L_{synch.}} = \frac{v_{max}}{v_{synch.}} = \frac{\mu_{max}}{\mu_{synch.}} \tag{3.2}$$

and

$$\frac{L_{min}}{L_{synch.}} = \frac{v_{min}}{v_{synch.}} = \frac{\mu_{min}}{\mu_{synch.}} \tag{3.3}$$

The GTW or detection windows for both cyclic layouts can be represented in a graph as relative mobility as a function of the switching phase.

For the determination of any detection window, it is necessary to distinguish between the two cyclic layouts, CYCE2 and CYCE3. The differences in the detection windows for the two cyclic layouts arises from differences in the arrangement of side channels.

3.2.3 The given time window (GTW)

a) CYCE3

In terms of detection window, layout CYCE3 is easier to describe than CYCE2. This is a result of two conditions dictated by the layout of CYCE2:

1) the requirement of maintaining a constant electric field in all sections of the main channel within all switching phases

2) the requirement to define all reservoirs as either inlets or outlets - a single reservoir cannot serve as both

As already defined above, the GTW determines the components remaining within a section of the main channel where the component of interest is located at a given time, t, where t is the synchronisation time, $t_{synch.}$. The GTW can be expressed in terms of the maximum and minimum distances a sample component could or should travel within one switching interval to remain within the section of the separation channel containing the component of interest. This is illustrated in Fig. 3.2.

This Figure shows the first four voltage switching steps (phase 1-4) which together describes one complete cycle. For layout CYCE3, it is assumed that the component of interest is at the midpoint of the corresponding side of the square-shaped separation channel (see Fig. 3.2) when a voltage switch occurs, as indicated by the X.

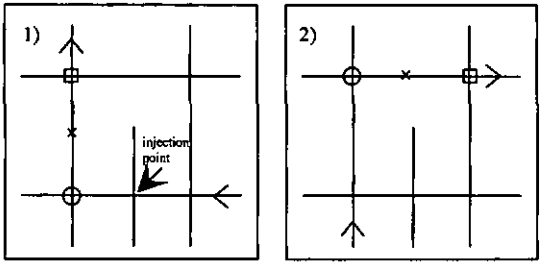

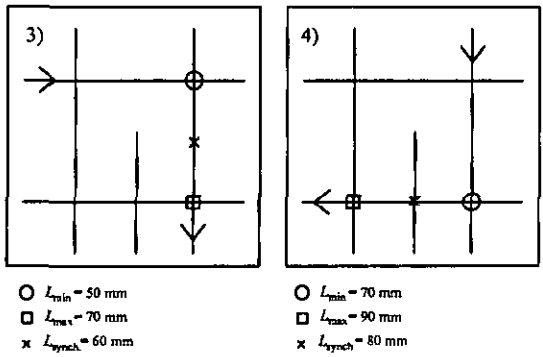

Figure 3.2 The initial four switching steps are schematically shown. The arrows indicate the direction of buffer flow. One side of the main channel is 20 mm in length. The X determines the location of the component to which the system is synchronized. A more detailed description of this figure is given in the text.

As shown in Fig. 3.2, it is possible to determine L_{max} and L_{min} for each phase of the cycle. In phase 1 (Fig. 3.2 ①), the slowest component indicated by a circle must have just passed the lower left corner of the main channel by the time the component of interest has reached the X, to stay within the GTW. This yields L_{min} = 10 mm. For the fastest component indicated by a square, the maximum travel distance allowed without leaving the main channel is given by L_{max} = 30 mm. This value is equal to the condition that the fastest component should not pass the intersection at the upper left corner of the main channel.

The second phase (Fig. 3.2 ②) illustrates the GTW after the first voltage switch has occurred. The electrodes to which the voltage is applied have changed, so that two other side channels serve as inlets and outlets for the buffer flow. The conditions for L_{max} and L_{min} can be determined in the same way as in phase 1.

The difference between L_{max} and L_{min} is always constant for all four phases. Table 3.1 gives the values for L_{max}, L_{min} and $L_{synch.}$ and the relative values for the first seven phases:

Table 3.1

phase	L_{min} in mm	L_{max} in mm	$L_{synch.}$ in mm	$L_{min}/L_{synch.}$	$L_{max}/L_{synch.}$
1	10	30	20	10/20	30/20
2	30	50	40	30/40	50/40
3	50	70	60	50/60	70/60
4	70	90	80	70/80	90/80
5	90	110	100	90/100	110/100
6	110	130	120	100/120	130/120
7	130	150	140	130/140	150/140

Values of L_{max}, L_{min} and $L_{synch.}$ determining the given time window, GTW, for the first seven switching phases for layout CYCE3. The first four switching phases are shown in figure 3.2.

Using the numbers for the relative length given in Table 3.1, it is possible to determine a general formula for the GTW. The formulas for the GTW for layout CYCE3 are:

$$\frac{L_{min}}{L_{synch.}} = \frac{1+(i-1)\cdot 2}{2+(i-1)\cdot 2} = \frac{\mu_{min}}{\mu_{synch.}} \tag{3.4}$$

$$\frac{L_{max}}{L_{synch.}} = \frac{3+(i-1)\cdot 2}{2+(i-1)\cdot 2} = \frac{\mu_{max}}{\mu_{synch.}} \tag{3.5}$$

where i determines the phase number with $i = 1, 2, 3, \ldots$.

The graph illustrating the GTW for CYCE3 is shown in Figure 3.4 (a).

b) CYCE2

To determine the GTW for the cyclic structure CYCE2, the question arises again regarding which location the fastest component is allowed to reach (or must the slowest component reach) within one switching interval, to stay within the section of the separation channel where the sample of interest is located.
For the cyclic structure CYCE2, the length of the section of separation channel in which the component of interest is located varies within the four switching phases.

This is a result of the above mentioned requirements.

1) the requirement of maintaining a constant electric field in all sections of the main channel within all switching phases

2) the requirement to define all reservoirs as either inlets or outlets - a single reservoir cannot serve as both

For a more complete discussion of the operation of the switching steps for CYCE2 the reader is referred to section 4.3.3.

Figure 3.3 shows again the first four switching steps resulting in one complete cycle.

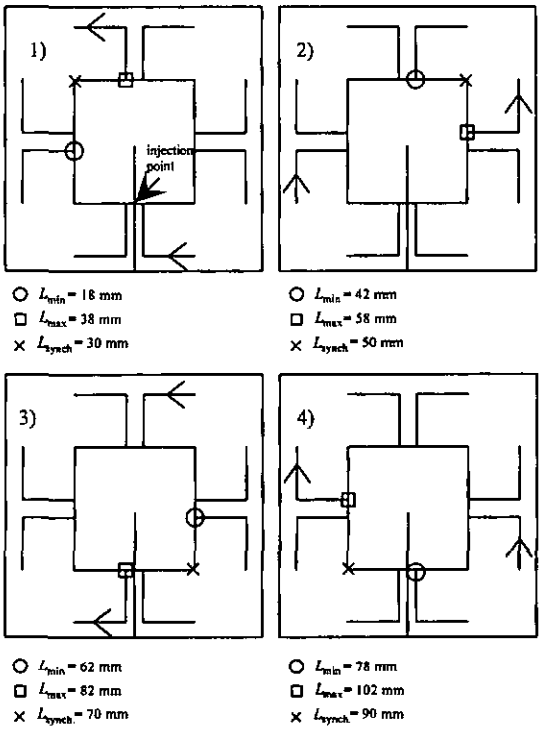

Figure 3.3 The initial four switching steps are shown schematically. The arrows indicates the direction of buffer flow. One side of the main channel is 20 mm in length. The X determines the location of the component to which the system is synchronized. The distance between two neighboring T-junctions is 4 mm. A more detailed description of this figure is given in the text.

For layout CYCE2, it is necessary to avoid any voltage switching if the sample of interest is close to a side channel intersection, as sample could be lost. Therefore, the

voltage switching is performed when the component of interest is at the corner of the separation channel, as indicated by the X in Fig. 3.3 Note that an *initial offset time* must be included in phase 1 of the first cycle to allow the component of interest to travel the extra distance from the point of injection to the first corner.
In Figure 3.3, as in Fig. 3.2, the slowest component staying within the GTW is indicated by a circle, whereas the fastest component is indicated by a square. The duration of the first phase is longer than phases 2 to 4 because of the above mentioned initial offset time. This has no influence on the following phases.
During phase 1, the slowest component has to pass the first side channel intersection at the left side of the square shaped separation channel (this side channel is used as a buffer inlet during phase 2). This condition is equivalent to a value for L_{min} of 18 mm. It should be noted at this stage that the distance between two side channel intersections along one side of the main channel is 4 mm. The fastest component should not move further than 38 mm during the first phase to stay within the GTW. The situation after the first voltage switching has occurred is shown in Fig. 3.3 ②. Again, we can determine the values for L_{min} and L_{max} to be 42 mm and 58 mm. The conditions for L_{max} and L_{min} for the following phases can be similarly determined. The GTW for CYCE2 can therefore expressed by an upper limit and a lower limit given by the relative values of L_{min} over $L_{synch.}$ and L_{max} over $L_{synch.}$. Table 3.2 gives the values for L_{max}, L_{min} and $L_{synch.}$ and the relative values for the first seven phases:

Table 3.2

phase	L_{min} in mm	L_{max} in mm	$L_{synch.}$ in mm	$L_{min}/L_{synch.}$	$L_{max}/L_{synch.}$
1	18	38	30	18/30	38/30
2	42	58	50	42/50	58/50
3	62	82	70	62/70	82/70
4	78	102	90	78/90	102/90
5	98	118	110	98/110	118/110
6	122	138	130	122/130	138/130
7	142	162	150	142/150	162/150

Values of L_{max}, L_{min} and $L_{synch.}$ determining the given time window for the first seven switching phases. The first four switching phases are shown in figure 3.2.

It is important to stress that the differences between L_{max} and L_{min} vary within the four different phases necessary to perform a whole cycle. This results in the need to distinguish between the four phases and therefore leads to four different formulas to describe the GTW of CYCE2. Using the numbers for the relative length given in Table 3.2, it was possible to determine general formulas for the description of the GTW. These formulas for the GTW for layout CYCE2 are given in Table 3.3:

Table 3.3

switching phase	$\frac{L_{min}}{L_{synch.}}$	$\frac{L_{max}}{L_{synch.}}$
$j.1$	$\frac{18+j\cdot 80}{30+j\cdot 80}$	$\frac{38+j\cdot 80}{30+j\cdot 80}$
$j.2$	$\frac{42+j\cdot 80}{50+j\cdot 80}$	$\frac{58+j\cdot 80}{50+j\cdot 80}$
$j.3$	$\frac{62+j\cdot 80}{70+j\cdot 80}$	$\frac{82+j\cdot 80}{70+j\cdot 80}$
$j.4$	$\frac{78+j\cdot 80}{90+j\cdot 80}$	$\frac{102+j\cdot 80}{90+j\cdot 80}$

Formulas for the *given time window* for the layout CYCE2. The variable j determines the cycle number ($j = 0, 1, 2, ...$) (in contrast to Table 3.1 where i determines the phase number!). These formulas are valid for the condition that the component of interest is located at the corner when a voltage switch occurs.

The graph of the two GTW for CYCE2 is shown in Figure 3.4 (b).
The given time window for CYCE2 is determined by the second switching phase because there the possible length of the part of the separation channel in which the component of interest is located has a local minimum.
Figure 3.4 illustrates what is called the "focusing effect" of the synchronized cyclic capillary electrophoresis system. As shown, the detection window narrows increasingly over the number of cycles performed This results in a "focusing" to the specific mobility to which the system is synchronized, to the exclusion of all other mobilities.

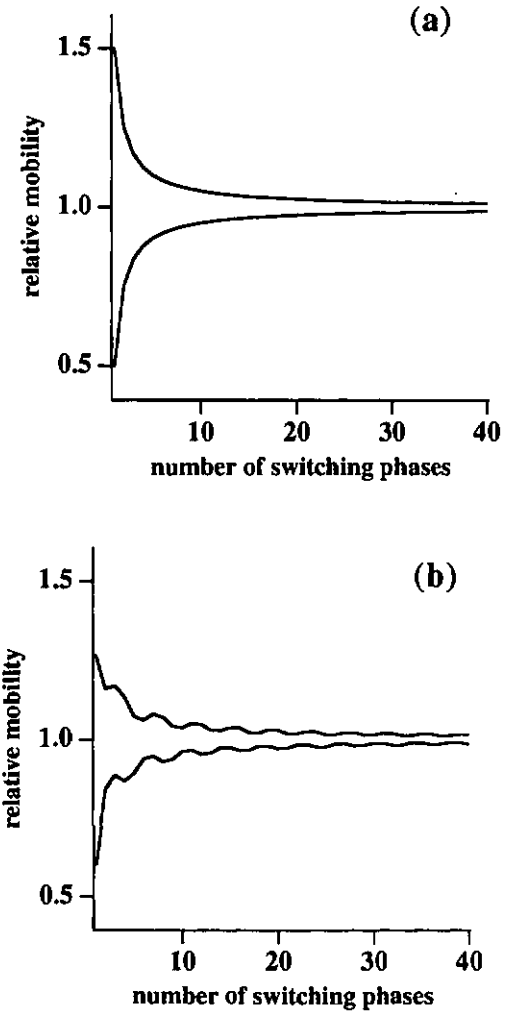

Figure 3.4 The *given time window* for CYCE3 and CYCE2 in terms of relative mobility as a function of switching phase. The GTW for CYCE3 is shown on the left-hand side (a) whereas the GTW for CYCE2 is shown at the right-hand side of this figure (b). This illustrates the so called focusing effect.

3.2.4 Complete description of the mobility window: "splitting effect"

The term "splitting effect" describes the filter-like property of SCCE systems already alluded to in Fig. 1.6, section 1.3.3. This effect arises during the cycling process, when the voltage switching sequence dictates that components having mobilities too large or too small to remain within the GTW are split off from the main sample (to which the system is synchronized) in each phase. The slowest components are subsequently transported in a direction opposite to that of the main sample in following phases. The fastest components are subsequently transported out of the system. It is of basic interest to know if the slower components can ever enter the detection window again during later switching phases. To answer this question, it is necessary to observe all portions of the sample split off at any time during the cyclic movement. An approach to solving this problem involves establishing the "mobility band" over the first few phases and checking for any regularities.

It is assumed that the injection of a sample consisting of an infinite number of different components with mobilities ranging from 0 to infinity is being considered. If any splitting occurs, we have to observe the portion split off as well until it is transported out of the main channel. Again, we have to distinguish between CYCE2 and CYCE3 due to their different geometries.

CYCE3

The description of this experiment of thought is easier for structure CYCE3. Voltage switching occurs always when the sample component to which the system is synchronized is at the midpoint of a side of the square shaped main channel. It is possible to distinguish three parts of the "mobility band" generated through the splitting effect:

1) the part of the mobility band split off from the rest of the sample and moving in the opposite direction (this part is always characterized by mobilities smaller than $\mu_{synch.}$)

2) the part of the mobility band staying within the detection window (this is equal to the GTW defined above).

3) the part of the mobility band with $\mu > \mu_{synch.}$ moving out of the separation channel during each phase

Figure 3.5 shows a simulation of an experiment on CYCE3, demonstrating the "splitting effect". It is assumed that a sample consisting of an infinite number of components with mobilities ranging from 0 to infinity is injected into the SCCE system CYCE3.

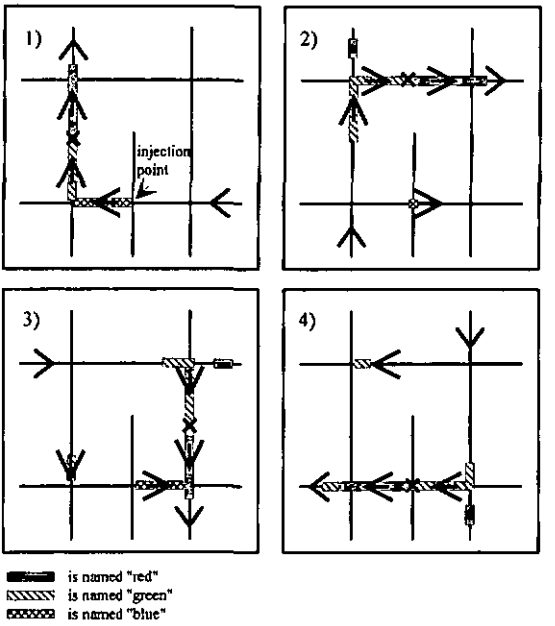

Figure 3.5 The initial four switching steps are shown schematically for layout CYCE3. The sample is assumed to consist of an infinite number of different components with mobilities ranging from 0 to infinity (comparable to a "mobility band"). The arrows indicate the direction of buffer flow. One side of the main channel is 20 mm in length. The X determines the location of the component to which the system is synchronized. A more detailed description of this figure is given in the text. The different sections of the mobility band are hatched but denoted by different colours, in order to simplify explanation.

As already explained for the GTW case, there is a part of the mobility band which stays in the system. For phase 1, this is indicated with red and green color. The green zone contains components with $\mu < \mu_{synch.}$, whereas the red zone contains components with $\mu > \mu_{synch.}$. Both of these mobility intervals will reach the next phase without leaving the system. All components with mobilities high enough to pass the upper left corner will leave the system during phase 1 and flow to waste. The blue colored mobility interval consists of mobilities which are too slow to remain in the GTW. Therefore, the corresponding components have not passed the lower left corner and remain within this part of the cyclic system.

During phase 2, the green part of the mobility band partially passes the upper left corner of the structure, and is therefore split into two parts upon the voltage switch between phase 2 and phase 3. One part moves within the GTW, whereas the part which has not passed the upper left corner during phase 2 is carried in the opposite direction during phase 3. This part will be moved out of the system for good at the lower left corner during phase 4.

The voltage switch from phase 3 to phase 4 again causes a splitting off of a segment of the green colored mobility band, which will be moved out at the upper left corner during phase 5 (this is not shown in Fig. 3.5).

Using distances normalized by the distance travelled by the component having $\mu_{synch.}$, it is possible to develop formulas for the description of the mobility band for the first 6 phases. These formulas for layout CYCE3 are given in Table 3.4:

Table 3.4

end of phase i	segment split off	staying in GTW	leaving during phase
i=1	$0 < \mu < \frac{10}{20}\mu_0$	$\frac{10}{20}\mu_0 < \mu < \frac{30}{20}\mu_0$	$\mu > \frac{30}{20}\mu_0$
i=2	$\frac{10}{20}\mu_0 < \mu < \frac{30}{40}\mu_0$	$\frac{30}{40}\mu_0 < \mu < \frac{50}{40}\mu_0$	$\mu > \frac{50}{40}\mu_0$
i=3	$\frac{30}{40}\mu_0 < \mu < \frac{50}{60}\mu_0$	$\frac{50}{60}\mu_0 < \mu < \frac{70}{60}\mu_0$	$\mu > \frac{70}{60}\mu_0$
i=4	$\frac{50}{60}\mu_0 < \mu < \frac{70}{80}\mu_0$	$\frac{70}{80}\mu_0 < \mu < \frac{90}{80}\mu_0$	$\mu > \frac{90}{80}\mu_0$ and the segment split off during phase 2
i=5	$\frac{70}{80}\mu_0 < \mu < \frac{90}{100}\mu_0$	$\frac{90}{100}\mu_0 < \mu < \frac{110}{120}\mu_0$	$\mu > \frac{110}{100}\mu_0$ and the segment split off during phase 3
i=6	$\frac{90}{100}\mu_0 < \mu < \frac{110}{120}\mu_0$	$\frac{110}{120}\mu_0 < \mu < \frac{130}{120}\mu_0$	$\mu > \frac{130}{120}\mu_0$ and the segment split off during phase 4
...	...	...	...

This table considers all sample segments generated by splitting off sample components during various phases for layout CYCE3. The segment within the first column (besides for i=1, see text below) will be moved out of the system two phases later (phase = i + 2). The part given in the right most column is moved out during the ith phase. Note that $\mu_0 = \mu_{synch.}$

1) segment split off

The sample portion split off during the switch between phase 1 and 2 is different from all other splitting events. As was already explained for the GTW, the condition for a component to stay within the GTW is that it pass at least the lower left corner (see Fig. 3.3) during the first switching phase. All components within the mobility interval $0 > \mu > \frac{1}{2}\mu_{synch.}$ which have not passed this corner will remain within this side of the main channel for all (!) subsequent switching steps. This is because the direction of buffer flow is reversed during phase 2 and 3 in this channel segment, leading to a movement of the split mobility band towards the lower right-hand corner. However, none of the components will pass this corner during pbase 2 and 3. During phases 4 and 5, the flow direction is reversed again, which results finally in oscillation of this mobility band about the injection point.

All other split segments shown in the left-most column of table 3.4 will be moved out of the system two switching steps later. Therefore, no split off part will move back into the detection window again.

2) part of the mobility band staying within the detection window
This part was already described in the section about the GTW and is equal to that.

3) part of the mobility band moving out during the corresponding phase
This part is equal to the upper limit of the GTW. Therefore, the GTW describes this case too.

Finally, it is possible to give a general formula for each of the three cases resulting from the "splitting effect" which describes the corresponding mobility interval for any phase *i*:

Table 3.5

segment split off during phase *i*	staying in GTW during phase *i*	leaving during phase *i*
$\frac{2i-3}{2i-2}\mu_0 < \mu < \frac{2i-1}{2i}\mu_0$ for $i > 1$	$\frac{2i-1}{2i}\mu_0 < \mu < \frac{2i+1}{2i}\mu_0$ for $i > 0$	$\mu > \frac{2i+1}{2i}\mu_0$ for $i > 0$ and the segment split off during phase $(i\text{-}2)$ for $i > 3$

Formulas describing the dependence of the three different segments of the mobility band (consisting of an infinite number of different components with mobilities ranging from 0 to infinity) on the phase number, *i*.

CYCE2
The same theoretical analysis can be made for the structure CYCE2. As in the case for the GTW, it is necessary to distinguish between the four switching phases. Again, we can distinguish three different mobility band sections during the cycling of an infinite number of different components with mobilities ranging from 0 to infinity. For CYCE2, we assume that the switching occurs when the sample of interest is located at the corner of the separation channel. Therefore, it is necessary to add an initial offset time to the duration of the first switching phase, to allow the analyte of interest to

travel the extra distance between the injection point and the first corner. This was considered for the formulas given below.
As in the CYCE3 case, three distinct sections of the mobility band are generated by the "splitting effect".
Figure 3.6 shows a simulation of an experiment with CYCE2. It is assumed that a sample consisting out of an infinite number of components with mobilities ranging from 0 to infinity is injected into the SCCE system CYCE2.

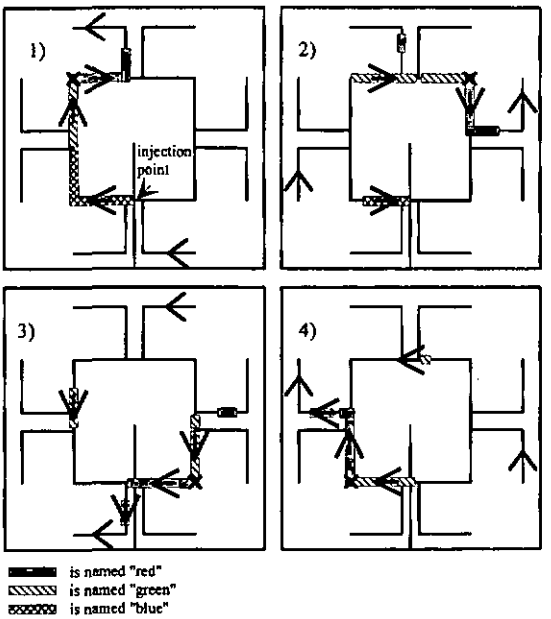

Figure 3.6 The initial four switching steps are shown schematically for layout CYCE2. The sample is assumed to consist of an infinite number of different components with mobilities ranging from 0 to infinity (otherwise known as the "mobility band"). The arrows indicate the direction of buffer flow. One side of the main channel is 20 mm in length. The X determines the location of the component to which the system is synchronized. A more detailed description of this figure is given in the text. The different sections of the mobility band are hatched but denoted by different colours, in order to simplify explanation.

As already explained for the GTW, there is a part of the mobility band which remains in the system. For phase 1, this is indicated with red and green. Again, the green zone contains components with $\mu < \mu_{synch.}$, whereas the red zone contains components with $\mu > \mu_{synch.}$. Both mobility intervals continue to the next phase without leaving the system. All components with mobilities high enough to pass the upper left-hand side channel intersection will leave the system during phase 1 through this side channel. The blue colored mobility interval containing the slowest moving components has not passed the lower left-hand side channel intersection and is moved backwards during phase 2. Observing the behavior of this mobility interval (blue) during phases 2 and 3, it can be seen that this segment will leave the system during phase 3.

During phase 2, the green part of the mobility band partially passes the upper left-hand side channel intersection. It is therefore split into two segments when the voltage is switched between phase 2 and phase 3. One segment continues on to the GTW of phase 3, whereas the segment which has not passed the upper left-hand side channel intersection during phase 2 reverses its direction. This segment will be moved out at the upper left-hand side channel during phase 4.

The voltage switch from phase 3 to phase 4 again causes a splitting of a segment of the green colored mobility band, which will be moved out through the upper left-hand side channel during phase 5 (this is not shown in Fig. 3.6).

Using distances normalized by the distance travelled by the component having $\mu_{synch.}$, it is possible to determine formulas for the description of the mobility band for the first 6 phases. These formulas for layout CYCE2 are given in Table 3.6:

Table 3.6

end of phase i	segment split off	staying in GTW	leaving during phase
i=1	$0 < \mu < \frac{18 \cdot 2}{3 \cdot 20}\mu_0$	$\frac{18 \cdot 2}{3 \cdot 20}\mu_0 < \mu < \frac{38 \cdot 2}{3 \cdot 20}\mu_0$	$\mu > \frac{38 \cdot 2}{3 \cdot 20}\mu_0$
i=2	$\frac{18 \cdot 2}{3 \cdot 20}\mu_0 < \mu < \frac{42 \cdot 2}{5 \cdot 20}\mu_0$	$\frac{42 \cdot 2}{5 \cdot 20}\mu_0 < \mu < \frac{58 \cdot 2}{5 \cdot 20}\mu_0$	$\mu > \frac{58 \cdot 2}{5 \cdot 20}\mu_0$
i=3	$\frac{42 \cdot 2}{5 \cdot 20}\mu_0 < \mu < \frac{62 \cdot 2}{7 \cdot 20}\mu_0$	$\frac{62 \cdot 2}{7 \cdot 20}\mu_0 < \mu < \frac{82 \cdot 2}{7 \cdot 20}\mu_0$	$\mu > \frac{82 \cdot 2}{7 \cdot 20}\mu_0$ and the segment split off during phase 1
i=4	no segment split off	$\frac{62 \cdot 2}{7 \cdot 20}\mu_0 < \mu < \frac{102 \cdot 2}{9 \cdot 20}\mu_0$	$\mu > \frac{102 \cdot 2}{9 \cdot 20}\mu_0$ and the segment split off during phase 2
i=5	$\frac{62 \cdot 2}{7 \cdot 20}\mu_0 < \mu < \frac{98 \cdot 2}{11 \cdot 20}\mu_0$	$\frac{98 \cdot 2}{11 \cdot 20}\mu_0 < \mu < \frac{118 \cdot 2}{11 \cdot 20}\mu_0$	$\mu > \frac{118 \cdot 2}{11 \cdot 20}\mu_0$ and the segment split off during phase 3
i=6	$\frac{98 \cdot 2}{11 \cdot 20}\mu_0 < \mu < \frac{122 \cdot 2}{13 \cdot 20}\mu_0$	$\frac{122 \cdot 2}{13 \cdot 20}\mu_0 < \mu < \frac{138 \cdot 2}{13 \cdot 20}\mu_0$	$\mu > \frac{138 \cdot 2}{13 \cdot 20}\mu_0$
...	...	...	...

This table considers all sample segments generated by the "splitting effect" during the switching sequence for layout CYCE2. The segments within the first column will be moved out of the system two phases later (phase $i + 2$). The segment given in the right most column is moved out during phase i. Note that $\mu_0 = \mu_{synch.}$

In contrast to layout CYCE3, there is no segment oscillating within any part of the separation channel. This means that the GTW really determines the detection window for CYCE2. The characteristic property of structure CYCE2 is that no segment of sample is split off during phase 4 of any cycle, whereas during all other phases a sample segment is split off and moved out two phases later (phase $i + 2$).

Finally, it is possible to give the general formulas for each of the four phases, and for all three segments which describe the corresponding mobility interval for any phase i:

Table 3.7

end of phase $j.i^*$	segment split off during phase i	staying in GTW during phase i	leaving during phase i
$j.1$	$0 < \mu < \frac{38+j80}{30+j80}\mu_0$	$\frac{18+j80}{30+j80}\mu_0 < \mu < \frac{38+j80}{30+j80}\mu_0$	$\mu > \frac{38+j80}{30+j80}\mu_0$
$j.2$	$\frac{18+j80}{30+j80}\mu_0 < \mu < \frac{42+j80}{50+j80}\mu_0$	$\frac{42+j80}{50+j80}\mu_0 < \mu < \frac{58+j80}{50+j80}\mu_0$	$\mu > \frac{58+j80}{50+j80}\mu_0$
$j.3$	$\frac{42+j80}{50+j80}\mu_0 < \mu < \frac{62+j80}{70+j80}\mu_0$	$\frac{62+j80}{70+j80}\mu_0 < \mu < \frac{82+j80}{70+j80}\mu_0$	$\mu > \frac{82+j80}{70+j80}\mu_0$
$j.4$	no segment split off	$\frac{62+j80}{70+j80}\mu_0 < \mu < \frac{102+j80}{90+j80}\mu_0$	$\mu > \frac{102+j80}{90+j80}\mu_0$

*with i = 1,2,3,4 and j number of the cycle

Formulas expressing the dependence of the three different segments of the mobility band (consisting of an infinite number of different components with mobilities ranging from 0 to infinity) on the phase number, i, and the cycle number, j. During phase i with $i > 2$, the segment which was split off during phase i-2 will leave the system as well.

3.3 Non idealities of SCCE

3.3.1 Corner effect

The term *corner effect* describes the bandbroadening caused by the movement of a sample plug around a corner. In the case of layout CYCE2, this corner is a 90° corner, as is also shown in Appendix A6. The corner effect can be treated according to several different models. In the first approach, we assume that the contour of the electrical field lines is not influenced by the corner. All particles will move around the corner following a path defined by a quarter circle. This results in a dead volume of 3.5 pL at each corner*. It is important to consider the diffusion of sample into this dead volume while the sample is passing the corner. This might result in tailing effects (and therefore in an additional bandbroadening) because the sample needs more time to move out of this region again. The average diffusion length is in the order of the maximum distance between the edge of the corner and the largest possible radius which still defines a circular path around the corner. Assuming a diffusion coefficient of $D = 10^{-10}$ m^2/s and a speed of $v = 1$ mm/s, a mean diffusion length can be calculated (with these assumed values) to be 4 µm, whereas the distance to the corner can be calculated to be 17 µm. The predicted value for the average path length for a particle moving around a 90 degree corner (in a channel with a rectangular shaped cross section) can be calculated with [EFF 95a]:

$$\left\langle l^2 \right\rangle = \frac{\int_0^{l_{max}} l^2 dl}{\int_0^{l_{max}} dl} \tag{3.6}$$

with $l = \frac{\pi}{2} r$ and $\frac{dl}{dr} = \frac{\pi}{2}$

where l is the maximum length a molecule can move around the corner under the condition that it has to follow the arc of the circle with the radius r

$$\left\langle l^2 \right\rangle = \frac{\pi^4}{48} r^2 \tag{3.7}$$

$\Leftrightarrow$

* this value can be calculated by taking the area difference of a square and the quarter of a circle with its midpoint at the corner of the square.

$$\langle l \rangle = \frac{\pi^2}{\sqrt{48}} r$$

$\Leftrightarrow$

$$l = 1.42 \cdot r \tag{3.8}$$

where r is the width of the channel, which is equal to 40 µm. For the SCCE device, CYCE2, l can be calculated to be 57 µm. This means that an additonal bandbroadening of 60 µm at each 90° corner should theoretically be considered.
A second, physically more realistic view of the corner effect should consider that the field lines of the applied electrical field will be different in the area of the corner than in a straight channel. This will cause a force on the charged sample molecules towards the inner radius of the corner and therefore reduce the bandbroadening effects caused by the corner.

3.3.2 Corner loss and sample loss

corner loss

The term *corner loss* describes the loss of sample at a T-junction. This is caused by the different flow resistances of the main channel and the side channels. The reason for the different geometries is related to obtaining the different electrical resistance ratios necessary to get the largest voltage drop over the main channel and not over the side channels. This was already described in section 2.2.2.

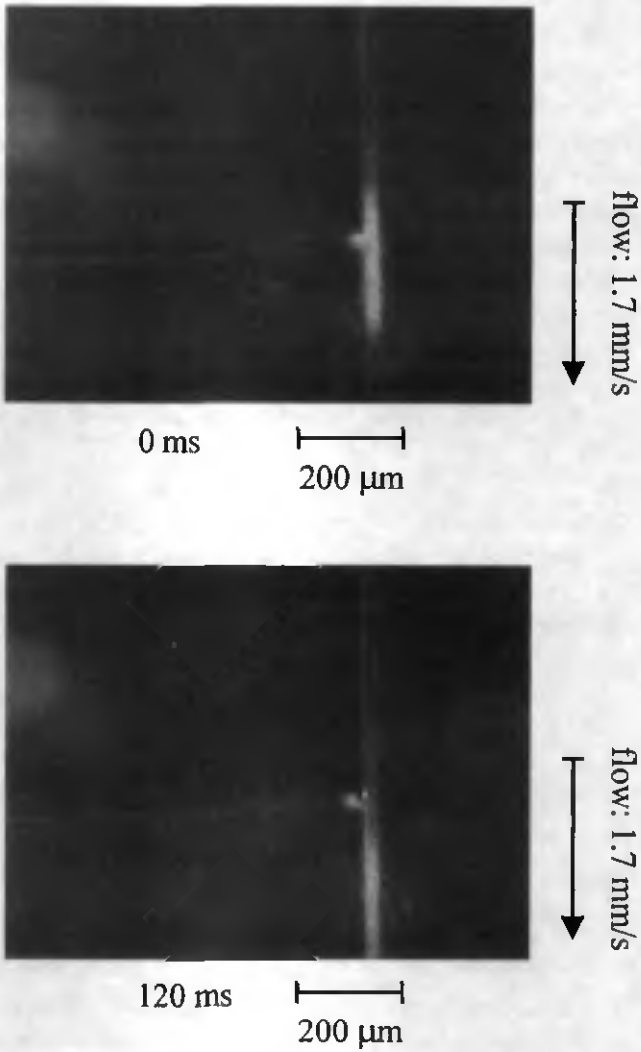

Figure 3.7 Video printouts of the corner loss at a T-junction due to the differences in flow resistance of the side channels and the main channel.

sample loss

Focusing to a specific mobility and therefore reducing the detection window causes a loss of all other components outside of the detection window. The advantage of getting rid of the components in which we are not interested can be also treated as another disadvantage of the system. This is because the focusing results in a limitation of the detectable mobilities (or components) within one sample, and causes a reduction in the amount of information which can be effectively obtained in one experiment.

If the detector is placed after the first quarter of the cycle it is not guaranteed that all sample components will pass the detector after the first voltage switch. This must be considered if one is interested in a first overview of all sample components.

3.3.3 Limitation of the "infinite" length

In contrast to the "infinite length" obtained theoretically with this system, there is a length limitation arising from the increasing bandwidth of the component of interest. The signal bandwidth can be described by

$$\sigma^2_{total} = \sigma^2_{const} + \sigma^2_{side\_1} + \sigma^2_{corner\_1} + 2\cdot\sigma^2_{T-junction\_1} + \sigma^2_{side\_2} + \sigma^2_{corner\_2} + 2\cdot\sigma^2_{T-junction\_2} + \ldots \quad (3.9)$$

$$= \sigma^2_{const} + \sum_{i=sides}\sigma^2_i + \sum_{j=corners}\sigma^2_j + 2\cdot\sum_{k=T-junction}\sigma^2_k$$

$$= \sigma^2_{const} + \sigma^2_{migr.dist.} + n\cdot\sigma^2_{corner} + 2\cdot n\cdot\sigma^2_{T-junction}$$

where σ_{const} is the signal bandwidth caused by all constant effects like injection, detection, and others, whereas $\sigma_{migr.dist.}$ is the bandbroadening caused by axial diffusion expected for the total migration distance, n is the number of corners (or sides), and the corner effect σ_{corner} is assumed to be a constant value (see corner effect in this section). For CYCE2, the term $\sigma_{T-junction}$ describes the bandbroadening caused at a T-junction (see corner loss in this section). For the cyclic layout CYCE3 this effect is already included in the term σ^2_{corner} because the side channels are included in a four way intersection at each corner of the main channel (see Appendix A6). The term $\sigma_{migr.dist.}$ can be expressed in terms of length σ_x and time σ_t:

$$\sigma_x = \sqrt{2\cdot D\cdot t} \quad (3.10)$$

$$\sigma_t = \frac{\sigma_x}{v} \tag{3.11}$$

where t is the time elapsed after injection, D is the diffusion coefficient, and v is the average migration speed of the component of interest.

For CYCE3, an upper limit to the number of cycles is given by the condition that no portion of the peak may be cut off, e.g.

$$4 \cdot \sigma_{total,x} < L \tag{3.12}$$

where L is the length of one side of the channel system and $\sigma_{total,x}$ is the total signal bandwidth in terms of length.

3.4 *Formulas and other mathematical utilities*

3.4.1 The variance of a square wave function

Theoretically the injected sample plug is geometrically defined (see injection process section 4.3.2), and has a rectangular shape (from a top view). The relation between the geometrically defined length of the plug (l), and the variance of the Gaussian distribution (due to axial diffusion) of the sample plug can be determined by calculating the variance of a square wave function. The variance of a steady function $f(x)$ is defined as:

$$\sigma^2 = \frac{\int f(x)\cdot(x-\bar{x})^2 dx}{\int f(x)\cdot dx} \tag{3.13}$$

where $\bar{x}$ is the mean value. With a square wave function $f(x)$:

$$f(x) = \begin{cases} 1 & a < x < b \\ 0 & x \le a \vee x \ge b \end{cases}$$

where $l = b - a$ and $\bar{x} = \frac{a+b}{2}$.

Eq. 3.13 can be reduced to:

$$\sigma^2 = \int_a^b f(x)\cdot(x-\bar{x})^2 dx \tag{3.14}$$

The variance of a rectangular function can therefore calculated to

$$\sigma^2 = \frac{1}{12}\cdot l^2 \tag{3.15}$$

3.4.2 The surface to volume ratio (heat dissipation)

It can easily be shown that the heat dissipation is more efficient in a channel with rectangular cross section than in a channel with a round cross section. This comes because the circumference of a given area has its minimum for a round shaped area. Therefore, a rectangular cross section enlarges the surface-to-volume ratio, resulting in a higher heat dissipation.

Chapter 4 Experimental

4.1 General aspects of the experimental setup

4.1.1 Preparation and filling of the chip

The device fabrication and assembly are described in chapter 2. To get an evenly charged channel surface, the channels were washed with 0.1 M NaOH. This procedure was done always before a new session of separation experiments was started. All channels were pressure-filled with buffer using filtered nitrogen (grade 99.999 %) at 5 bar. To avoid air bubbles stacking at the interface between the pipette tips and the glass chip, Hamilton microliter syringes of 50 µl and 100 µl volume (Hamilton company, Reno, Nevada, USA), were used to deliver buffer into the reservoirs. These fine tip syringes allow the filling of the reservoirs (pipette tips) without getting air bubbles caught at the end of the pipette tip. All reservoirs, except for the central reservoir, were filled with equal amounts of buffer. Usually the central reservoir was filled with an equivalent amount of sample solution. This was necessary to avoid any hydrostatic effects. All solutions used were filtered through a *Sterile Acrodisc*® (Gelman Sciences, Ann Arbor, MI, USA) filter with 0.2 µm pore size. It was found that the presence of fingerprints or other sources of dirt on outer surfaces of the chip could lead to leakage current upon application of high voltage. Therefore, it was important to ensure that outer surfaces were clean before an experiment. This was done by rinsing the chip with clean water or some solvent. Figure 4.1 shows a photograph of the filled chip with reservoirs and electrodes.

4.1.2 Apparatus

Figure 4.2 shows a schematic diagram of that part of the experimental setup developed for the control of the high voltage power supplies. In total, up to ten high voltage power supplies (FUG Elektronik Model HCN 12 500, Rosenheim, Germany) were used to provide the high potentials required for the experiments. Preliminary experiments were performed using only five high voltage power supplies. This number was increased to ten to permit control of the applied potential at every reservoir. All power supplies used have an input plug where the output voltage of the power supply could be controlled with an external voltage between 0 and +10 V. This possibility was used for the experiments. The power supplies were connected to the external electrolyte reservoirs by Pt electrodes via a set of 16 high voltage relais (Magnecraft, Chicago). The relais allowed computer control of the power supplies

while ensuring isolation of the computer from the power supplies. An Apple Quadra Computer (Mac Quadra 700 20/160) was used for all experiments.

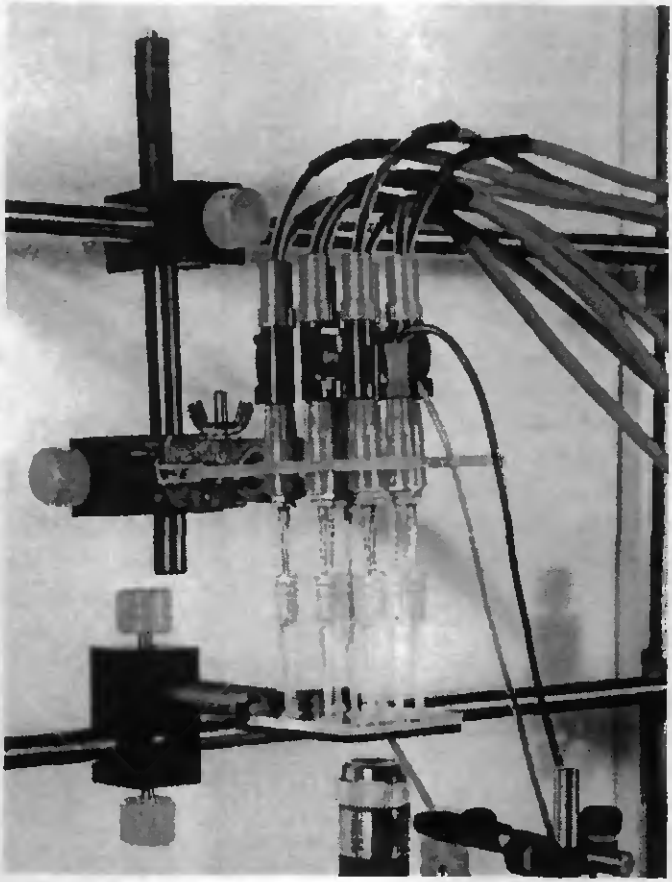

Figure 4.1 Photograph of the chip with electrodes inserted into the filled reservoirs.

The Pt electrodes were combined into a set, resembling a plug. This plug was made in-house and allowed simultaneous contact to all ten reservoirs at once (see Fig. 4.1). The current was monitored by an auto-ranging pico amperometer (485 Keithley, Cleveland, Ohio) between a solvent reservoir and ground. The analog output of the pico amperometer was hooked up to the computer as well.

All buffer reservoirs were connected to a high voltage power supply. Both the sample and waste reservoirs of the injection channel could be connected to high voltage

power supplies as well as to ground. Figure 4.2 shows a diagram of how all components for the control of the high voltage power supplies are wired up.

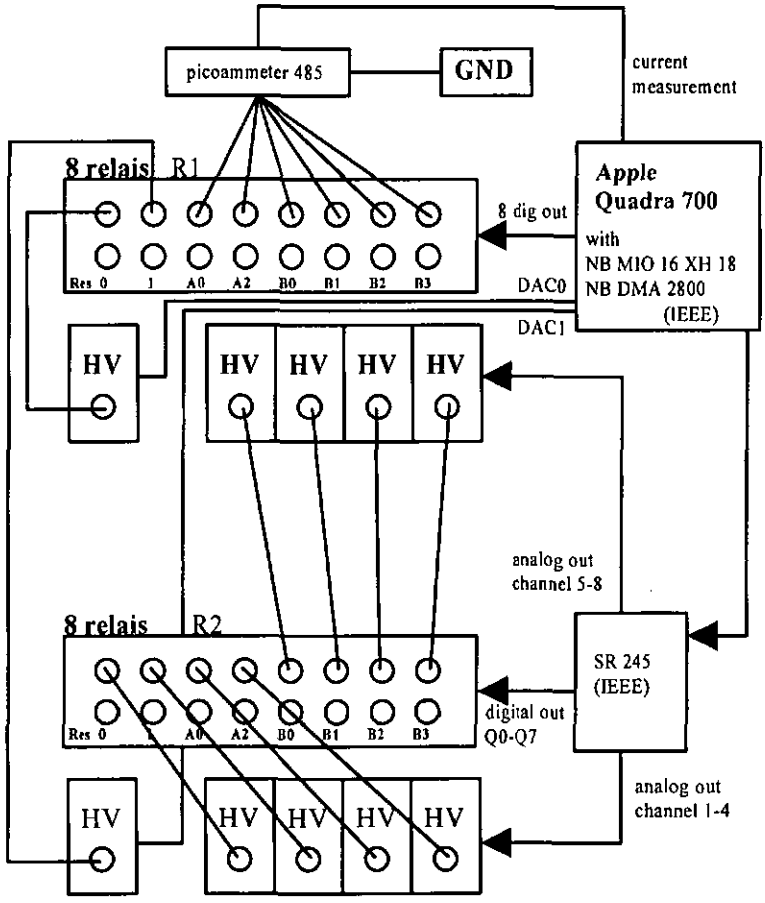

Figure 4.2 Diagram showing the connection between all components necessary to control the output voltage of all ten high voltage power supplies (HV). The sixteen relais are placed into two homemade housings (R1 and R2). The picoammeter is placed between six relais connected to ground electrodes and ground.

All sixteen relais were controlled with TTL signals generated by two electronic boards mounted in the computer. One board is an analog-digital / digital-analog converter

(National Instruments, NB MIO 16 XH 18) and the second is an IEEE board (National Instruments, NB DMA 2800). The IEEE board was used to control an external electronic board (SR 245, Computer Interface Module, Stanford Research Systems (SRS), Sunnyvale, CA, USA) which generated 8 TTL signals for eight of the sixteen relais, as well as eight analog signals (0-10 Volt) to set the high voltage power supplies to the voltage required. The eight TTL outputs from the NB MIO 16 XH 18 board were used to control the remaining relais. The NB MIO 16 XH 18 board was also used to provide the system with two additional analog output signals and to perform the analog-digital conversion. These two analog output channels were connected to the two high voltage power supplies used for the injection. Table 4.1 gives an overview of the control functions of both electronic boards used for the system. The use of two sources for the TTL signals was necessary because of the already mentioned change from five to ten high voltage power supplies. A change in the control software was necessary as well.

Table 4.1

	NB MIO 16 XH 18	SR 245
number of digital output channels	8	8
number of analog output channels	2	8
used for	control of eight relais and setting of the injection voltage	control of eight relais and setting of the separation voltage

Electronic boards and their properties used for controlling the ten high voltage power supplies and the sixteen relais.

4.1.3 Software for controlling the system for SCCE

The software to control all different elements of the system for SCCE was homemade using the software package LabView 2.2.1 (National Instruments, Austin, TX, USA). It consists of several parts which were programmed separately and then combined to one program. This was done to allow more convenient handling of all parts at once. Figure 4.3 shows a block diagram of the different steps involved during one run.

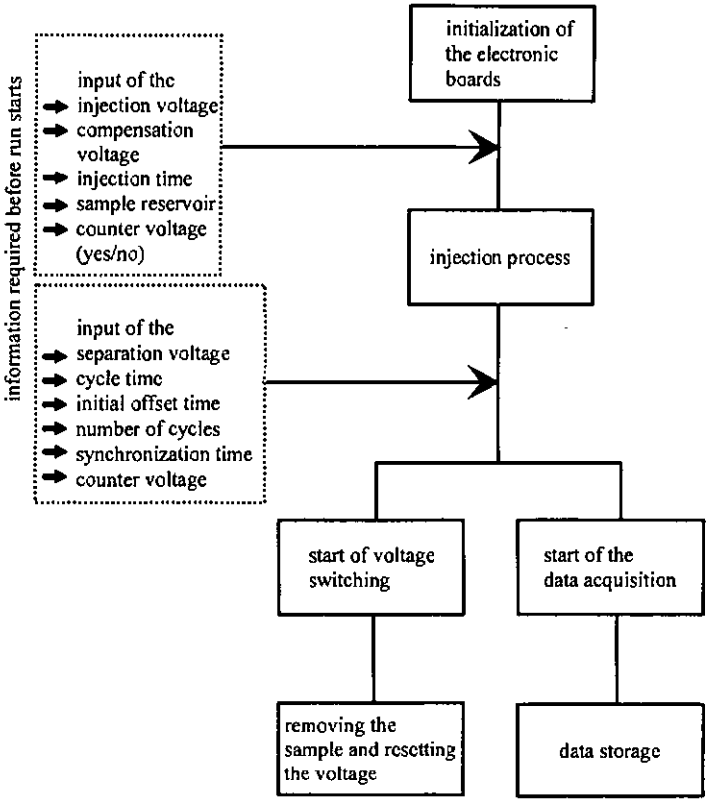

Figure 4.3 Block diagram showing schematically the main procedures of the software used for controlling the voltage, the synchronization and the data acquisition.

voltage control

All ten reservoirs of the SCCE chip are connected to a high voltage power supply. These power supplies have an external input to preset them to a specific output voltage. For the SCCE software it was necessary to distinguish between four different voltages:

injection voltage The injection voltage is applied to one of the two reservoirs used for the sample injection. Both reservoirs are connected to a power supply to permit a change of sample reservoir and change of the direction of electroosmotic flow.

compensation voltage To obtain a good injection quality, a compensation voltage is applied to the two injection reservoirs simultaneously with the separation voltage. This voltage is set at a value which causes the unused sample to be pushed back into the channels by buffer solution, thus avoiding any additional leaking into the separation channel.

separation voltage The separation voltage is used for the separation of the sample. Four high voltage power supplies used for the separation are set to given values before a separation starts.

counter voltage The counter voltage was used to lower corner loss. This was done by causing a slight counter flow of buffer out of the side channels towards the main channel. All counter voltage values necessary for a run were stored in a specific file and loaded into the system during the initializing step at the beginning of the run. Counter voltages were not applied in all experiments.

relais control

The final application of the voltage was done by using high voltage relais as switches. Switching was performed by generating a TTL signal for changing the state of the relais. The switching for moving the sample around the cyclic channel system was done in a "for-loop". The number of times this loop was executed was set before the run was started (see listing in Appendix A7).

timing

A time program determining the length of time each voltage is applied was necessary to perform a controlled run. All times were set to their respective values before the program was started. The different times are:

injection time	Time during which an electrical field is applied between the two injection reservoirs
compensation time	Time in which the sample is pushed back into the two injection channels to avoid leakage of sample into the separation channel after injection.
initial offset time	For layout CYCE2, it was necessary to avoid switching steps if the sample of interest was close to a side channel intersection. Therefore, an initial offset time is added to the total running time to ensure that the sample of interest was located away from any intersections of side channels with the main channel upon a voltage switch.
interval time (synchronization time)	The interval time is the time between two voltage switching steps when moving the sample around the system. Four times the interval time thus yields the cycle time.
extra acquisition time	Additional time for the data acquisition to make sure that all the sample of interest has passed the detector. During this time, the separation channel is completely filled with electrolyte solution.

data acquisition

As already mentioned, the data acquisition was performed using an analog / digital converter board (see 4.1.2 Apparatus). This board has a sampling frequency of 55 kHz, which allows a maximum time resolution of 20 µs. For application with cyclic capillary electrophoresis, this time resolution is not necessary. In fact, it would result in a huge amount of data, which would cause storage problems as well as run-time problems of other parts of the software. Therefore, it was decided to use a much lower time resolution of 20 ms. To maintain runtime precision, the data were stored in the random access memory (RAM) and displayed after the whole separation was done.

4.2 Setups for the different detection schemes

4.2.1 Laser-induced fluorescence (LIF) detection

Optical setup

The experimental setup used for the laser-induced fluorescence (LIF) detection is shown in Figure 4.4. An air-cooled Ar^+-ion laser was used at 488 nm and 5 mW (Omnichrome Mod. 532 AP, Chino, California) to induce the fluorescence. The laser beam was coupled into a 600 µm core diameter optical fiber, which was mounted underneath the separation channel at 45° to the surface of the device. Thus, a few mm of the separation channel was illuminated with the unfocused output of the fiber. A droplet of Triton X-100 serving as a refractive index matching fluid (alkylphenylpolyethyleneglycol) contacted the end of the fiber. Triton X-100 (Fluka Chemie Ltd., Buchs, Switzerland) has an index of refraction of 1.491 [FLU 93] which is very similar to the index of refraction of the HOYA SLW type glass used (n=1.52) [HOY 84]. To collect the induced fluorescence, a homemade microscope body with a microscope objective (Leitz NPL Fluotar L, 25 x, N.A. 0.35, working distance 17 mm) was mounted perpendicularly underneath the glass chip. A pinhole (diameter 1 mm) is placed in the focal plane of the objective. A detection window of 40 µm results, which corresponds to a detection volume of 12.6 pL. The collected light was measured by a Hamamatsu R1477 photomultiplier tube (PMT) (Hamamatsu, Japan) mounted in an integrated detection module (SMT, Seefeld, Germany, Mod. NV 30-1). To reduce the effect of unwanted room light and scattered laser light, a 514 nm interference filter (Spindler & Hoyer GmbH, Göttingen, Germany) was placed between the objective and the PMT. As shown in Figure 4.4, the whole detection unit is mounted on an X-Y translation stage (Spindler & Hoyer, Göttingen, Germany). This allows easy alignment to the separation channels, and makes various locations for detection accessible.

In earlier experiments, a second optical fiber instead of the microscope tube was used for the collection of the fluorescence. The fiber was immersed into a hole drilled down from the top close to the separation channel. Triton X-100 was used as a refractive index matching fluid in this case as well. The other end of the collection fiber was attached to a PMT.

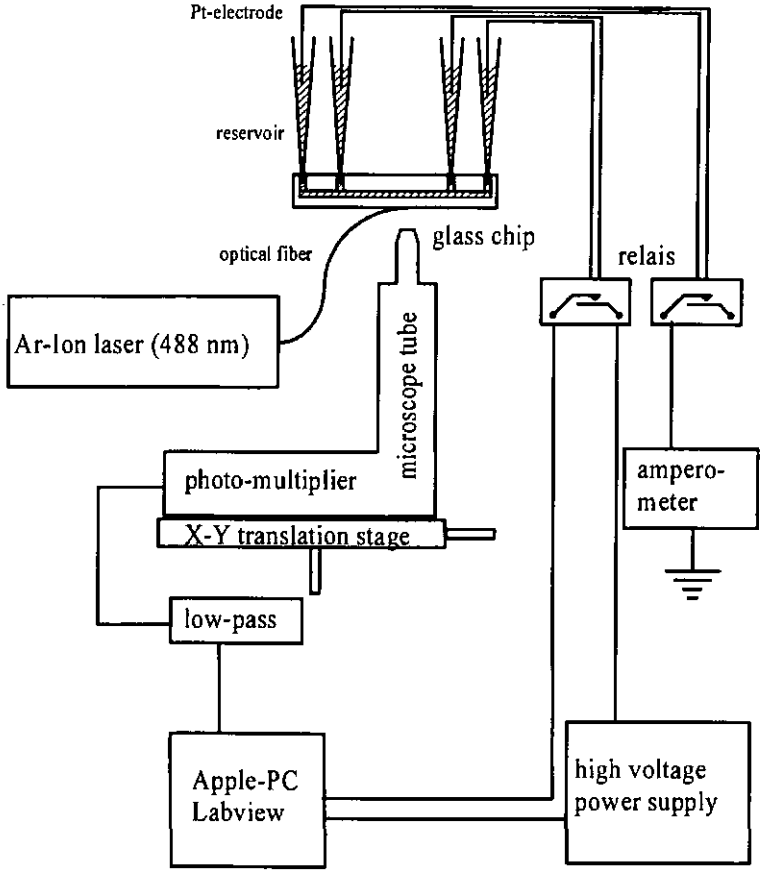

Figure 4.4 Scheme of the experimental setup showing the optical fiber used to induce fluorescence, the microscope tube with the photomultiplier used for detection and the glass chip with the electrodes.

Data acquisition.

The output signal of the PMT was recorded using the analog input of the A/D converter (NB MIO 16 XH 18 board) of the Apple Quadra Computer. A low-pass filter (Avens Signal Equipment Corp., Elmhurst, NY, Model AP-255-5) was used to reduce the noise in the signal. The low pass filter was used at cutoff frequencies between 10 Hz and 50 Hz. To provide the programming environment, the software

package LabView 2.2.1 (National Instruments, Switzerland) was used. This package allows data acquisition and potential control to be managed simultaneously.

4.2.2 Hologram-based refractive index measurements

A refractive index (RI) measurement using a laser as a light source is usually performed using standard optical elements like lenses, beam splitter and mirrors to split a single laser beam into two coherent beams. These optical elements can be integrated into one micromachined optical device or holographic optical element (HOE). A novel hologram-based RI detector for capillary electrophoresis was presented by Beat Krattiger and Alfredo Bruno, Ciba-Geigy Ltd., Corporate Analytical Research, Basel Switzerland [BRU 91], [KRA 94a], [KRA 94b]. A holographic optical element (HOE) manufactured using standard micromachining processes was used to generate the two coherent beams necessary for this type of detection. This HOE-based RI detector was the basis for a detector adapted for the synchronized cyclic capillary electrophoresis on chip.

Principle of the refractive index detection.

The principle of the hologram-based refractive index measurement is shown in Fig. 4.5. A collimated coherent beam of light is partially deflected by the HOE placed at a given angle ($\approx 30°$) with respect to the illumination beam. The HOE acts as nearly superimposed focusing lenses laterally displaced by a distance D, ($D \approx 14$ μm) [KRA 94a]. Therefore, the illumination beam is split into two coherent beams and focused onto the plane where the channel is positioned. One beam is directed through the channel, and is therefore called the probe beam. The second beam acts as the reference beam, passing only through the glass plate. As shown in Fig. 4.5, both beams fan out and interfere in the far field, resulting in an evenly spaced fringe pattern, which can be detected using a diode array. Interference occurs because both beams originate from the same light source. A change in refractive index within the microchannel will induce a phase change in the probing beam, resulting in a lateral shift of the fringe pattern.

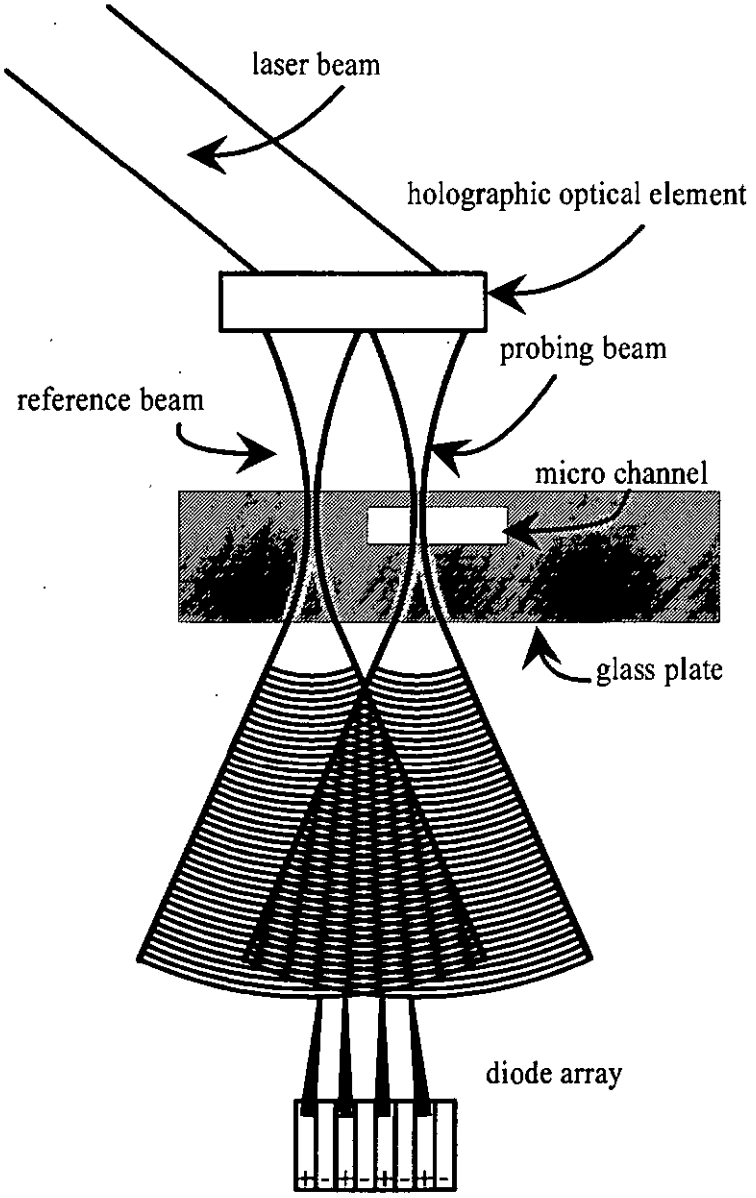

Figure 4.5 Scheme of the detection principle of refractive index detection

Optical setup

The optical setup for the refractive index detection is shown in Figure 4.6. It is a similar setup to the one described in [KRA 94a]. A diode laser light source (Model LDM 145, Imatronic Inc., Batavia, IL, USA) was used at a wavelength of 670 nm and 3 mW. A collimating lens is mounted in front of the laser diode to collimate the laser's output. A precision current source (Mod. LDX 3412, ILX Lightwave, MT, USA) is used to drive the laser diode. The HOE is glued at the correct angle ($\approx 30°$) on a machined plastic pipe and connected to the laser diode. This was done to shield the laser beam and avoid schlieren effects. The refractive index of gases and other media is dependent on their density. Due to temperature inhomogeneities and local air movement, density changes occur, with corresponding local changes in refractive index. This results in a shift of the laser beams with respect to one another, and causes unwanted noise. This effect is called a schlieren* effect. The HOEs have been manufactured according to standard photolitographic procedures [TED 93]. The deflection efficiency of the HOEs ranged from 16% to 32% from batch to batch [KRA 94a]. A glass plate glued on the emulsion side of the HOE using refractive index matching glue prevented drift caused by humidity variations.

To get a stable laser output, the laser diode was set to room temperature using a Peltier element (Melcor, Trenton, NJ, USA) and a temperature controller (LDT 5901B, ILX Lightwave, MT, USA). The laser diode, as well as the HOE, is mounted on a motor controlled X-Y translation stage (Spindler & Hoyer, Göttingen, Germany). This allows easy alignment of the probe beam to propagate through the separation channel, whereas the reference beam passes through the structure beside the channel.

* "The word Schlieren in German means streaks or striae. It's frequently capitalized because all nouns are in German and not because there was a Mr. Schlieren." [HEC 87]

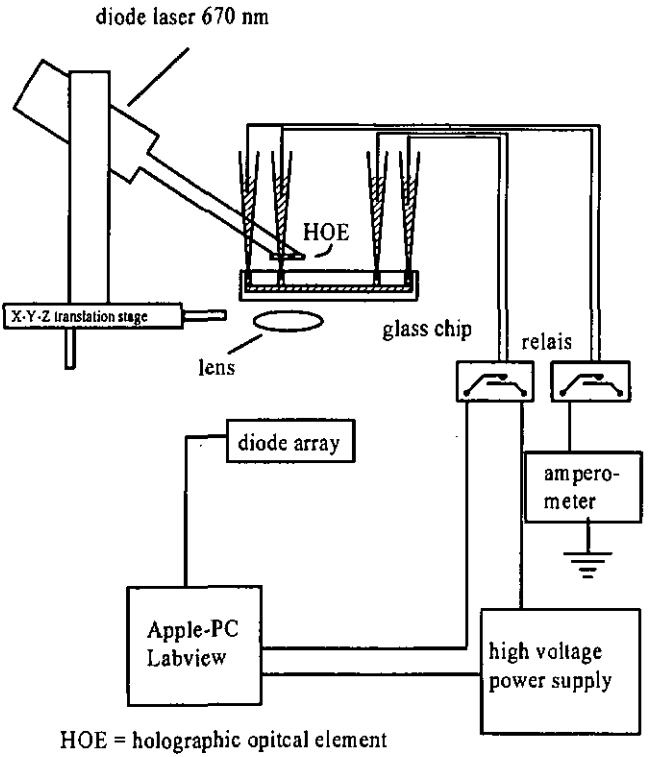

Figure 4.6 Scheme of the experimental setup showing the glass chip with reservoirs and electrodes, the diode laser, the holographic optical element (HOE) and the diode array. The control unit for the high voltage power supplies is the same as that used for LIF detection.

A cylindrical lens (Newport Corp., Fountain Valley, CA, USA) is used to compress the fringe pattern along one direction. The fringes are equally spaced and are monitored by a photo diode array, in essence a position sensitive detection system. The photo diode array (Model KOM 2045, Siemens, Fürth, Germany) is mounted on a translation stage (Microbench, Spindler & Hoyer, Göttingen, Germany) to make it possible to zero the signal. The photo diode array consists of eight single diodes (four pairs) and is wired in parallel to combine the signals of the four fringes. This means that the wiring is performed in a way to get the summation of the four signal differences of each diode pair. With this setup, the lateral shift of the fringe pattern caused by the sample passing through the probing beam is converted to a voltage. The Apple Quadra computer is used to perform the data acquisition as for LIF detection.

4.3 Procedures

4.3.1 Leakage current check and resistance measurement

To ensure that all channels of the SCCE device are filled with electrolyte, and to make sure that there is no leakage current caused by incomplete bonding of the two glass plates, a leakage current check is performed. This check can be combined with a measurement of the electrical resistances of the different channels. The measurement of the electrical resistances is necessary to enable the application of a counter voltage to avoid "corner losses". The counter voltage is applied to the side channels of the SCCE devices, which requires determination of their electrical resistances. Figure 4.7 shows the SCCE device (CYCE2) as a wiring diagram with the different resistors. The first approach is to assume that all side channels have the same electrical resistance and the square shaped channel can be divided into four equal resistors representing the four sides of the separation channel. Together with the resistors which stand for the injection channel, three different resistors can be measured.

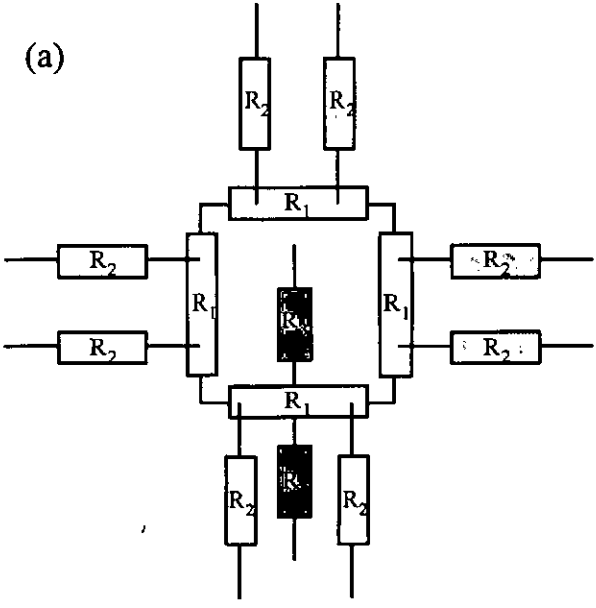

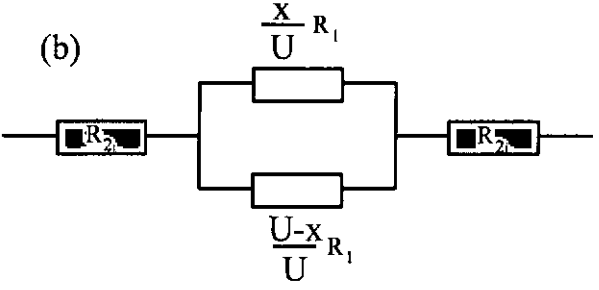

Figure 4.7

(a) Wiring diagram representing the SCCE chip (CYCE2). All relevant channels are represented by resistors.

(b) Applying a voltage between two of the eight side channels results in a wiring diagram consisting of three different resistors (two side channels and the main channel). Four different current dividers are achievable out of a set of eight side channels. In our case U = 80 (circumference of the main channel in mm). To get the set of equations referred to in the text, one has to take x, the possible distance between two side channels in mm, out of the set {16, 20, 36, 40}. These values represent the different possibilities of partitioning the main channel in terms of length. R_i, R_j are the two resistors representing the side channels over which the voltage is being applied with $i \neq j$.

Another approach assumes that all ten side channels have different electrical resistances due to slight variations in channel geometry. Therefore, it is necessary to determine eleven different resistors to describe the electrical behaviour of the system (eight side channels, one side of the main channel, and the two injection channels). This assumption is due to the fact that the geometry of the side channel is more complicated than the main channel geometry. Applying a voltage between two electrodes out of a system with ten electrodes results in 55* possibilities. Neglecting the two electrodes used for the injection, only eight over 2 cases must be considered. This results in 28** different possibilities for applying a voltage. The whole set of 28 possibilities can be described by the wiring diagram shown in Figure 4.7(b). The easiest approach for trying out all 28 possibilities would be to connect each electrode with high voltage as well as with ground. This would require 16 high voltage relais. This number can be reduced to 14 high voltage relais if two electrodes (out of the eight) are connected only to one source, whether to a high voltage power supply or to

---

* the number can be calculated using the combinatorial expression: $\binom{11}{2} = \frac{11!}{(11-2)!\,2!} = 55$

** $\binom{8}{2} = 28$

ground. This would still allow the measurement of all possible currents without reducing the possibilities. Therefore, with 14 high voltage relais all 28 current divider arrangements could be measured. As mentioned in chapter 4.1.2, only 16 TTL signals were available and therefore 16 high voltage relais were controllable (without using any multiplexing system). Four out of the 16 were used to connect the two electrodes for the injection with high voltage as well as with ground. Therefore, only 12 high voltage relais remained for the resistance measurement. Eight were used for the connection to a high voltage power supply (see Figure 4.8), and the remaining four were used for the connection to ground. For the first ground electrode, 7 different possibilities then exist for application of a voltage for the resistance measurement, for the second ground electrode 6 possibilities and so on, resulting in $7+6+5+4=22$ possibilities. Therefore, only these 22 out of the 28 possibilities for a voltage application can be tested.

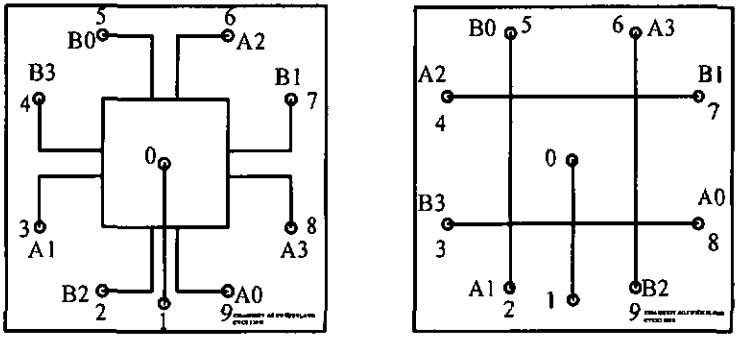

(a) CYCE2 (b) CYCE3

Figure 4.8 Schematic layout of the two SCCE devices (a) CYCE2 and (b) CYCE3. The numbers are referred to in the text. All reservoirs named with an A plus number are connected only to a high voltage power supply where as all reservoirs named with a B plus number are connected via two relais with high voltage and ground.

Neglecting the two electrodes used for the injection reduces the measurement of the resistances to the resistors of the eight side channels and the resistor of the main channel. Applying a voltage between two of these eight electrodes always results in a current dividing system. Therefore, three different resistors are involved assuming that the main channel has a constant cross-section. This results in a set of equations with nine unknowns. To solve an inhomogeneous system of linear equations with 9

independent variables (8 side channel resistors and the main channel resistor), 9 independent linear equations are necessary [BRO 84].
Nine equations must be taken out of the 22 possibilities to calculate all nine resistors. To reduce the number of possibilities, a condition was given that only two out of the four possibilities to form a current divider should be used. It was chosen to be the 50% / 50% case and the 25% / 75% case (compare to Figure 4.7 (b)). This results in ten independent equations represented by the following pairs of electrodes:

Table 4.2

diagonally applied voltage 50% / 50%	"quarterly" applied voltage 25% / 75%
A0/B0	A0/B1
A1/B1	A1/B0
A2/B2	A2/B3
A3/B3	A3/B2
	B0/B1
	B2/B3

Sets of electrodes used to measure the current for calculating the nine different resistor values (eight side channels and one quarter of the main channel). Numbering refers to Figure 4.8 (a).

All ten equations were used to calculate the resistances. This was done in a software routine which performed the measurement of the different currents and used them to calculate the nine resistor values.

4.3.2 Injection methods

An advantage of micromachined glass devices for CE is the possibility to use different injection schemes by designing special injection geometries. The injection methods used for SCCE experiments were determined by the four-way intersection formed by the injection channel and the separation channel. Two different injection methods were performed. They can be applied to both SCCE devices.

a) geometrically defined injection

This injection method was possible in both SCCE layouts, shown in Fig. 4.8(a) and (b). To inject a sample, a voltage was applied between reservoir 0 and reservoir 1 (see Fig. 4.8). Assuming that the sample was placed in reservoir 0, the polarity of the applied voltage was chosen to generate electrokinetic movement from reservoir 0

towards reservoir 1. In this way the intersection of the separation channel and the injection channel was filled. In order to do this, a voltage in the order of 500 V to 1000 V was applied for about 10 to 15 s. The *injection time* (see section 4.1.3) determines the relative composition of the injected sample. That means it is necessary in practice to apply the injection voltage until even the slowest component has reached the intersection. A representative amount of sample within the intersection area could thus be ensured. In the next step of the injection process, the separation voltage was applied diagonally to the device between reservoirs A0 and B0 (see Fig. 4.8) to move the sample clockwise towards reservoir B0. Simultaneously a *compensation voltage* (see section 4.1.3) is applied to reservoir 0 and 1, causing a slight flow of buffer towards both injection reservoirs, thus avoiding any additional leaking of sample into the separation channel. This three-way flow results in well defined injection plugs. The quantity injected with this method is mainly dependent on the geometry of the intersection. A delay between filling the intersection and starting the separation will cause additional broadening of the injected sample plug, due to diffusion of the sample into the main channel. This broadening is proportional to the square root of the delay time. With this method, it is possible to inject volumes in the range from 20 to 30 pL.

b) electrokinetic injection

Another injection method used for preliminary experiments and well known in standard CE is called electrokinetic injection. It is performed by replacing one buffer reservoir with the sample vial and applying an injection voltage along the capillary. Usually a field strength 3 to 5 times lower than that used for the separation is applied [NEI 92]. Introduction of sample to the capillary is caused by electroosmotic migration as well as by electrophoretic migration. Therefore, the separation starts already during the injection process.

Transferring this injection method to the SCCE device has the great advantage that no vials must be exchanged to inject a sample with the electrokinetic injection method. An injection can be achieved by applying a voltage diagonally to the structure between reservoirs A0 and B0. Simultaneously, the electrode immersed in the sample reservoir is set to a voltage causing a sample flow towards the main channel. This sample flow is only possible if the applied injection voltage results in an electrical field between the intersection (which is at a certain potential at this point due to the diagonally applied voltage) and the electrode used for the injection. Typical values for both the diagonally applied voltage and the injection voltage are 2'500 to 5'000 V. For CYCE2, the potential at the intersection while applying the separation voltage

between A0 and B0 can be calculated to be 84% of the applied voltage (under the condition that the high voltage is applied to reservoir A0). Switching off the injection voltage can be combined with the application of a compensation voltage to avoid any additional leaking of sample into the separation channel, as in the geometrically defined injection method. The amount of sample introduced into the system is linearly dependent on the amount of time the injection voltage is applied. It can be calculated using equation 4.1.

$$V_{inj.} = \left(\mu_{ep} + \mu_{eo}\right) \cdot A \cdot t \cdot E \qquad (4.1)$$

where $V_{inj.}$ is the injected volume, A is the cross-section of the injection channel, t the injection time and E the resulting electrical field between the electrode used for the injection and potential at the intersection.

c) other injection methods on planar glass structures

To complete the picture about injection methods, two other schemes used for the injection process will be briefly described. These two methods were not used for this work.

double T injection

Another geometrically defined injection process was used and described in [EFF 93], [EFF 94a], [EFF 94b]. Two side channels connected within a defined distance to a main separation channel form two T-junctions, or a double T-junction. Moving sample through one side channel into the main channel and out via the second side channel will fill the geometrically defined volume in the main channel with sample. The quantity is determined by the distance along the main channel separating the two side channels. This plug can be moved away by applying a voltage along the main channel.

geometrically defined injection using countervoltage

This geometrically defined injection method was first described in [JAC 94e] where it is named *pinched injection*. To reduce broadening of the injected plug due to diffusion and other effects, this method was developed. It is a very similar injection method to the one used for this work and described at the beginning of this section (geometrically defined injection). During a defined injection time a voltage is applied between reservoir 0 and 1 (see Fig. 4.8 (a)) causing a stream of sample towards reservoir 1. An additional voltage is applied to reservoirs B2 and A0, also resulting in

a flow of buffer towards reservoir 1. Therefore, the sample within the intersection is compressed to form a thinner stream and the influence of diffusion to broaden this stream is reduced.

4.3.3 Separation

The separation of an injected sample was performed by switching the electrodes to which the voltage was applied, synchronized to the mobility of the component of interest. Four switching steps are used. The switching steps necessary to perform one cycle are:

1) A0 /B0
2) A1 / B1
3) A2 / B2
4) A3 / B3

The procedure is valid for both SCCE layouts and the numbering refers to Figure 4.8 (a) and (b). Interval times depend on the applied voltage and range in the order of less than ten seconds up to 25 s.

Chapter 5 Results and Discussion

5.1 Characterisation of the SCCE structures

5.1.1 Equivalent circuit analysis

As already mentioned in chapter 2, the devices for SCCE were fabricated by etching channels into a glass surface. The cyclic layouts were designed in a way that the larger voltage drop occurs across the main or separation channel, with only a smaller drop over the side channels. Therefore, the ratio of electrical resistance of the main channel (R1) and the electrical resistance of the side channel (R2) is of great importance. The dimensions given by the manufacturer for the precision of the etched channel dimensions are:

depth: 10 ± 2 µm*
width: 40 ± 4 µm

For the layout CYCE2, this results in a calculated ratio, based on geometric considerations (see Appendix A6 for dimensions), of the resistance of one side of the main channel (R1) to one of the side channels (R2) of $9 \pm 30\%$. For CYCE3, this ratio was calculated to be $10 \pm 30\%$.
It was possible to determine the resistance ratios experimentally by filling the channels with an electrolyte and measuring current, I, as a function of the applied voltage. The buffer used was 20 mM $B(OH)_3$ / 100 mM TRIS at pH 9. By applying voltage to several pairs of electrodes, it was possible to obtain the electrical resistances of all the channels. At this point, it is important to mention that for the measurement of current within a CE system, it was necessary to allow the system to attain a constant current value after applying a voltage. The time needed for this was in the order of seconds. During this equilibration time, concentration differences between the reservoirs to which the voltage was applied could be equalised. In addition, temperature gradients due to joule heating effects were allowed to establish and stabilise. The values for the electrical resistance given below were calculated from current values which had a standard deviation smaller than 0.15 µA. The procedure described in section 4.3.1 was used to calculate the resistance values. A typical example of such a current measurement for both layouts is shown in Table 5.1.
A measurement of the conductivity of the buffer (20 mM $B(OH)_3$ / 100 mM TRIS at pH 9) resulted in a value of 0.61 mS/cm. The value for the resistance, R1, using this conductivity value was calculated to 0.8 GΩ which is the same order of magnitude as

* standard deviation

measured values. Thus leakage currents are not a problem, which in turn means the device has been properly bonded and assembled.

Table 5.1

current I1-I4 50 % / 50 %	current I5-I10 25 % / 75 %	values for the resistance R2-R5*	values for the resistance R6-R9*
1.62 μA	2.082 μA	0.185 GΩ	0.263 GΩ
1.63 μA	1.860 μA	0.252 GΩ	0.179 GΩ
1.61 μA	1.851 μA	0.261 GΩ	0.190 GΩ
1.61 μA	2.093 μA	0.265 GΩ	0.176 GΩ
	1.968 μA		
	1.964 μA		

Results of current measurements used to calculate the resistances of the side channels of the cyclic layout CYCE2. The voltage used for the measurement was 2'500 V. The given values for current I1 to I10 are the means of 20'000 single values. I1 to I4 were the values for the current obtained by applying the voltage diagonally across the device, resulting in a current divider of 50 % / 50 %. The current values I5 to I10 were measured for the current divider case of 25 % / 75 % (see section 4.3.1). Before measuring the different currents, the system was allowed to equilibrate for three seconds. *The numbering refers to the numbering for the reservoirs (see figure 4.8).

Using the values listed above, a mean for the two current splitting cases can be calculated to:

1) 50 % / 50 % case: $I = 1.618 \pm 0.008$ μA
2) 25 % / 75 % case $I = 1.970 \pm 0.095$ μA

For a single **CYCE2** device, the values for the electrical resistances were measured to be (20 mM $B(OH)_3$ / 100 mM TRIS pH 9):

$R1 = 1.22 \pm 0.08$ GΩ
$R2 = 0.20 \pm 0.02$ GΩ

This results in a ratio of $R1/R2 = 6 \pm 1$, which is not as good as expected, but still within the range calculated for the given dimensions ($9 \pm 30\%$).

For **CYCE3**, the values for the electrical resistances were measured to be (20 mM $B(OH)_3$ / 100 mM TRIS):

$R1 = 1.55 \pm 0.02\ G\Omega$
$R2 = 0.17 \pm 0.01\ G\Omega$

This results in a value for $R1/R2 = 9 \pm 0.7$ which is much closer to the expected value of 10 ±30%. A reason for the difference between CYCE2 and CYCE3 which results in the difference between measured and calculated results may be found in the fact that layout CYCE2 is more complicated than layout CYCE3, and therefore more difficult to reproduce using micromachining techniques applied to glass as a substrate. The range of R1/R2 ratios will therefore be larger for CYCE2 than for CYCE3 - in other words, R1/R2 will vary more for CYCE2 than CYCE3. This must also considered for the application of counter voltages.

The values for the resistance ratios are also important for calculating the resulting electrical field strengths obtained within the separation channel. The voltage which drops over the main channel can be calculated with

$$U_{main\_ch.} = \frac{1}{1+\frac{R2}{R1}} \cdot U_{appl.} \qquad (5.1)$$

where $U_{main\_ch.}$ is the voltage which drops over the main channel and $U_{appl.}$ the voltage applied diagonally to the structure. The application of 5'000 V results therefore in an electrical field strength of 1'125 V/cm for the separation channel of CYCE3, and 1'075 V/cm for the separation channel of CYCE2.

5.1.2 Measurement of the diffusion coefficient of fluorescein

To obtain some preliminary data to characterise the properties of the cyclic layouts, fluorescein was used as a fluorescent sample for initial experiments. The diffusion coefficient of fluorescein was first determined by the following experiment.

A sample of 100 µM fluorescein in 50 mM TRIS / 50 mM $B(OH)_3$ buffer (pH 8.5) was injected on structure CYCE3 using the electrokinetic injection method described in section 4.3.2. The sample plug was moved towards the lower left-hand corner without allowing the sample plug to pass this corner. The sample plug was then moved back and forth over a distance of 1.66 ± 0.1 mm. The sample plug was moved back and forth, passing the detector placed at L = 4 mm. The switching was performed manually, resulting in a much larger path travelled by the plug between the first and second detection. Figure 5.1 (a) shows the detector signal obtained. The spikes between the peaks are due to the switching of the high voltage power supplies. Not all cables used for the data acquisition were shielded for these experiments, resulting in induction of a signal. The velocity of the sample plug was calculated to be 0.22 ± 0.01 mm/s. The unfocused laser power during this experiment was measured to be 6 mW. The decrease in signal observed in Fig. 5.1 results in part from a bleaching effect, which is the term used to describe the degradation of fluorescein molecules exposed to the laser light.

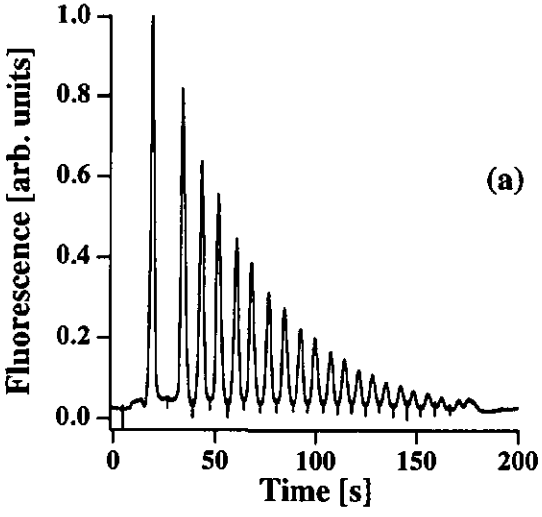

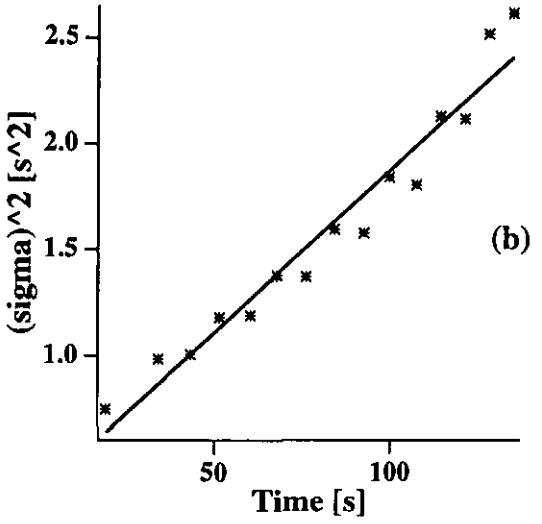

Figure 5.1

(a) Signal of an injected sample plug of 100 µM fluorescein in 50 mM TRIS / 50 mM $B(OH)_3$ buffer at pH 8.5 into structure CYCE3. The sample plug was moved back and forth, passing the detector several times. The detector was placed at L = 4 mm. The diagonally applied voltage was 500 V. The decrease of signal results from the bleaching of the fluorescein.

(b) The variance of the detected peaks as a function of time. The symbols are measured values, whereas the line represents a calculated fit.

The fit function for Figure 5.1 (b) is given by

$$\sigma^2 = K_0 + K_1 \cdot t \tag{5.2}$$

with $K_0 = 0.34 \pm 0.09$ s² and $K_1 = 0.015 \pm 0.001$ s.
Assuming that the total variance, σ^2_{total}, can be expressed in terms of s² by

$$\sigma^2_{total} = \sigma^2_{inj.} + \sigma^2_{det} + \frac{2Dt}{v^2} \tag{5.3}$$

the intercept of the fit function in Figure 5.1 (b) defines the contribution of the detection and injection process to the total variance. As already explained in section 4.1.2, a pinhole 1 mm in diameter was used within the LIF-detection system to define the detection window. Together with the microscope objective used, which had a factor 25 magnification, this results in a detection window of 40 µm. Therefore, σ^2_{det} can be calculated to be 1.3 E-10 m² using Eq. 3.15. The injected plug length can then be calculated to be 425 µm (Eq. 3.15). The slope of the graph corresponds to a diffusion coefficient of 3.7 ± 0.6 E-10 m²/s. This value corresponds well to the

independently measured diffusion coefficient of 3.3 ± 0.2 E-10 m^2/s [HAR 92a]. Another measurement of D = (3.4 ± 0.3) E-10 m^2/s for fluorescein in pH 8.5 buffer was obtained by [DEL 48].

5.1.3 Injection process

a) CYCE3

As mentioned in section 4.3.2, it is possible to perform a geometrically defined injection. Figure 5.2 shows a typical example of an injected sample plug formed on the CYCE3 structure. Again, the sample was 100 µM fluorescein. The injection procedure could be performed with two successive steps (numbering of the reservoirs refers to Figure 4.8):

1) 15 s application of U_{inj} = 500 V between reservoir 0 and 1 (injection voltage)
2) U_{sep} = 5'000 V ("separation" voltage) between A0 and B0 and simultaneously U_{comp} = 400 V (compensation voltage) for 2 s to reservoir 0 and 1. This yield a sample plug of approximately 110 pL.

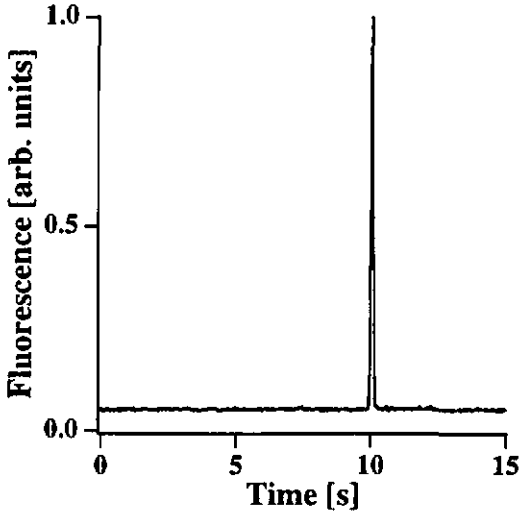

Figure 5.2 Example of an injected peak (CYCE3) detected at L = 20 mm. Sample: 100 µM fluorescein, buffer: 20 mM $B(OH)_3$ / 100 mM TRIS at pH 9, Usep = 5'000 V, injection with 500 V for 15 s and Ucomp = 400 V for 2 s.

The repetitive injection of ten peaks yields the following values for the reproducibility of the geometrically defined injection process:

σ	=	0.04 s ± 2 %
t_{max}	=	10.0 s ± 0.2 %
signal (maximum)	=	0.85 V ± 4 %

The number of theoretical plates achieved can then be calculated to be N = 62'500 ± 2'750.* To obtain these values, the original data were fit assuming a Gaussian distribution. The error given for the measurement of the migration time (t_{max}) is mainly determined by the time resolution of the data acquisition system. Due to the application of counter voltage, the velocity of the peak is reduced in comparison to what is expected for an applied separation voltage of 5'000 V. Instead of 2.2 mm/s, only 2.0 mm/s was measured.

The theoretically achievable maximum number of theoretical plates for a given length of L = 20 mm can be calculated to be 57'000, using D = 3.4 E-10 m^2/s and $\sigma^2_{det} = \sigma^2_{inj}$ = $1.3*10^{-10}$ m^2. This value does not fall in the given error interval obtained for the measured value, being somewhat lower. This is surprising, since bandbroadening due to axial diffusion only would cause a broader peak than was detected here. The contribution to the total variance of the peak due to axial diffusion can be calculated to be $68*10^{-10}$ m^2, whereas the variance of the measured peak is $64*10^{-10}$ m^2. It can be assumed that the peak must be influenced by the corner; therefore, it is of basic interest to know what happens to the peak while passing the corner.

Using a VCR system and positioning the camera over the corner, it was ascertained that for structure CYCE3, loss of sample occurred when a sample plug rounded a corner. Two parts were split off the sample plug and carried into the two side channels. Effectively, the plug was cut off at the ends, which reduced the width of the peak in an undefined manner and artificially increased N.

To prevent this, it might be possible to apply a counter voltage to the side channels, causing a flow towards the main channel. This will be examined in more detail in section 5.1.4.

Another explanation for the unexpectedly high number of theoretical plates lies in the nozzle-like corner layout (see Appendix A6). It might be possible that there is a "focusing effect" due to the special shape of the corner. This possibility was not examined in more detail.

* using an error propagation analysis, where Δt and $\Delta\sigma$ have the values given above [WAL 89].

It was also found that apodization of the peak in such an undefined manner did not always occur. The example shown here gives a worst case scenario obtained with this layout. Much better results obtained with the layout are given in section 5.2.

b) CYCE2

The geometrically defined injection process was tested also using structure CYCE2. An electropherogram obtained after the injection of a 200 µM FITC (fluorescein isothiocyanate) is shown in Figure 5.3. The detection point was at L = 20 mm, the diagonally applied voltage was 5'000 V, and the injection was performed using 500 V for 10 s. No compensation voltage was used. This yielded a sample plug of approximately 150 pL.

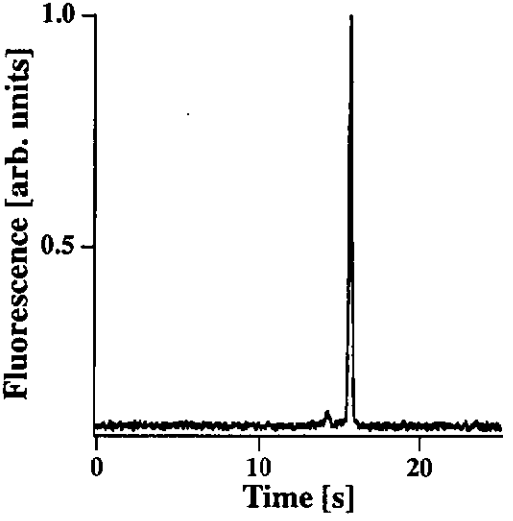

Figure 5.3 Example of an injected peak (CYCE2) detected at L = 20 mm. Sample: 200 µM FITC, buffer: 20 mM $B(OH)_3$ / 100 mM TRIS at pH 9, U_{scp} = 5'000 V, injection with 500 V for 10 s and no U_{comp}.

For this experiment, a fresh sample of FITC was used and therefore no side peak due to the hydrolysis of FITC was detected. The small peak to the left of the FITC peak is most likely an impurity. Again, it was possible to measure the following values describing the reproducibility of the geometrically defined injection process:

σ	=	0.09 s ± 7%
t_{max}	=	15.64 s ± 0.2 %
signal (maximum)	=	0.29 V ± 8 %

The number of theoretical plates achieved experimentally can then be calculated to be $N = 30'200 \pm 630$, in comparison with the theoretically expected maximum number of theoretical plates, calculated to be approximately 57'000, using the same values as for CYCE3. This is not perfectly correct because FITC probably has a slightly different diffusion coefficient than fluorescein. For the sake of simplicity, however, it was assumed to be approximately the same. Again, the question arises concerning the large difference between the measured value and the calculated value of N. It is necessary to observe what is happening at the corner of this layout when a sample is moving around it. For layout CYCE2, no loss of sample can be caused by the corner, but as already explained in section 3.3.1, an additional bandbroadening would be expected due to the "corner effect".

5.1.4 Corner effect

Different experiments were carried out to examine what is called the "corner effect". This effect is responsible for the bandbroadening of a sample plug passing a corner in the structure CYCE2. Another effect which could be examined with the same experimental setup was the bandbroadening caused by passing a T-junction type intersection between the main channel and a side channel. Both effects were already explained in section 3.3.1 and 3.3.2. These experiments were performed using layout CYCE2.

a) moving back and forth around a corner

The first examination of the corner effect involved moving an injected sample plug back and forth around a corner. The detector was placed at L = 25.6 mm, which is between the upper left-hand side channel and the upper left corner. Figure 5.4 (a) shows the scheme of CYCE2, the detection point and the path travelled by the sample plug. An extension of this experiment examined the influence of a side channel intersecting the main channel in a T-junction. For this, the plug was moved across an intersection during its counterclockwise mode. This is illustrated in Fig. 5.4 (b).

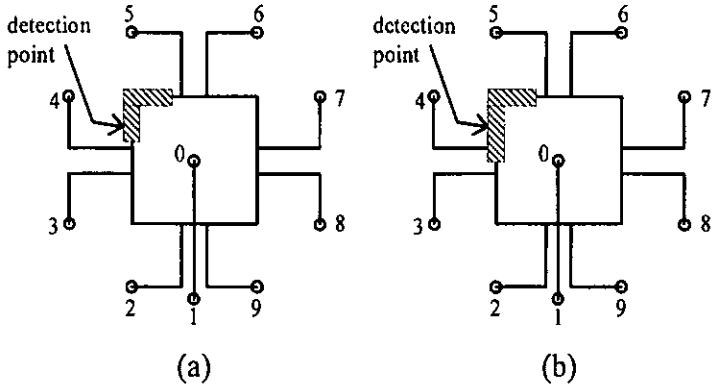

Figure 5.4 Schematic illustration of the path travelled by the sample plug for the examination of (a) the corner effect and (b) the bandbroadening of the sample plug caused by passing a T-junction. The path is indicated by the hatched box. The detection point is indicated with an arrow.

A voltage of 2'500 V applied between reservoir 9 and 5 (see Fig. 5.4) and alternating in polarity was used to move the sample back and forth. The sample was again 100 µM fluorescein in 50 mM TRIS / 50 mM $B(OH)_3$ buffer (pH 8.5). For investigation of the corner effect, two conditions were given for the path length travelled by the sample, as shown in Figure 5.4 (a).
During the clockwise movement, the sample had to pass the corner before the direction of the buffer flow was reversed.
During the counterclockwise movement the sample was not allowed to reach the intersection between the main channel and the upper left-hand side channel before the next voltage switch occurred.
Figure 5.5 shows the detector signal obtained with this experimental setup.

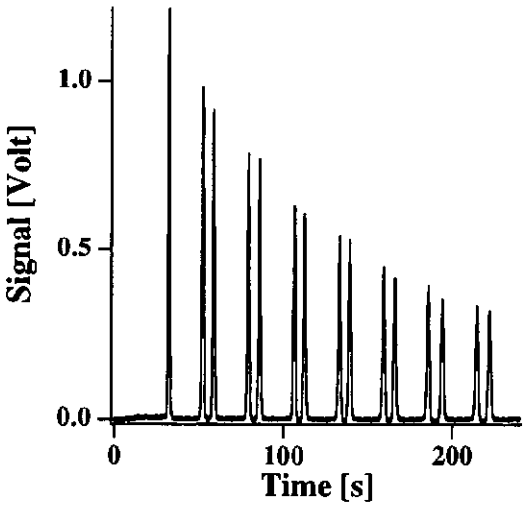

Figure 5.5 Detector signal obtained by moving a 100 µM sample of fluorescein back and forth around the upper left-hand corner of layout CYCE2. Between each "pair" of peaks, the sample has passed the corner twice. The decrease of signal results from the bleaching effect, as well as broadening of the peaks.

The detector signal obtained for the experiment including the upper left-hand T-junction is given in Figure 5.6. It is of special interest that in this experiment some additional peaks appear. These peaks will be called "ghost" peaks in the following discussion. An explanation for this effect is given below.

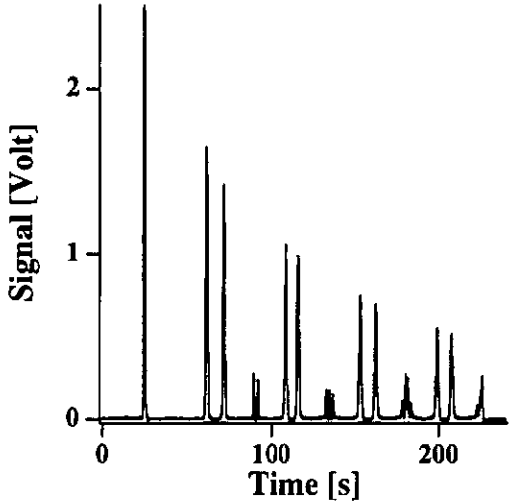

Figure 5.6 Detector signal obtained by moving a 100 µM sample of fluorescein back and forth around the upper left-hand corner of layout CYCE2 and a location between the two side channels on the left-hand side. Between each "pair" of peaks, the sample has passed the corner twice. The decrease of signal results from the bleaching effect and bandbroadening due to the "corner effect" and to passing a T-junction (see section 3.3.1).

It is possible to pinpoint the location where these ghost peaks must be generated from their migration times. These peaks were generated when sample passed the T-junction, to be directly followed by a voltage switch. According to an effect much like corner loss, it can be concluded that a part of the sample plug was split off while passing the T-junction, and was moved back into the separation channel again upon switching. To prevent this effect for any separation experiments, it was decided to switch the voltage when the sample of interest was located away from any intersection, at a corner of the main channel. This was why an initial offset time was added to the beginning of a cycling experiment.
This effect also made it impossible to determine the contribution to bandbroadening due to passing a T-junction because the splitting resulted in a narrower peak. No reasonable data for the bandbroadening could therefore be obtained. For measurement of the contribution resulting from passing a T-junction, the reader is referred to the results presented in the following section (b).
The bandbroadening due to passing a corner can be calculated to be:

$\sigma^2_{corner} = 64.1 \pm 3.7 * 10^{-10}\ m^2$

This value was much higher than expected. An additional experiment which would permit evaluation of the influence of a T-junction was carried out, as described in the following section.

b) detection of an injected peak at different locations

Another experiment to determine the influence of a corner or a T-junction was performed by detecting an injected peak at various locations. For this, the detector was placed at 0.6 mm, 9.0 mm, 15.0 mm, 20.0 mm, 23.0 mm, and 60.0 mm. The distances refer to distance from the injection point. The moving direction was chosen to be clockwise. Figure 5.7 shows an example of a measurement obtained at each corresponding detection point. Every experiment was performed five times. Comparing the measured peak widths and taking into account the number of corners and side channels passed by the corresponding peak, it was possible to determine values for the bandbroadening caused by a corner and the bandbroadening due to T-junctions. Because voltage switching was carried out when the sample was at a corner of the separation channel, losses of sample at the T-junction due to voltage switching were prevented. Thus, a more precise measurement of $\sigma^2_{T-junction}$ was possible.

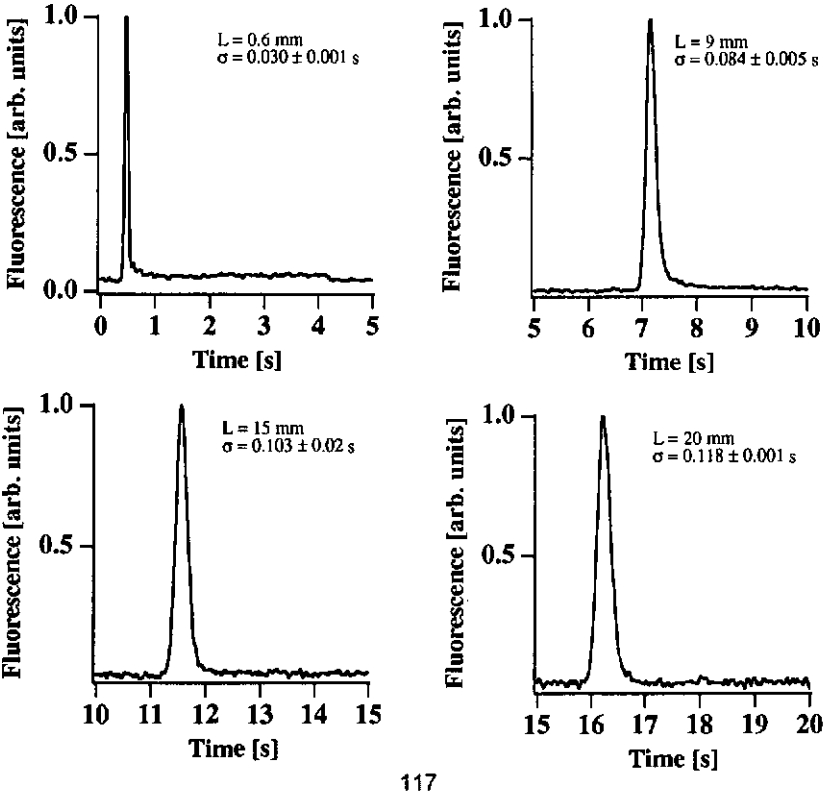

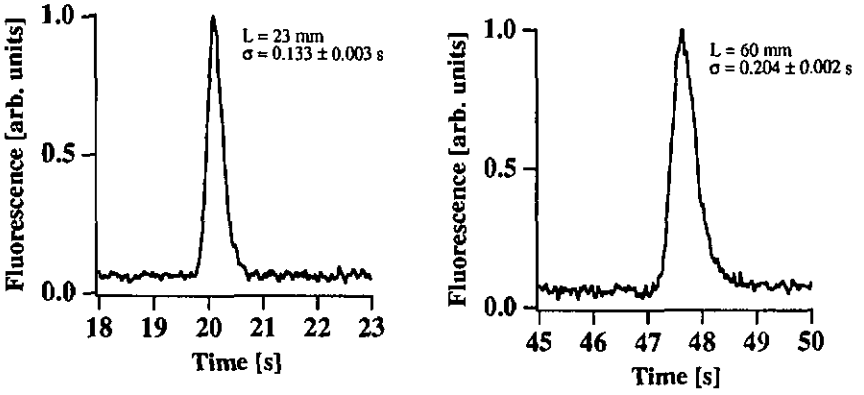

Figure 5.7 Examples of the measured signal obtained after injecting a sample of 100 μM fluorescein. The detector was placed at different locations (L), given in the corresponding figure.

The contributions to the total variance of a moving peak were found to be:

for a T-junction:
$\sigma^2_{T\text{-junction}} = 30 \pm 11 * 10^{-10}\ m^2$

for a corner:
$\sigma^2_{corner} = 37 \pm 7 * 10^{-10}\ m^2$

Considerations regarding the "corner effect"

First of all, it is important to stress that bandbroadening is caused by moving a sample plug around a corner. Comparing various data, which also includes the data obtained during the investigation of the injection process (see section 5.1.3), results in a variation of σ^2_{corner} from less than $10 * 10^{-10}\ m^2$ to $64 * 10^{-10}\ m^2$. This is the range of likely values which can be given for this effect at the moment. Further investigations and many more experiments would be necessary to obtain more precise data, and to pinpoint the causes of the observed experimental variability for σ^2_{corner}.

5.2 Typical SCCE results

5.2.1 Cycling of a single component

On the basis of preliminary experiments, we were able to show that movement of a sample around a cyclic structure was possible using solely electrokinetic pumping. This experiment was done with a sample containing only one component, using the cyclic structure CYCE3. As shown in Figure 5.8, ten complete cycles were achieved. The detector was placed at the midpoint between the lower left-hand and the upper left-hand corner (see figure 4.8). The applied voltage for the cyclic movement was 2'500 V, resulting in an electrical field strength in the separation channel of about 500 V/cm. Taking into account that only 2'000 V drops along the separation channel, "only" 2'000 V were used to obtain this result. The first signal was recorded after the sample had travelled along a quarter of the square. The next two peaks were recorded after the first and a quarter and second and a quarter cycles, respectively. The time needed for one cycle was about 67.8 ± 0.1 s. This corresponds to a electrokinetic velocity of 1.2 mm/s. It is important to remember that while a sample was driven around the system, it was detected each time it passed the detection point. This might be confusing for the reader familiar with conventional CE systems, where the sample is detected only once, at the end of the capillary.

The precision of the migration time indicates that the voltage control and switching system were operating in the desired way. It shows also that it is possible to move a sample around a cyclic structure only by switching the electrodes to which the voltage is applied. Therefore, this was the first demonstration of the idea behind the synchronized cyclic capillary electrophoresis system.

It was found that the number of theoretical plates per peak increased linearly with the number of cycles completed. The maximum theoretically expected value for the number of theoretical plates for the tenth peak was calculated to be $1.4*10^6$.

The rapid decrease of the signal intensity observed in Fig. 5.8 is very significant. This was caused by three different effects. One was photochemical bleaching of the fluorescein, which arises when a high illumination intensity is used (see also Figure 5.1) [HIR 76]. A second effect responsible for the decrease of the signal was axial diffusion. The third effect was the loss of a small amount of the sample plug at the corners (CYCE3), as was described earlier (see section 5.1.3).

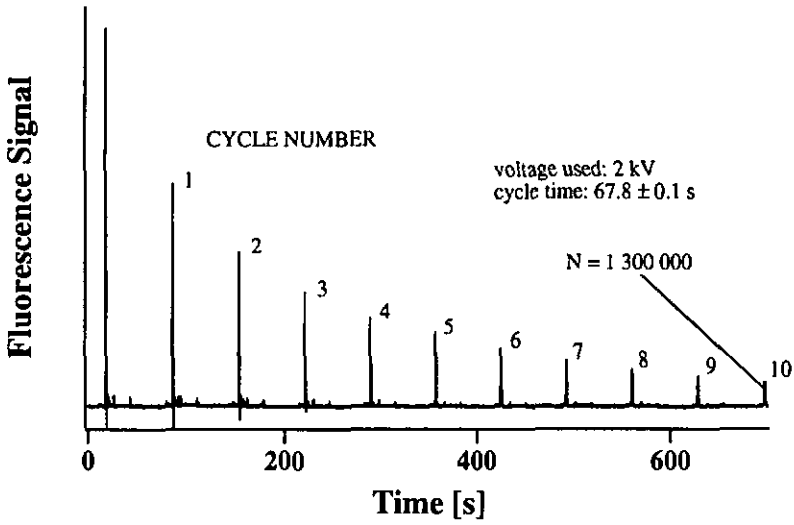

Figure 5.8. Synchronized cyclic electropherogram obtained after injection of 100 µM fluorescein. Ten complete cycles were detected. The first peak was obtained when the sample first passed the detector placed midway between the lower left-hand and the upper left-hand corner (see figure 4.8). A significant decrease in signal intensity was apparent. The number of theoretical plates for the last detected peak was calculated to be 1'300'000. Device used for this experiment: CYCE3

5.2.2 Separation of FITC-labelled amino acids

CYCE3

The first separation obtained with the SCCE system (CYCE3) was performed using the sample described in [EFF 93]. The sample consisted of six amino acids: arginine (Arg), glutamine (Gln), phenylalanine (Phe), asparagine (Asn), serine (Ser), and glycine (Gly). These amino acids were labelled overnight with FITC (fluorescein isothiocyanate) using a method described in [EFF 93]. The voltage applied for the separation was 5'000 V. Figure 5.9 shows the electropherogram obtained after the first quarter of a cycle. It was found that there were two intervals of mobililities to which the system could be synchronized.

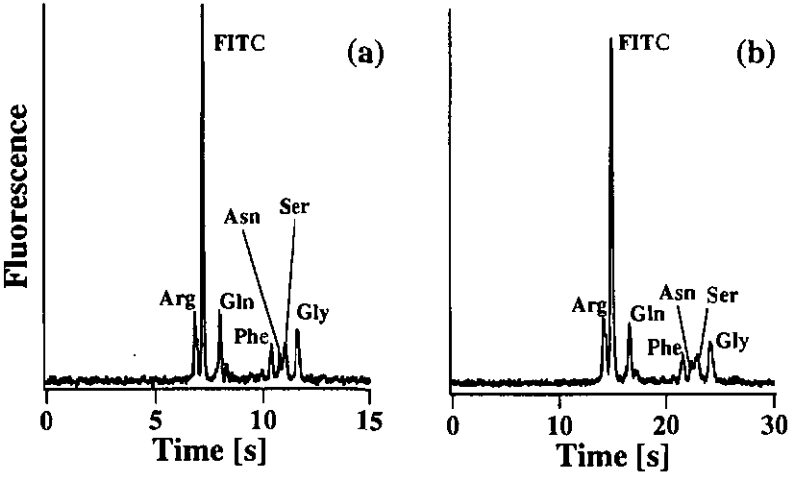

Figure 5.9 (a) Electropherogram of six FITC (fluorescein-isothiocyanate) - labelled amino acids. Formal concentration of each amino acid: 100 µM. Buffer solution: 20 mM boric acid / 100 mM Tris (pH 9.0). A voltage of 5'000 V was applied which corresponds to an electrical field of 1'125 V/cm. The detector was placed at L = 20 mm. For the glutamine peak, a number of theoretical plates was found to be 40'000.

(b) The same electropherogram obtained with application of 2'500 V (E = 560 V/cm).

It was now possible to synchronize the system to a specific electrokinetic mobility. Considering Fig. 5.9 (b), $t_{synch.}$ was set to 22 s for the first run. This meant a "focusing" to the section of the electrophcrogram in which the four amino acids Phe, Asn, Ser, and Gly were found. Figure 5.10 shows the electropherogram obtained after moving the sample around for one complete cycle.

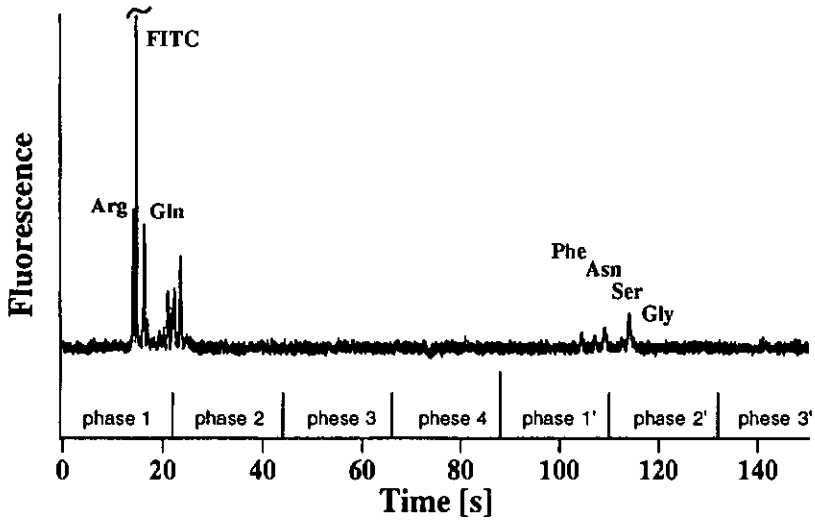

Figure 5.10 Electropherogram of six FITC-labelled amino acids recorded under the same conditions as shown in Fig. 5.9 (b). The voltage applied was 2'500 V. The switching frequency of the voltage applied was synchronized to the four slower components (Phe, Asn, Ser, Gly). Each phase lasted 22 seconds. The FITC peak, as well as the two faster components (Arg, Gln), were driven out of the system in a manner similar to component (3) in Fig. 1(c). After one complete cycle, the four components of interest passed the detector again (phase 1' and 2').

Changing the synchronisation time from 22 s to 15 s, a different electropherogram was obtained, as shown in Fig. 5.11. In this case, the system was synchronized to the faster components of the sample (Arg, FITC, Gln).

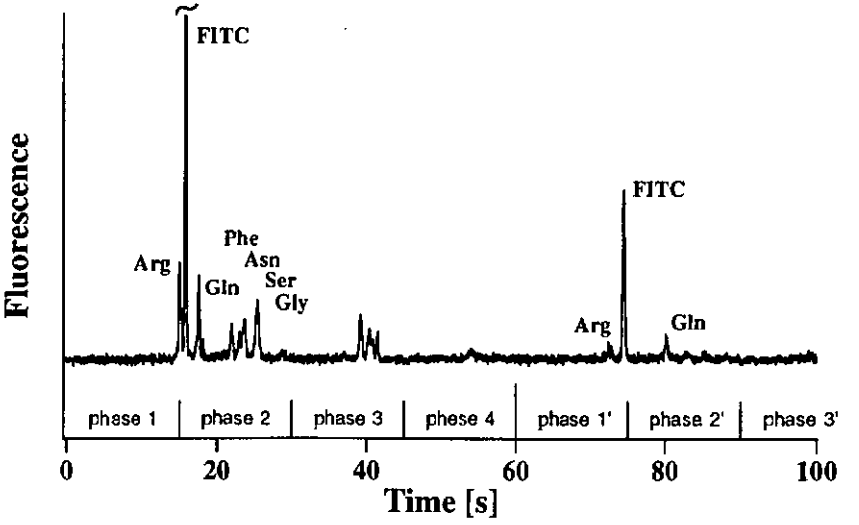

Figure 5.11 Electropherogram of six FITC-labelled amino acids recorded under the same conditions as shown in Fig. 5.9. The voltage applied was 2'500 V (E = 560 V/cm). The switching frequency of the voltage applied was synchronized to the three faster components (Arg, FITC, Gln). Each phase lasted 15 seconds. After the initial separation, the slower components passed the detector again (phase 3) because of a change in the direction of liquid flow in a manner similar to component (1) in figure 1.6 (d) and (e). These components were subsequently driven out of the system, as shown in figure 1.6 (f). After one complete cycle, only the components of interest passed the detector again (Phase 1' and 2').

As already predicted by theory, it can occur that components which have smaller electrophoretic mobilities than the sample to which the system is synchronized will be excluded from the detection window and be forced to reverse the direction in which they are travelling. This occurred to the components Phe, Asn, Ser, Gly (see Fig. 5.11) which were too slow to pass the next corner (in this case the upper left-hand, see Fig 4.8). As a result, they passed the detector again in phase 3 as they moved in the opposite direction, producing a mirror image of the quartet of peaks recorded in phase 2.

CYCE2

Another experiment was performed using the structure CYCE2. In this case the sample chosen was a mixture of isoleucine (Ile), lysine (Lys) and acridine orange (AO) in a 20 mM boric acid / 100 mM Tris buffer (pH 9.0). The amino acids were again labelled with FITC and the concentration of each component was chosen to be 200 μM. The injection process was performed using an injection voltage of 1'000 V for 15 s. The separation voltage was chosen to be 5'000 V. No compensation voltage was used in this case. Figure 5.12 shows the electropherogram obtained after the sample has travelled a quarter of a cycle.

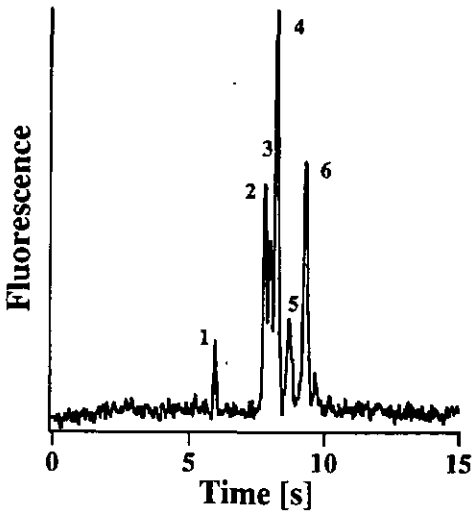

Figure 5.12 Electropherogram of a sample of isoleucine, lysine, and acridine orange (200 μM each), obtained after the first quarter using structure CYCE2. The detector was placed at L = 20 mm. Injection was performed using 1'000 V for 15 s. The separation was carried out using a separation voltage of 5'000 V (E = 1'125 V/cm).

Six peaks are detected due to the likely presence in the sample of FITC, as well as its hydrolysis product and impurities. Setting the system to a synchronisation time of $t_{synch.}$ = 8 s resulted in the electropherogram shown in Figure 5.13.

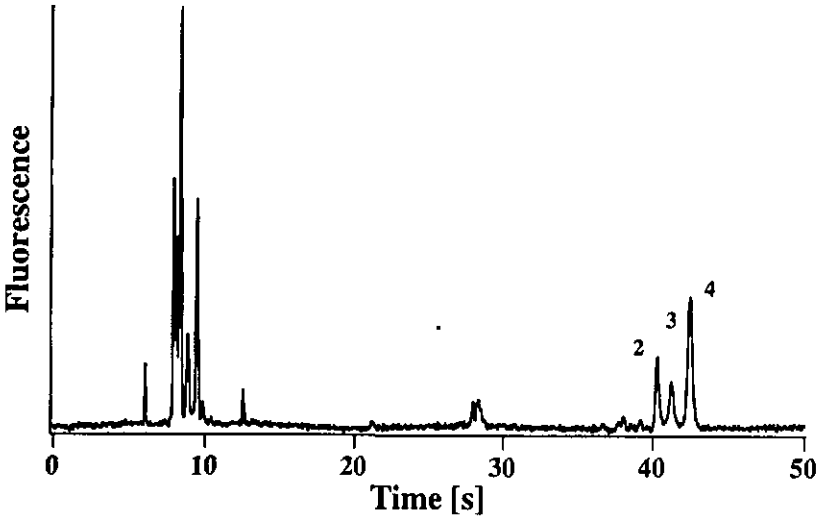

Figure 5.13 Electropherogram obtained after moving the sample (see figure 5.12) around one and a quarter cycles. The synchronisation time was set to 8 s, with the initial offset time 4 s. Injection: 1'000 V for 15 s, separation voltage: 5'000 V (E = 1'125 V/cm), and L: 20 mm.

The value for the resolution obtained (Equ. 1.24) for these three peaks (number 2, 3 and 4) after moving around one complete cycle can be calculated to be larger than two (R_s = 2.1 and 2.2).
Changing the synchronisation time from 8 to 9 s, a different electropherogram was obtained. This is shown in Figure 5.14 (a) and (b).

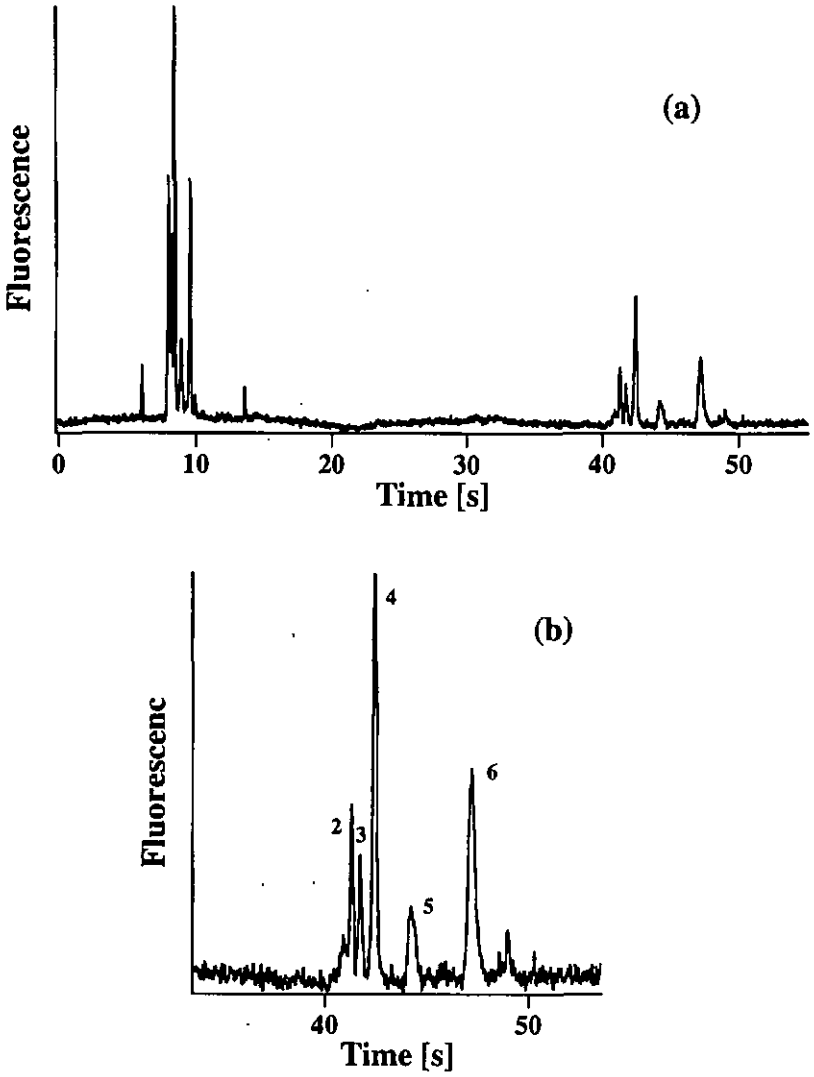

Figure 5.14

(a) Electropherogram obtained under the same conditions as the one shown in figure 5.13. The only difference is the synchronisation time, which was set to 9 s, with an initial offset time of 4 s. Injection: 1'000 V for 15 s, separation voltage: 5'000 V, and L: 20 mm.

(b) Expanded view of the part of the electropherogram recorded when the sample passed the detector a second time, after being moved around one and one quarter cycles.

Calculating the value for the resolution results in a baseline resolution for all 5 peaks (obtained values for the resolution are: 1.6 for peaks 2 and 3, 2.3 for peaks 3 and 4, 5.2 for peaks 4 and 5, and 4.1 for peaks 5 and 6).
Considering Fig. 5.13 ($t_{synch.}$ = 8 s), and using the theoretical description of the mobility window (see section 3.2.4), it was possible to account for the disappearance of the two slower peaks. Using Fig. 5.12 showing all six peaks, it was possible to assign numbers ranging from 1 for the fastest to 6 for the slowest component. For each component, the location reached during a switching phase can be calculated. Table 5.2 contains these calculated distances.

Table 5.2

end of phase	moving time [s]	l_1 [mm]	l_2 [mm]	l_3 [mm]	l_4 [mm]	l_5 [mm]	l_6 [mm]	l_{min} [mm]	l_{max} [mm]
1	12	39.6	29.6	29.2	28.2	26.5	25.4	18	38
2	8	--	49.4	48.6	47	44.5	42.4	42	58
3	8	--	69.2	68.0	65.8	61.9	59.4	62	82
4	8	--	88.9	87.5	84.6	--	--	78	102
5	8	--	108.7	106.9	103.4	--	--	98	118

Distances travelled by the 6 components (see figure 5.12) at the end of the corresponding phase calculated for a synchronisation time of 8 s. The velocities used to calculate these numbers are given below. The two right-most columns determine the interval of length defining the *given time window*.

Comparing the distances travelled by the six components (during phase 1 to 5) with the interval determined by the *given time window* (GTW) (two right-most columns) allows the determination of the precise path travelled by the different components (see section 3.2.3 and 3.2.4). It was possible to confirm that during the voltage switching with a synchronisation time of 8 s, component number 1 was moved out during the first phase. This conclusion can be drawn from the fact that l_1 is larger than l_{max}. This component was moved out through side channel number 5 (B0) (see Figure 4.8 or 5.4). Component number 5 and 6 were split off between phase 3 and 4 and left the separation channel during phase 5 through the same side channel as component 1. As shown in Table 5.2, l_5 and l_6 are smaller than l_{min} of phase 3. The last row of table 5.2 indicates the peaks passing the detection system a second time after being moved around the structure. It can be concluded that all of these three components would stay within the GTW at least for the next phase.

The following velocities, measured over five experiments, were used to calculate the numbers given in table 5.2 and table 5.3:

v_1 = 3.3 ±0.02 mm/s v_2 = 2.47 ± 0.003 mm/s v_3 = 2.43 ± 0.002 mm/s
v_4 = 2.35 ± 0.003 mm/s v_5 = 2.21 ± 0.01 mm/s v_6 = 2.12 ± 0.01 mm/s

The same calculation can be done for a synchronisation time of 9 s. The distances travelled by each component are given in table 5.3.

Table 5.3

end of phase	moving time [s]	l_1 [mm]	l_2 [mm]	l_3 [mm]	l_4 [mm]	l_5 [mm]	l_6 [mm]	l_{min} [mm]	l_{max} [mm]
1	12	42.9	32.1	31.6	30.6	28.7	27.6	18	38
2	8	--	54.3	53.5	51.7	48.6	46.6	42	58
3	8	--	76.6	75.3	72.9	68.5	65.7	62	82
4	8	--	98.8	97.2	94.0	88.4	84.8	78	102
5	8	--	121.0	119.1	115.2	108.3	103.9	98	118

Distance travelled by the 6 components (see figure 5.12) at the end of each phase calculated for a synchronisation time of 9 s. The velocities used to calculate these numbers are given above. The two right-most columns determine the distance intervals of length defining the *given time window*.

The last row of table 5.3 predicts that five out of the six components will pass the detection point a second time. This corresponds perfectly with the measurement shown in Figure 5.14. It is also possible to conclude that components 2 and 3 will be moved out of the separation channel during phase 5 because they are moving out of the detection window.
The result of this experiment corresponds perfectly to what is expected by theory. In this case, a change of the synchronisation time by only 1 s changes the course of the separation drastically. This opens the possibility to use this SCCE chip for fraction collection.

5.2.3 Separation of a tryptic digested sample of melittin

An example of a separation of a tryptic digested sample of melittin (from bee venom) is shown in Figure 5.15. The digestion was performed according to the method described in [SCH 91b]:

1 mL of 1 mM melittin sample in 20 mM boric acid / 100 mM Tris (pH 9.0)
adding 400 µL of 1 mM FITC in acetone
adding 10 µM trypsin
storing for 15 min. at 20°C
adding 0.1 mL of 1M acetic acid to stop the digestion
adding 0.1 mL of 1M sodium hydroxide to neutralise the acetic acid

The tryptic digestion of melittin results into the following six (five different) fragments:

1) Gly - Ile - Gly - Ala - Val - Leu - Lys
2) Val - Leu - Thr - Thr - Gly - Leu - Pro - Ala - Leu - Ile - Ser - Trp - Ile - Lys
3) Arg
4) Lys
5) Arg
6) Gln - Gln

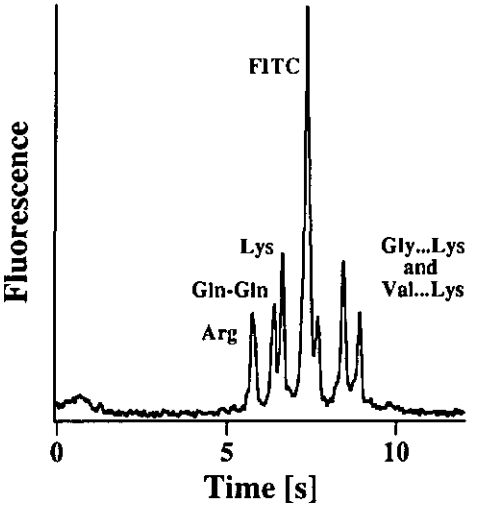

Figure 5.15 Electropherogram of tryptic digested melittin in a running buffer of CAPS pH 11 (Fluka Chemie, Buchs, Switzerland). Separation conditions: L = 22 mm, E = 1'125 V/cm. Digestion and labelling were performed in 20 mM boric acid / 100 mM Tris (pH 9.0). U_{inj} = 1'000 V for 15 s. Peak assignment was done by individual runs with each of the smaller fragments.

For the two larger fragments the numbers of theoretical plates were measured to be:

N = 22'500 (for the slower one) and
N = 31'500 (for the faster one)

Due to the fact that the larger fragments were adsorbing to the capillary walls, it was not possible to perform a multi cycle experiment with this sample. To achieve a cycling of such a sample, it would be necessary to cover the channel surface with an appropriate coating (see Appendix A2). To determine the different components single runs with Arg, Lys, and Gln - Gln were performed.

5.3 Effects of the application of counter voltage - advanced fluid handling

5.3.1 Reasons for the decrease of the signal

A significant problem of both of the cyclic structures is the loss of sample while passing an intersection between the main channel and a side channel, (CYCE2) or a corner (CYCE3). As already shown in Figure 5.8 (the movement of one component around CYCE3 for ten cycles), the signal decreases drastically over the performed cycles. Three reasons were assumed to contribute to that decrease:

1) axial diffusion
2) photochemical bleaching
3) loss of sample at the corner (or T-junction)

It was possible to determine the extent to which each of these effects contribute to signal loss. In order to do this, it was necessary to perform an integration over each of the detected peaks shown in Figure 5.8 and 5.1. The resulting graph is shown in Figure 5.16. No sample loss due to diffusion could be assumed. Therefore, the peak area obtained for axial diffusion alone was set constant and can be set equal to one.

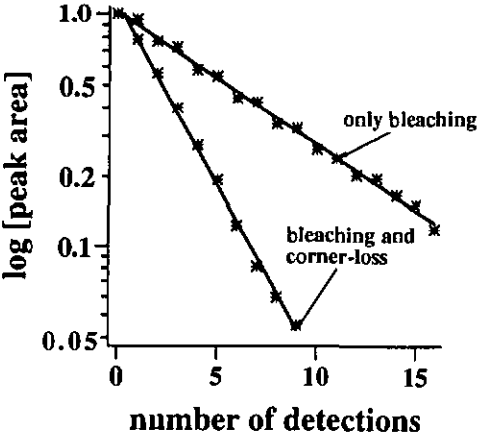

Figure 5.16 Comparison of the peak areas obtained from data in Figs. 5.1 and 5.8 as a function of the number of detections. The graph representing the data of a sample plug exposed to the detection system (and therefore bleached) is indicated as "only bleaching". The graph indicated as "bleaching and corner loss" was obtained by the integration of each of the peaks obtained by moving the sample ten times around the structure CYCE3. The lines indicate fits calculated for these data. The fit parameters are given below.

The fit function for Figure 5.16 is given by

$$\log\{\text{peak area}\} = K_0 + K_1 \cdot t \qquad (5.4)$$

with $K_0 = 0.1 \pm 0.04$ and $K_1 = -0.36 \pm 0.01$ for "bleaching and corner-loss"
and $K_0 = 0.02 \pm 0.002$ and $K_1 = -0.13 \pm 0.002$ for "only bleaching"

The slope of both graphs given in Figure 5.16 determines the decrease in peak area as a function of detection number. It should be noted for interpretation of the data that between each measured point on the graph "bleaching and corner loss", the sample was moved around one complete cycle. This must be considered for the interpretation of the obtained data. The values for the loss of sample due to bleaching and corner loss can be calculated to be:

loss of sample due to bleaching: -13 ± 3 % for each detection process
loss of sample due to the corner effect (CYCE3): -23 ± 0.01 % for each completed cycle

As a result of this experiment, it was concluded that the detection process itself reduced the amount of detectable sample by 13 %. This could be avoided by using the detection system only at the very end of a separation loop. In other words, the laser must be kept switched off until the very end of a separation. Therefore, it is necessary to ensure that the switching process is very precise, so as to make it unnecessary to observe the peak of interest each time passing the detection point. Another solution to this problem, of course, is to implement a different detection scheme, such as refractive index measurement. Preliminary results obtained with such a detection scheme are presented in section 5.4.
Loss of sample at the corner (CYCE3) or T-junction (CYCE2) could be reduced using counter voltages applied to the side channels. This is necessary because a loss of sample amount of 23 % per cycle is unacceptable. First results obtained using a counter voltage setup are presented in section 5.4.3.

5.3.2 Photochemical bleaching of fluorescein

The effect of the photochemical degradation of fluorescein was also measured in the following experiment, the result of which is shown in Fig. 5.17. After the laser was turned off, the capillary underneath the detection system was filled with a solution of 100 µM fluorescein in 20 mM boric acid / 100 mM Tris (pH 9.0). In the next step, the

sample flow was stopped and the data acquisition system was switched on. Finally, the laser was switched on again, causing a rapid increase of the acquired signal. Due to the bleaching effect this signal subsequently decreased very rapidly. This degradation can be fitted by an exponential-decay function (Eq. 5.5). Again, the laser power was set to a value of 6 mW.

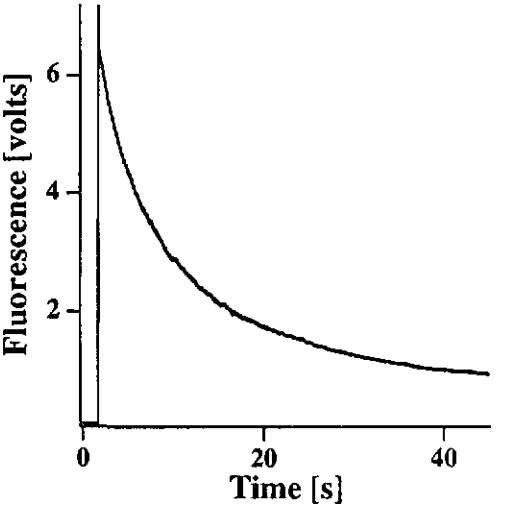

Figure 5.17 A typical decay function for the photochemical degradation of a fluorescein sample. The procedure for that measurement is explained above. The sample was 100 µM in 20 mM boric acid / 100 mM Tris (pH 9.0).

Ten successive measurements were performed and all data obtained were fit with the following fit-function:

$$\text{fit - function} = K0 + K1 \cdot \exp(-K2 * x) \tag{5.5}$$

This was resulting in a value for K2 of $0.13 \pm 0.01\ s^{-1}$.

This is equal to a loss of sample due to bleaching of $13 \pm 0.01\ \% s^{-1}$.
In the previous measurement, a value for the loss of sample per detection was found to be 13 %. At first glance, this is the same value as found above. However, the two values should be interpreted differently.
For the detection scheme used for all of these experiments, it was never possible to illuminate only the geometrically defined detection length of 40 µm (defined by the

objective and the used pinhole). Usually the laser beam was adjusted to illuminate a certain length of the separation channel. This length was in the range of approximately 2 to 3 mm. The plug observed to get the results shown in Fig. 5.1 therefore never left the illuminated area of the main channel and was bleached continually. This corresponds with the experimental setup for the photochemical decay experiment in Fig. 5.17 where one detection point was also illuminated all the time. Nevertheless, both values are comparable only in the case when the sample needs one second to pass the illuminated area of the separation channel during one detection.

5.3.3 The application of counter voltage

The number obtained for the loss of sample due to corner loss shows that there is a need to reduce or better yet, prevent this effect completely. Again, a VCR system was used and the camera was positioned over the intersection of a side channel and the main channel (T-junction) on the structure CYCE2. Successive injections (electrokinetic injection type) were performed, and the plug moved along the main channel to pass the T-junction. A printout of two of these pictures obtained was already shown in Figure 3.7. It was found that for structure CYCE2, loss of sample occurred when a sample plug passed this intersection. During the observation of the intersection a counter voltage was applied, which set a potential at the intersection such that a slight counter flow of buffer out of the side channel towards the main channel was generated. Now no sample loss was observed anymore. A careful observation of this counter flow showed that the peak was diluted due to a flow of buffer towards the main channel. Changing the value of the counter voltage by just a few volts (less than ten volts) reversed the flow. With this setup, then, it was possible to get an indication of the sensitivity required for flow control through the application of a counter voltage.

Monitoring solution flows was facilitated at times by the appearance of minuscule dust particles, which were clearly visible. The location of a particle could be controlled very precisely by changing the counter voltage in an appropriate way. A particle could be moved back and forth within the side channel, while buffer flowed through the main channel. This experiment clearly showed the possibility for advanced fluid handling with volumes ranging in the order of nanoliters (the volume of one side channel of CYCE2 was calculated to be 21 nL).

It was possible, then, to distinguish three different situations, depending on the applied counter voltage:

1) flow out of the side channel towards the main channel
2) equilibrium; no flow within the side channel
3) flow from the main channel towards the side channel

To obtain values for the counter voltage needed to achieve a particular flow, it was necessary to know the electrical resistance of each side channel. These values could be determined by applying a voltage to various pairs of electrodes and measuring the current. As already explained in sections 4.3.1 and 5.1.1, it was possible to calculate the various electrical resistances from such a set of current measurements. With values for the electrical resistances of the side channels, values for counter voltage could be calculated using Ohm's law. These values for each of the eight side channels were stored in a data file, which was automatically read during the initialisation phase of the switching control software before an experiment was started. In order to achieve a slight flow towards the main channel, for a separation voltage of 2'500 V the values for the counter voltages ranged from 476 V up to 2'036 V. One example is given in Table 5.4. It is necessary to remember that a sample of interest passes two side channels within one voltage switching phase. Therefore, it is necessary to control the counter voltages applied to two side channels only during one voltage switching phase. An exception to this rule is given for phase 1 of the first cycle. There, the component must pass three side channels instead of two due to the initial offset time added to the switching time for that phase. Again, it is assumed that the switching occurs when the sample of interest is at a corner of the device.

Table 5.4

counter voltage applied to:	phase 1	phase 2	phase 3	phase 4
first side channel passed	2'036* V 1'322 V	1'190 V	1'187 V	1'308 V
second side channel passed	1'144 V	1'010 V	476 V	598 V

Example for the calculated values obtained for the counter voltage which must be applied to the side channels passed by the sample of interest during the corresponding switching phase. *During the very first phase the sample has to pass three side channels due to the initial offset time.

Figure 5.18 shows two injections detected on structure CYCE2, after the sample plug has passed the first three side channels (see Figure 5.6). One injection (a) was performed without application of counter voltage to these side channels and one (b) was obtained with counter voltage.

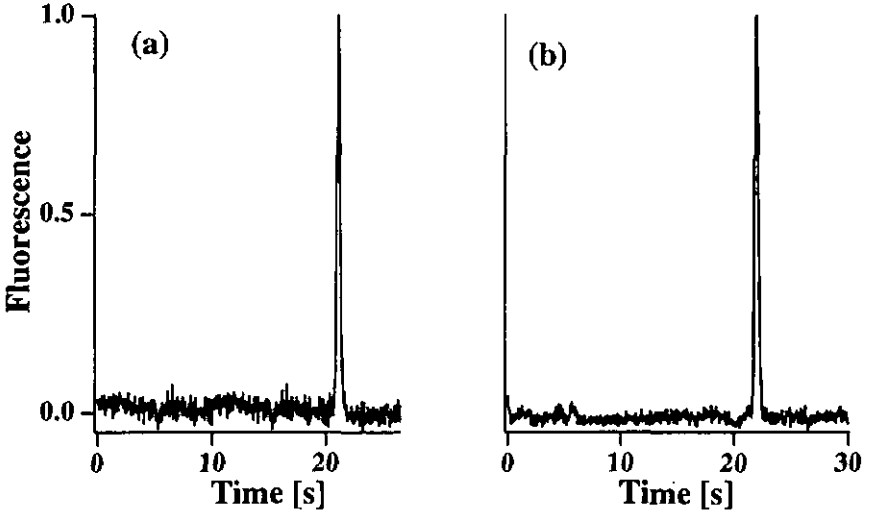

Figure 5.18 Injected sample of fluorescein detected after passing the two side channels on the left-hand side of structure CYCE2. (a) shows the case without application of any counter voltage (b) with counter voltage.

During the experiment, the order of runs with and without counter voltage was random, to exclude any systematic effects. Ten experiments were performed using counter voltage and five were performed without counter voltage.

Integration over the peak areas were resulting into the following values for:
(a) without counter voltage 0.16 ± 0.06
(b) with counter voltage 0.30 ± 0.09.

The peak area obtained in the case with application of a counter voltage was twice as large as the case without counter voltage.

It was much easier to control the potential of two side channels than doing the same procedure for a complete cycle in which eight side channels must be considered.

Figure 5.19 shows an overlay of two electropherograms obtained by moving a single component (fluorescein, 100 μM) around structure CYCE2 for two and a quarter cycles. This overlay contains both cases, with and without counter voltage. For this experiment, it was necessary to stay on the "safe side" while applying a counter voltage. Remembering the three possible cases of flow caused by application of counter voltage, one has to exclude the case of flow towards the side channel, which would move the sample plug out of the system. Therefore, the counter voltage was chosen to cause a slight flow towards the main channel resulting in additional broadening of the measured peak.

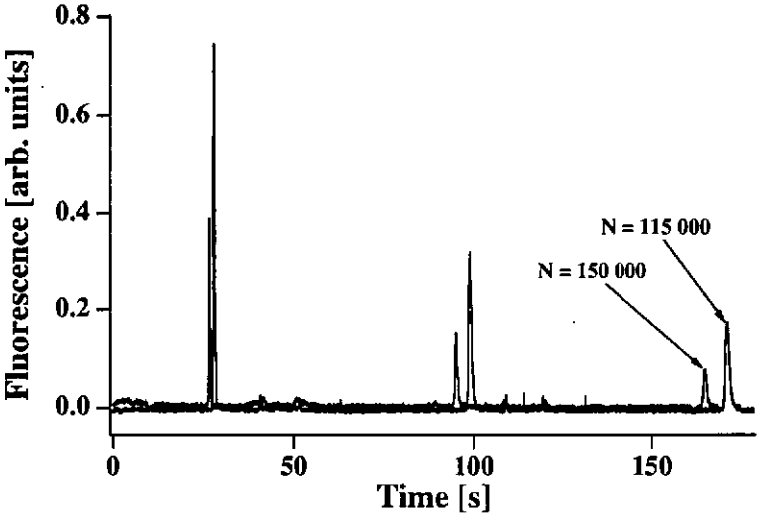

Figure 5.19 Overlay of two cycling experiments with and without counter voltage. The higher but broader peaks were obtained with the application of counter voltage. The smaller but less broad peaks represent the case with no counter voltage applied.

With the application of counter voltage, the peak area measured was increased by a factor of two. The theoretical number of plates obtained was only 75% of the value calculated for the case without any counter voltage. This results from the additional bandbroadening caused by buffer flow towards the main channel and into the sample zone.

final remarks about the application of counter voltage

The application of counter voltages and therefore complete control of the potential at all electrodes seems to be a solution to the corner loss problem. However, it is much more complicated to achieve than expected. It was never possible to drive a sample around the structure for more than two and a quarter cycles. A small change in electrical resistance (which cannot be excluded for resistances in the order of GΩ) reversed the counter flow, resulting then in a loss of the sample which was much worse than 23% per cycle. At this point, it might be necessary to stress another fundamental systematic problem of the counter voltage setup used. As already explained, the electrical resistances of all channels were determined by performing current measurements before any cycling experiment was started. Later changes of any of the resistances during an experiment could not be taken into account and might result in reversing the flow direction within a side channel. Therefore, it would be better to build an on-line control which enables changes to the applied counter voltage during a separation.

5.3.4 Comparison of the two layouts CYCE2 and CYCE3

The results describing bandbroadening due to the corner effect and sample losses as a result of device geometries allow a brief comparison of the differences between the two layouts used for these experiments. The advantage of CYCE3 lies in the fact that there are only four locations (the four corners) which influence peak shape and therefore separation efficiency. This number neglects the intersection of the injection channel with the main channel. It was found for CYCE3 that a loss of sample occurs at the corners. In addition, an "amputation" of the sample occurs, which means that the peak width after passing the corner was smaller than before. Additional studies are required to fully describe what happens when the peak passes the nozzle-like corner. CYCE2 in comparison has in total 12 locations where the peak can be altered in some way (eight side channels and four corners). The influence of the T-junctions especially was expected to be much lower than experimentally observed. Applying a counter voltage (see section 5.3.3) could reduce or, in the optimum case, prevent the adverse effect of the T-junction on sample bandbroadening and loss.
Another difference already explained in section 3.2.4 shows that due to their geometries, slight differences in detection windows are apparent. A main disadvantage of layout CYCE3 with respect to the detection window results from the fact that there might exist a mobility interval in the sample which will never leave the separation channel. Under other circumstances, this property could prove to be

beneficial, allowing the device to be used as a microreactor [AVI 93], [BAO 92]. In the CYCE2 case, all components outside the detection window will leave the channel without any interference to the remaining sample.
A combination of advantageous characteristics of both layouts should result in better separation efficiencies. This would include longer side channels to reduce the relative influence of any bandbroadening caused by a corner. It is also clear that improved device design would include fewer side channels intersecting with the main channel. One possible route to accomplishing this has already been demonstrated in CYCE3, where two side channels intersect the main channel at one location. Similar considerations will be incorporated into future designs.

5.4 Results obtained with the RI detection system

5.4.1 Injection of a single component

The results obtained with the RI detection system are preliminary results demonstrating the feasibility of other detection schemes in chip-based separation systems. Using the setup described in section 4.2.2, it was possible to perform the injections shown in Figure 5.20.

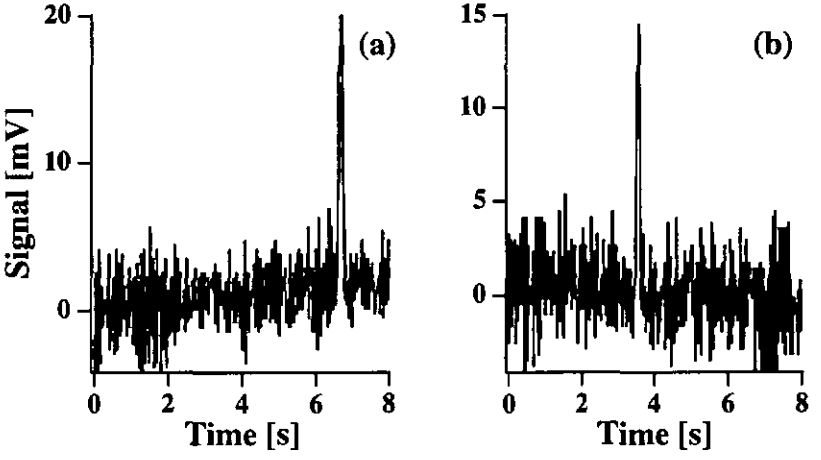

Figure 5.20 Injection of a sample of sucrose (concentration ≈ 30 mM) in 20 mM boric acid / 100 mM Tris (pH 9.0), detected with the RI detection system with two different electrical field strengths in the separation channel. The injection was performed using 1'000 V for 15 s. (a) Electric field strength 500 V/cm, L = 20 mm. (b) Electric field strength 1'000 V/cm, L = 20 mm.

The repetitive injection of four peaks for each electric field strength results in the following measurable values describing also the reproducibility of the geometrically defined injection process:

for E = 1'000 V/cm

σ = 0.02 ± 0.002 s

t_{max} = 3.54 ± 0.01 s

and for E = 500 V/cm

σ = 0.05 ± 0.001 s

t_{max} = 6.68 ± 0.01 s

Therefore, the number of theoretical plates obtained can be calculated to be:

N = 31'300 ± 20% for E = 1'000 V/cm

N = 17'800 ± 4% for E = 500 V/cm

5.4.2 Preliminary results

Figure 5.21 shows a separation performed using only the first quarter of the cycle (20 mm). The sample was a mixture of sucrose, N-acetyl-glucosamine, and raffinose, each with a concentration of 33 mM. The buffer used for this experiment was chosen to be a 100 mM $B(OH)_3$ buffer adjusted with 1 M NaOH to a pH of 9 [KLO 94].

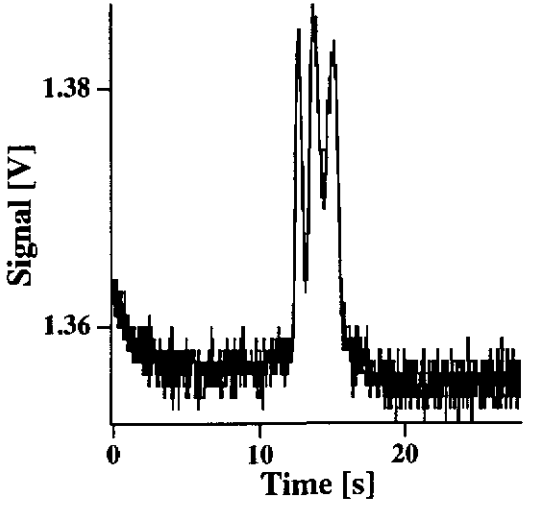

Figure 5.21 This figure shows the separation of a sugar sample (sucrose, N- acetyl-glucosamine and raffinose) at a concentration of 33 mM each moved along one quarter of the structure CYCE2. E = 500 V/cm, L = 20 mm.

Work with the RI-detection system was performed at the very end of the work done for this thesis. It was not a goal to achieve very good detection limits, but rather to show that in principle the system of SCCE is open to detection schemes other than the laser-induced fluorescence detection. Thus, the RI setup was not optimized. However, a detection limit in the lower μM range can be estimated from the data obtained from [BRU 94] for the raffinose peak These preliminary results look very promising and it would be very interesting to combine several different detection schemes into one setup.

Chapter 6 Conclusion and Outlook

general conclusions

It was shown that micromachining technologies can be combined with the analytical technique of capillary electrophoresis to produce planar glass devices for CE. A new concept for synchronized cyclic capillary electrophoresis system was realized and demonstrated. Two cyclic layouts were designed and fabricated. A setup for testing these first cyclic devices was built, and the devices were tested. A single component was cycled around the structure using only electrokinetic forces as a pump. It was shown that synchronizing the system to a specific mobility interval of injected components using a specific synchronization time results in an increase of resolution. Therefore, "focusing" a separation to a specific mobility is possible.

separation with SCCE

Using the SCCE system, it was possible to achieve rapid separation times ranging from minutes to seconds. It was shown that with this method, high plate numbers can be obtained using low voltages for the separation process. This could be accomplished by using the cyclic device to simulate a capillary of infinite length with a constant electric field strength. For example, a sample plug of fluorescein was cycled around the device 10 times, to yield an N of 1'300'000. This experiment simulated a capillary 80 cm long with a constant electrical field strength of 500 V/cm. No separations in which such high plate numbers were required to achieve resolution of sample components were carried out. Nevertheless, it was shown that SCCE can be used to perform separations similar to conventional CE.

liquid handling

Controlled liquid handling could be performed by changing the synchronization time. Correlation between theory and experimental result showed that precise prediction of the path traveled by each component is possible. This indicates that the system can be used for fraction collection [EFF 95b]. Further development is necessary to achieve a completely controlled system for the liquid handling. This includes further examination of the utility of counter voltage application for prevention of sample loss. A possible approach for future experiments would be a setup similar to the Wheatstone bridge for measuring unknown resistances. For such a setup, all reservoirs must be hooked up to high voltage supplies via an amperometer. The voltage at which no current is measured with this amperometer is then the counter voltage required to implement a "no-flow" situation at intersecting channels. This would then allow an

on-line control and adjustment of the applied counter voltage. A more precise control of all flows within the channels during a separation would be possible.

non-idealities

The different non-idealities like "corner effects" and "corner losses" were studied in various experiments. After initial experiments with layout CYCE3, the examination of the "corner effects" and "corner losses" were performed using structure CYCE2. Bandbroadening was determined due both by passing a corner and a T-junction were determined. The loss of sample at a T-junction could be reduced using a setup with counter voltage. In general, the bandbroadening of a sample peak caused by passing a corner was much higher than theoretically expected. Therefore, further experiments are necessary to obtain more reliable data for the examination of the bandbroadening caused by the "corner effect".

remarks regarding future layouts

The two cyclic layouts were first approaches for the verification of the idea of SCCE. It was found that both layouts have their characteristic non-idealities. For future layouts, it was concluded that an increase in the length of the channels would be advantageous. This would reduce the relative influence resulting from any corner effect and therefore increase the separation efficiency. The advantage of distinguishing strictly between side channels serving as inlets or outlets for the electrolyte was shown. For a future design, however, it is suggested to use different channels for inlets and outlets but combine them into one channel near the main channel so as to form only one T-junction. This would reduce the number of T-junctions, and therefore their contribution to any sample loss or bandbroadening.

detection schemes

Besides the laser-induced fluorescence detection scheme based on conventional optical components, a hologram-based refractive index measurement was tested. Neither detection scheme was optimized.

Further investigations should also include feasibility studies of absorbance detection. This would expand the number of possible analytes that could be analyzed using the SCCE system enormously. In the future, a combination of all three optical detection schemes (fluorescence, refractive index and absorbance) could be combined into one detection system, resulting in a truly universal detection unit. Finally, the feasibility of integrated optics would allow the miniaturization of the detection system and would make the integration of this instrument into a single chip possible.

final conclusions and outlook

The idea of synchronized cyclic capillary electrophoresis was realized and proven feasible. The theoretical advantages of the system were demonstrated, though unexpected problems in device design were discovered. Thus, a future direction of this research should involve development of new layouts for SCCE. Further optimization of the technique will allow clear demonstration of the impact this capillary electrophoresis technique will have on laboratory separation systems and on-line monitoring of chemical components.

Summary

A novel concept for repeated column switching in capillary electrophoresis is presented. Using micromachining techniques, two different types of planar glass structures have been fabricated (CYCE2 and CYCE3), which contain four capillaries of 20 mm length arranged in a square. This square-shaped channel is used as a separation channel. Eight side channels intersected this separation channel, serving as inlets and outlets for electrolyte. Another channel crossing the main channel perpendicular to the midpoint of one side of the square is used for sample injection. At the end of each side channel, a reservoir was placed, into which the electrodes to apply a voltage to the various channels were immersed. By switching the electrodes to which the voltage is applied, it is possible to move an injected sample around the separation channel using only electrokinetc forces.

Theoretical considerations predict the achievement of high plate numbers. After moving a single component around the structure for ten cycles, 1'300'000 theoretical plates were obtained. Separations of FITC-labelled amino acids were used to clarify the principle of SCCE. It was possible to perform rapid separations with separation times ranging from some minutes down to a few seconds. The theoretically predicted focusing of the detection window over a number of cycles onto a very narrow mobility band within the sample, as dictated by the synchronisation time set for voltage switching, was demonstrated. It was shown that the system can be used for fluid handling in the nL and sub-nL volume range.

Non-idealities such as bandbroadening due to the sample plug passing a corner, and the loss of sample at the T-junctions (CYCE2) or at the corner (CYCE3), were examined. The magnitude of most of these effects were determined.

Laser-induced fluorescence as well as hologram-based refractive index measurements were used as detection methods.

Appendix

A1 Conversion between equations in the CGS unit-system and SI unit-system (selection nf some equations and symbols) [JAC 83b].

	CGS unit-system	SI unit-system
Poisson equation	$\Delta\Phi = -\frac{4\pi}{\varepsilon}\rho$	$\Delta\Phi = -\frac{\rho}{\varepsilon_0}$
electrical field (potential, potential difference)	$E(\Phi,V)$	$\sqrt{4\pi\varepsilon_0}\,E(\Phi,V)$
dielectric constant	ε	$\frac{\varepsilon}{\varepsilon_0}$
conductivity	σ	$\frac{\sigma}{4\pi\varepsilon_0}$
electroosmotic velocity	$v_{eo} = \frac{\varepsilon\zeta}{4\pi\eta}E$	$v_{eo} = \frac{\varepsilon\varepsilon_0\zeta}{\eta}E$

with the dielectric constant $\varepsilon_0 = 8.854\ 10^{-12}$ As/Vm.

A2 Methods to control electroosmotic flow. *The abbreviation EOF stands for electroosmotic flow, *c* for concentration (table obtained from [NEI 92b] and modified).

Variable	Result	Comment
electric field	-proportional change in EOF*, if $\zeta \neq 0$ (ζ = zeta potential)	-separation efficiency and resolution may decrease when lowered -Joule heating may result when increased
pH	-EOF decreased at low pH and increased at high pH (for glass surfaces)	-most convenient and useful method to change EOF -may change charge of solute and therefore selectivity
ionic strength	-decreases zeta potential and EOF when increased	-high ionic strength generates high current and possible Joule heating -low ionic strength problematic for sample adsorption -contamination -instability of electrolyte if $c_{buffer} \leq 10^{-5}$ M -may distort peak shape if conductivity different from sample conductivity (if $c_{sample} > c_{buffer}$) -limits sample stacking if reduced
temperature	-changes viscosity 2-3% per °C, EOF increased if temperature increased	-often useful since temperature is controlled instrumentally
organic modifier	-changes zeta potential and viscosity (usually decreases EOF)	-complex changes, effect most easily determined experimentally -may alter selectivity

surfactant	-adsorbs to capillary wall via hydrophobic and/or ionic interactions -EOF can be increased or decreased	-anionic surfactants can increase EOF -cationic surfactants can decrease or reverse EOF -can significantly alter selectivity
neutral hydrophilic polymer	-adsorbs to capillary wall via hydrophobic interactions -EOF decreased by shielding	surface charge and increasing viscosity
covalent coating	-chemical bonding to capillary wall	-many modifications possible (hydrophilicity or charge) -stability often problematic

A3 Cleanroom classes [FIT 94]

cleanroom class	maximum number of particles						
	per cubic foot (≅ 28.32 l)					per liter	
100 000	-	-	-	100 000	300	3 500	10.6
10 000	-	-	-	10 000	70	350	2.5
1 000	-	-	-	1 000	7	35	0.2
100	-	750	300	100	-	3.5	-
10	350	75	30	10	-	0.35	-
1	35	7.5	3	1	-	-	-
maximum particle size in micrometer	0.1	0.2	0.3	0.5	5.0	0.5	5.0

A4 List of symbols

symbol	description	units	equation	page
v	velocity	m s^{-1}	(1.1)	8
E	electric field of strength	V m^{-1}	(1.1)	8
μ_i	effective mobility	m^2 V^{-1} s^{-1}	(1.1)	8
μ_{ep}	electrophoretic mobility	m^2 V^{-1} s^{-1}	(1.1)	8
μ_{eo}	electroosmotic mobility	m^2 V^{-1} s^{-1}	(1.1)	8
$\vec{F}_e$	electrical force	As V m^{-1}	(1.2)	8
q	charge	As	(1.2)	8
e	elementary charge	As	(1.2)	8
$\vec{F}_f$	frictional force	N	(1.3)	9
η	dynamic viscosity	kg m^{-1} s^{-1}	(1.3)	9
r_i	radius of the moving particle	m	(1.3)	9
f_i	friction coefficient	kg s^{-1}	(1.4)	9
v_{ep}	electrophoretic velocity	m s^{-1}	(1.6)	10
L_d	length of the capillary from the injection side to the detector	m	(1.6)	10
t_m	migration time	s	(1.6)	10
V	applied voltage	V	(1.8)	10
L_t	total length of the capillary	m	(1.8)	10
μ_1	total mobility of component 1	m^2 V^{-1} s^{-1}	(1.8b)	10
μ_2	total mobility of component 2	m^2 V^{-1} s^{-1}	(1.8b)	10
ζ	zeta potential	V	(1.9)	11
ε	dielectric constant of the medium		(1.9)	11
ε_0	dielectric constant for vacuum	As V^{-1} m^{-1}	(1.9)	11
N	number of theoretical plates		(1.10)	16
σ^2_{tot}	total variance of a measured Gaussian peak	m^2	(1.10)	16
σ^2_{diff}	contribution to bandbroadening due to axial diffusion	m^2	(1.11)	17
σ^2_{inj}	contribution to bandbroadening due to injection	m^2	(1.11)	17
σ^2_{det}	contribution to bandbroadening due to detection	m^2	(1.11)	17
σ^2_{temp}	contribution to bandbroadening due to temperature effects	m^2	(1.11)	17

σ^2_{ads}	contribution to bandbroadening due to adsorption	m^2	(1.11)	17
σ^2_{others}	contribution to bandbroadening due to other effects	m^2	(1.11)	17
D	diffusion coefficient	$cm^2\ s^{-1}$	(1.12)	17
μ_{tot}	overall mobility	$m^2\ V^{-1}\ s^{-1}$	(1.13)	17
L	migration distance	m	(1.14)	18
H	height equivalent to a theoretical plate	m	(1.15)	18
R_s	resolution		(1.18)	18
ΔL	difference in location	m	(1.20)	19
$\Delta\mu_{ep}$	difference in mobility	$m^2\ V^{-1}\ s^{-1}$	(1.21)	19
$\overline{L}$	mean distance	m	(1.21)	19
$\overline{\mu_{ep}}$	mean mobility	$m^2\ V^{-1}\ s^{-1}$	(1.22)	19
d	inner diameter of the channel	m	table 1.1	23
N_{max}	maximum achievable number of theoretical plates		table 1.1	23
σ^2_{bb}	all other contributions to the band broadening	m^2	table 1.1	23
Q	generation of heat per unit length	Wm^{-1}	(1.26)	24
γ	electrical conductivity	$\Omega^{-1}m^{-1}$	(1.26)	24
A	capillary cross section	m^2	(1.26)	24
L	length	m	table 1.2	26
A	area	m^2	table 1.2	26
V	volume	m^3	table 1.2	26
k	surface roughness		table 1.2	26
v	velocity	$m\ s^{-1}$	table 1.3	26
a	acceleration	$m\ s^{-2}$	table 1.3	26
m	mass	kg	table 1.3	26
t	time	s	table 1.3	26
F	force	N	table 1.3	26
ρ	density	$kg\ m^{-3}$	table 1.3	26
η	dynamic viscosity	$N\ s\ m^{-2}$	table 1.3	26
ν	kinematic viscosity	$m^2\ s^{-1}$	table 1.3	26
Re	Reynolds number		(1.27)	27
sw	number of voltage switchings		(2.1)	50
$L_{synch.}$	length to which the system is synchronized	m	(3.2)	60

L_{min}	minimum length allowed to move to stay within the GTW	m	(3.3)	60
L_{max}	maximum length allowed to move to stay within the GTW	m	(3.2)	60
$v_{synch.}$	velocity to which the system is synchronized	$m\ s^{-1}$	(3.2)	60
v_{min}	minimum velocity allowed to stay within the GTW	$m\ s^{-1}s$	(3.3)	60
v_{max}	maximum velocity allowed to stay within the GTW	$m\ s^{-1}$	(3.2)	60
$\mu_{synch.}$	mobility to which the system is synchronized	$m^2\ V^{-1}\ s^{-1}$	(3.2)	60
μ_{min}	minimum mobility allowed to stay within the GTW	$m^2\ V^{-1}\ s^{-1}$	(3.3)	60
μ_{max}	maximum mobility allowed to stay within the GTW	$m^2\ V^{-1}\ s^{-1}$	(3.2)	60
μ_0	mobility to which the system is synchronized	$m^2\ V^{-1}\ s^{-1}$	table 3.4	71
σ^2_{side}	contribution to bandbroadening due to axial diffusion along one side	m^2	(3.9)	80
σ^2_{corner}	contribution to bandbroadening due to corner effects	m^2	(3.9)	80
$\sigma^2_{T\text{-}side}$	contribution to bandbroadening due to a T-junction	m^2	(3.9)	80
V_{inj}	injected volume	$m^3\ s^{-1}$	(4.1)	101
$U_{main\_ch.}$	voltage drop at main channel	V	(5.1)	105
$U_{appl.}$	voltage applied	V	(5.1)	105

A5 List of abbreviations

abbreviation	complete name
CE	capillary electrophoresis
SCCE	synchronized cyclic capillary electrophoresis
TAS	total analysis system
CAPS	cyclohexylamino-propanesulfonic acid
CSEM	Centre Suisse d'Electronique et de Microtechnique, Neuchâtel
CYCE1	cyclic capillary electrophoresis device 1
CYCE2	cyclic capillary electrophoresis device 2
CYCE3	cyclic capillary electrophoresis device 3
FITC	fluorescein isothiocyanate
IMT	Institute de Microtechnique, Neuchâtel
ISFET	ion selective field effect transistor
HPLC	high pressure liquid chromatography
LC	liquid chromatography
µ-TAS	miniaturized total analysis system
OPA	o-phthaldialdehyde
RI	refractive index
TRIS	2-amino-2-hydroxymethyl-1,3-propanediol

A6 Layout and dimensions of the structures CYCE1, CYCE2, CYCE3

layout CYCE2 (dimensions given in mm)

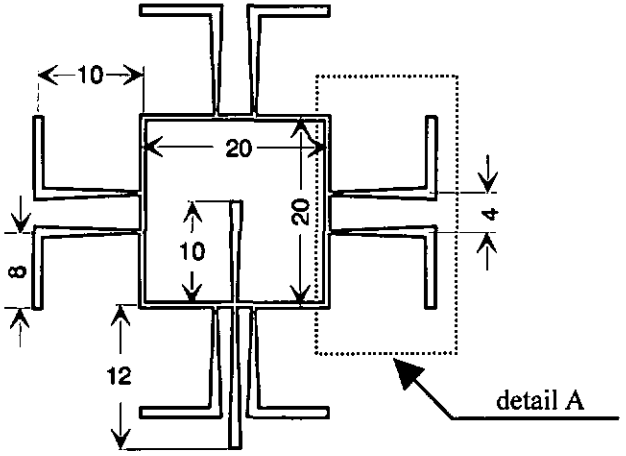

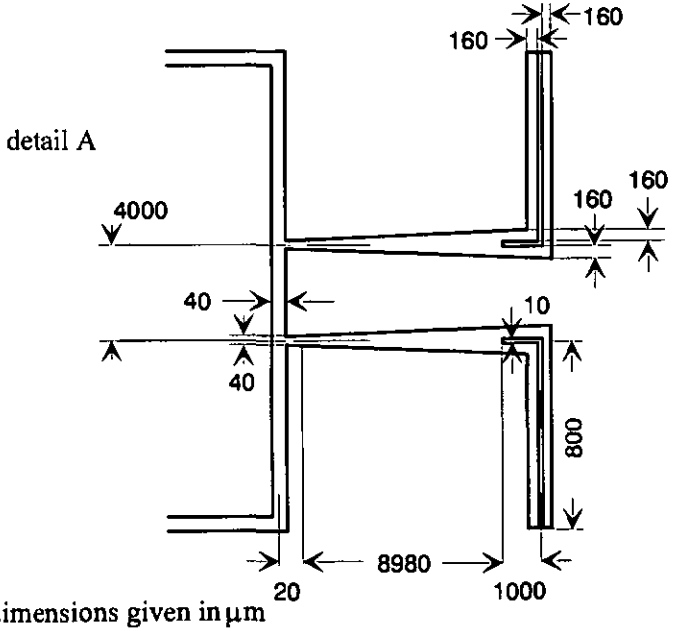

dimensions given in μm

layout CYCE3 (dimensions given in mm)

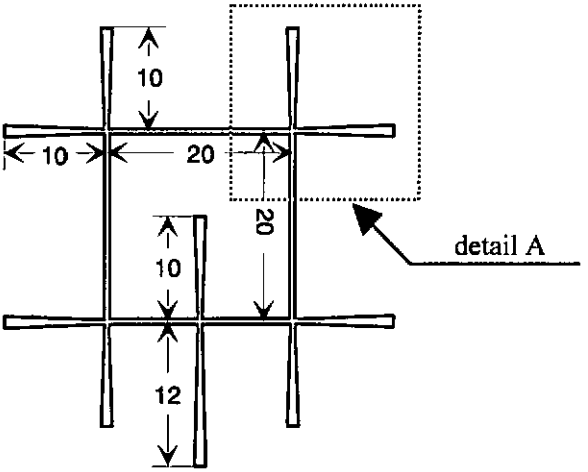

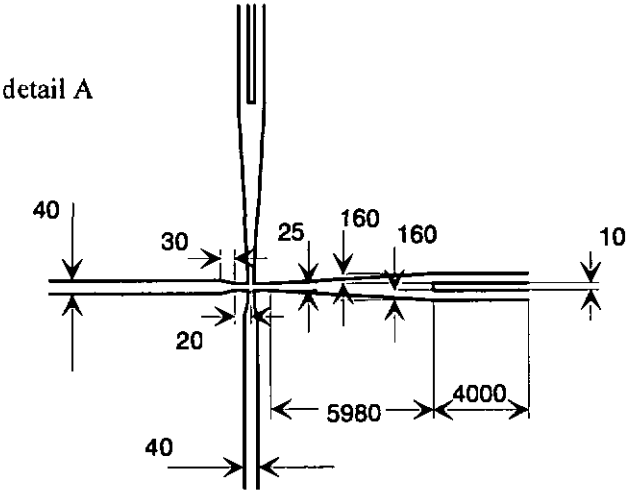

dimensions given in µm

layout CYCE1 (dimensions given in mm)

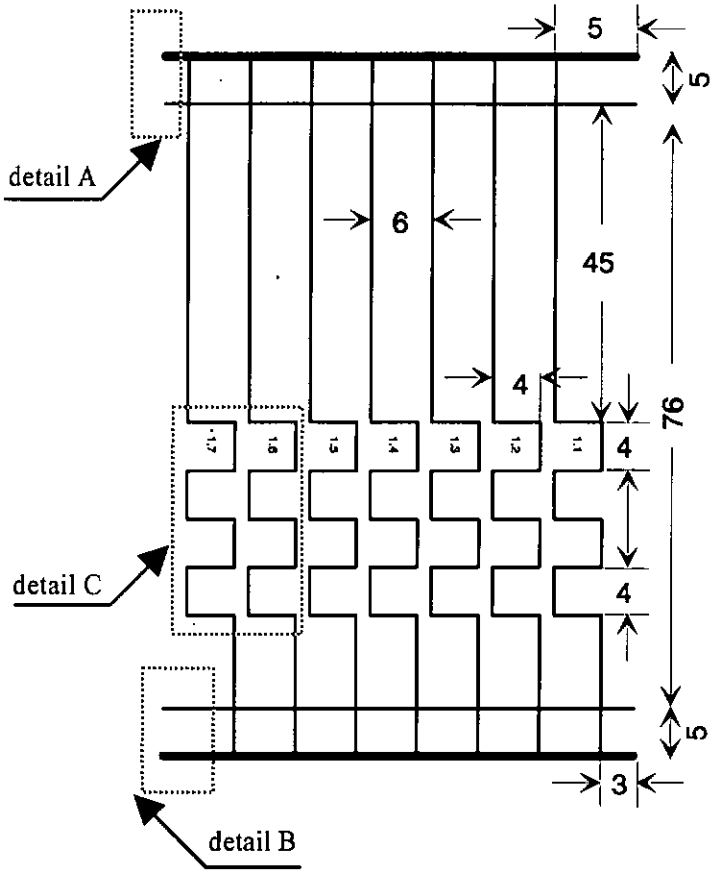

detail A

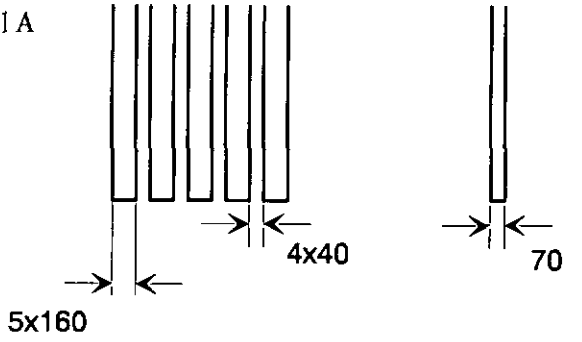

detail B

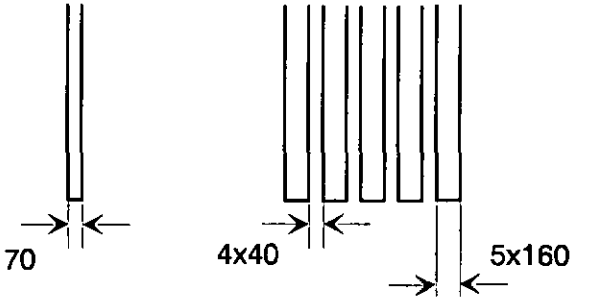

detail C

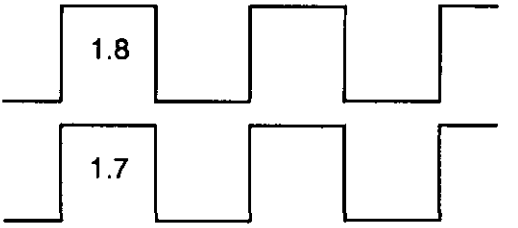

for more details
see "corner design"
for layout CYCE1

corner design for CYCE1

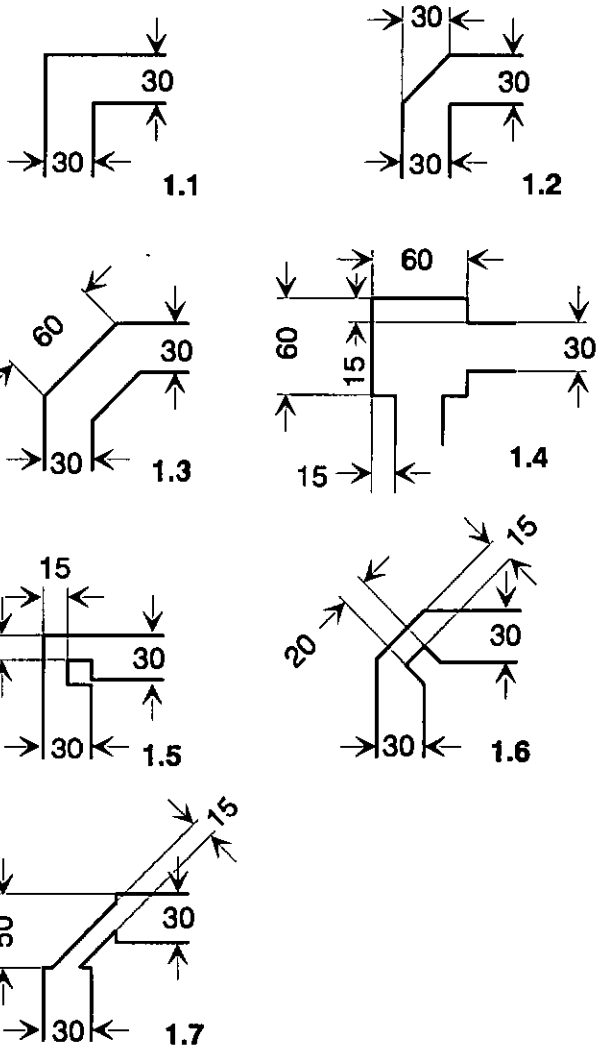

dimensions given in µm

References

[ALT 63] Altmann, J.P.; *Das neue Lehrbuch der Glasätzerei*, Verlag A.W. Gentner, Stuttgart, Germany (1963) 29-69.

[AND 93] Andreev, V.P.; Lisin, E.E.; *Chromatogrophio*, 37 (1993) 202-210.

[AVI 93] Avila, L.Z.; Whitesides, G.M.; *J. Org. Chem.*, 58 (1993) 5508-5512.

[BAO 92] Bao, J.; Regnier, F.E.; *J. Chromatogr.*, 608 (1992) 217-214.

[BEC 91] *Introduction to Capillary Electrophoresis*, Beckmann Handbook (1991).

[BER 75] Bergmann Schäfer; *Lehrbuch der Experimentolphysik*, Bd. 1, Mechanik, Akustik, Wärme, H. Gobrecht, de Gruyter, Berlin, Germany, (1975) 344.

[BER 90] Bergethon, P.R.; Simons, E.R.; *Biophysical Chemistry*, Springer Verlag, New York (1990) 258-266.

[BER 94] Van den Berg, A.; Van der Wal, P.D.; Van der Schoot, B.H.; de Rooij, N.F.; *Sensors Materials*, 6 (1994) 23-43.

[BER 95] van den Berg, A.; Bergveld, P. (eds.); *Micro Total Analysis Systems*, Kluwer Academic Publishers, The Netherlands (1995).

[BIR 60] Bird, E.B.; Stewart, W.E.; Lightfoot, E.N.; *Transport Phenomena*, John Wiley and Sons, New York (1960) 160.

[BOH 91] Bohl, W.; *Technische Strömungslehre*, Vogel Fachbuch Verlag, Würzburg, Germany (1991) 112-114.

[BOU 86] Bousse, L.; Meindl, J.D.; in Davis, J.A.; Hayes, K.F. (eds.); *Geochemical Process at Mineral Surfaces*, Chemical Society, Washington DC (1986) 79-98.

[BOU 91] Bousse, L.; Mostarshed, S.; *J. Electroanal. Chem.*, 302 (1991) 269-274.

[BRO 84] Bronstein, I. N.; Semendjajew, K.A.; *Taschenbuch der Mathematik*, Verlag Harri Deutsch, Thun, Switzerland (1984) 159.

[BRU 91] Bruno, A.E.; Krattiger, B.; Maystre, F; Widmer, H.M.; *Anal. Chem.*, 63 (1991) 2689-2697.

[BRU 94] Bruno, A.E.; Maystre, F.; Krattiger, B.; Nussbaum, P.; Gassmann, E.; *Trends Anal. Chem.*, 13 (1994) 190-198.

[BUR 93a] Burggraf, N.; Manz, A.; de Rooij, N.F.; Widmer, H.M.; *Anal. Methods Instrum.*, 1 (1993) 55-59.

[BUR 93b] Burggraf, N.; Manz, A.; de Rooij, N.F.; Widmer, H.M.; *Transducers '93* Digest of Technical Papers, ed. Institute of Electrical Engineers of Japan, Tokyo (1993) (ISBN 4-9900247-2-9) 399-402.

[BUR 93c] Burggraf, N.; Manz, A.; Effenhauser, C.S.; Verpoorte, E.; de Rooij, N.F.; Widmer, H.M.; *J. High Resolut. Chromatogr.*, 16 (1993) 594-596.

[BUR 94] Burggraf, N.; Manz, A.; Verpoorte, E.; Effenhauser, C.S.; Widmer, H.M.; de Rooij, N.F.; *Sensors and Actuators B*, 20 (1994) 103-110.

[BÜT 91] Büttgenbach, S.; *Mikromechanik*, Verlag B.G. Teubner, Stuttgart, Germany (1991).

[CHA 13] Chapman, D.L.; *Phil. Mag.* ("The London, Edinburgh and Dublin Philosophical Magazine and Journal of Science"), 25 (1913) 475-481.

[COW 95] Cowen, S.; Craston, D.; in Van den Berg, A.; Bergveld, P. (eds.), *Micro Total Analysis Systems*, The Netherlands (1995) 295-298.

[CUL 94] Culbertson, C.T.; Jorgenson, J.W.; *Anal. Chem.*, 66 (1994) 955-962.

[DEL 48] Delahay, P.; *Bull. Soc. Chem.*, 15 (1948) 348-350.

[DOS 93] Dose, E.V.; Guiochon, G.; *J. Chromatogr.*, A652 (1993) 163-275.

[EDM 85] Edmonds, T.E.; *Trends Anal. Chem.*, 4 (1985) 220-224.

[EFF 93] Effenhauser, C.S.; Manz, A.; Widmer, H.M.; *Anal. Chem.*, 65 (1993) 2637-2642.

[EFF 94a] Effenhauser, C.S.; Paulus, A.; Manz, A.; Widmer, H.M.; *Anal. Chem.*, 66 (1994) 2949-2953.

[EFF 94b] Effenhauser, C.S.; *Anal. Methods Instrum.*, 1 (1994) 172-176.

[EFF 95a] personal communication with Effenhauser, C.S., Corporate Analytical Research, Ciba Geigy Ltd., Basel, Switzerland (1994).

[EFF 95b] Effenhauser, C.S.; Manz, A.; Widmer, H.M.; *Anal. Chem.*, 67 (1995) 2284-2287.

[EKS 90] Ekström, B.; Jacobson, G.; Öhman O.; Sjödin, H.; international patent: WO 91/16966 (1990).

[FAN 94] Fan, Z.H.; Harrison, D.J.; *Anal. Chem.*, 66 (1994) 177-184.

[FET 93] Fettinger, J.C.; Manz, A.; Lüdi, H.; Widmer, H.M.; *Sensors and Actuators*, 17B (1993) 19-25.

[FIL 91] Fillipini, C.; Sonnleitner, B.; Fiechter, A.; Bradley, J.; Schmid, R.; *J. Biotechnology*, 18 (1991) 153-160.

[FIT 94] Fitzner, K., *Spektrum der Wissenschaft*, 10 (1994) 104-108.

[FLU 93] Fluka chemicals catalogue 1993, Fluka Chemie Ltd., Buchs, Switzerland.

[FOR 89] F. Foret; P. Bocek; in Chrambach, A.; Dunn M.J.; Radola, B.J. (eds.), *Advances in Electrophoresis*, Vol. 3, VCH Verlagsgesellschaft, Weinheim, Germany (1989) 271-347.

[GER 82] Gerthsen; Kneser; Vogel; *Physik*, Springer Verlag, berlin, Germany (1982) 417.

[GID 91] Giddings, J.C.; *Unified Separation Science*, John Wiley & Sons, New York, 1991.

[GLO 77] Glöckner, W.; *Chemie*, Fischer Kolleg 4, Fischer Taschenbuch Verlag, Frankfurt am Main, Germany (1977) 89.

[GOU 17] Gouy, M.G.; *Ann. de Phys*,. 9e serie, t. VII. (Mars-Avril 1917), 129-184.

[GRA 90] Graber, N.; Lüdi, H.; Widmer, H. M.; *Sensors & Actuators*, B1 (1990) 239-243.

[GUI 83] Guilbault, G.G.; *Anal. Chem. Symp. Ser.*, 17 (1983) 637.

[HAR 91] Harrison, D.J.; Manz, A.; Glavina, P.G.; *Transducers '91*, Digest of Technical Papers, IEEE 91CH2817-5, New York (1991) (ISBN 0-87942-586-5) 792-795.

[HAR 92a] Harrison, D.J.; Manz, A.; Fan, Z.; Lüdi, H.; Widmer, H.M.; *Anal. Chem.*, 64 (1992) 1926-1932.

[HAR 92b] Harrison, D.J.; Manz, A.; Fan, Z.; Luedi, H.; Widmer, H.M.; *Anal. Chem.*, 64 (1992) 1926-1932.

[HAR 93a] Harrison, D.J.; Fluri, K.; Seiler, K.; Fan, Z.; Effenhauser, C.S.; Manz, A.; *Science*, 261 (1993) 895-897.

[HAR 93b] Harrison, D.J.; Fan, Z.; Seiler, K.; Manz, A.; Widmer, H.M.; *Anal. Chim. Acta*, 283 (1993) 361-366.

[HAR 93c] Harrison, D.J.; Glavina, P.G.; Manz, A.; *Sens. Actuators B*, 10 (1993) 107-116.

[HEC 87] Hecht, E.; *Optics*, Addison-Wesley Publishing Company (1987) 576.

[HEL 79] Helmholtz, H.; *Ann. d. Phys. u. Chem.*, 7 (1879) 337-382.

[HEW 94] Hewlett Packard, Palo Alto, CA, USA, US-patent No.: US-5,328,578, priority date: Jul. 12, 1994

[HIR 76] Hirschfeld, T.; *Applied Optics*, 15 (1976) 3135-3139.

[HOG 94] Hogan, B.L.; Lunte, S.M.; *Anal. Chem.*, 66 (1994) 596-602.

[HOY 84] HOYA Corporation electronics division, product information for precision-polished glass substrates (1984).

[JAC 83a] Jackson, J.D.; *Klassische Elektrodynamik*, de Gruyter, Berlin, Germany (1983) 37.

[JAC 83b] Ref. [JAC 83a] p. 980.

[JAC 94a] Jacobsen, S.C.; Hergenröder, R.; Koutny, L.B.; Ramsey, J.M.; *Anal. Chem.*, 66 (1994) 1114-1118.

[JAC 94b] Jacobsen, S.C.; Koutny, L.B.; Hergenröder, R.; Moore, A.W. Jr.; Ramsey, J.M.; *Anal. Chem.*, 66 (1994) 3472-3476.

[JAC 94c] Jacobsen, S.C.; Hergenröder, R.; Koutny, L.B.; Ramsey, J.M.; *Anal. Chem.*, 66 (1994) 2369-2373.

[JAC 94d] Jacobson, S.C.; Hergenroder, R.; Moore, A.W. Jr.; Ramsey, J.M.; *Anal. Chem.*, 66 (1994) 4127-4132.

[JAC 94e] Jacobson, S.C.; Hergenroder, R.; Koutny, L.B.; Warmack, R.J.; Ramsey, J.M.; *Anal. Chem.*, 66 (1994) 1107-1113.

[JAN 89] Jansson, M.; Emmer Å.; Roeraade J.; *J. High Resolut. Chromatogr.*, 12 (1989) 797-801.

[JOR 81] Jorgenson, J.W.; Lucacs K.D.; *J. Chromatogr.*, 218 (1981) 209-216.

[KLO 94] personal communication with Klockow-Beck, A., Corporate Analytical Research, Ciba Geigy Ltd., Basel, Switzerland (1994).

[KNA 90] Knapp, J.; Andreae, G.; Petersohn, D.; *Sensors & Actuators*, A21-A23 (1990) 1080-1083.

[KNE 90] Kneubühl, F.K.; *Repetitorium der Physik*, B.G. Teubner, Stuttgart, Germany (1990) 158-160.

[KOR 66a] Kortüm G.; *Lehrbuch der Elektrochemie*, Verlag Chemie GmbH, Weinheim, Germany (1966) 167.

[KOR 66b] Ref. [KOR 66a] p. 407.

[KOR 66c] Ref. [KOR 66a] p. 186.

[KOU 95] Koutny, L.B.; Taylor, T.A.; Schmalzing, D.; Nashabeh, W.; Yao, X.-W.; Fuchs, M.; poster presented on the HPCE' 95, January 29 - February 2, 1995, Würzburg, Germany, poster No. P-401.

[KRA 94a] Krattiger, B.; Bruin, G.J.M.; Bruno, A.E.; *Anal. Chem.*, 66 (1994) 1-8.

[KRA 94b] Krattiger, B.; dissertation, University of Neuchâtel, Institute of Microtechnology, Neuchâtel, Switzerland (1994).

[LI 92] Li, S.F.Y.; *Capillary Electrophoresis*, Elsevier, Amsterdam, The Netherlands (1992).

[LUE 90] Lüdi, H.; Garn, M. B.; Bataillard, P.; Widmer, H.M.; *J. Biotechnology*, 14 (1990) 71-79.

[MAN 86] Manz, A.; dissertation, ETH Zürich, No. 8135 (1986).

[MAN 90a] Manz, A.; Graber, N.; Widmer, H.M.; *Sensors and Actuators B*, 1 (1990) 244-248.

[MAN 90b] Manz, A.; Miyahara, Y.; Miura, J.; Watanabe, Y.; Miyagi, H.; Sato, K.; *Sensors Actuators B*, 1 (1990) 249-255.

[MAN 91a] Manz, A.; Fettinger, J.C.; Verpoorte, E.; Haemmerli, S.; Widmer, H.M.; in Krahn, R.; Reichl, H. (eds.), *Micro System Technologies 91*, Vde Verlag, Berlin, Germany (1991) 49-54.

[MAN 91b] Manz, A.; Harrison, D.J.; Fettinger, J.C.; Verpoorte, E.; Lüdi, H.; Widmer, H.M.; *Transducers '91*, Digest of Technical Papers, IEEE 91CH2817-5, New York (1991) (ISBN 0-87942-586-5) 939-941.

[MAN 91c] Manz, A.; Ciba-Geigy Ltd., Basel, Switzerland, European patent application No. EP-91810952.1, priority date: Dec. 06, 1991, Japanese patent application No. JP-92/351257, priority date: Dec. 06, 1991, US-patent No.: US-5,296,114, Mar. 22, 1994.

[MAN 91d] Manz, A.; Fettinger, J.C.; Verpoorte, E.; Luedi, H.; Widmer, H.M.; Harrison, D.J.; *Trends Anal. Chem.*, 10 (1991) 144-149.

[MAN 91e] Manz, A.; Harrison, D.J.; Verpoorte, E.M.J.; Fettinger, J.C.; Luedi, H.; Widmer, H. M.; *Chimia*, 45 (1991) 103-105.

[MAN 92a] Manz, A.; Harrison D.J.; Verpoorte, E.M.J.; Fettinger, J.C.; Lüdi, H.; Widmer, H.M.; *J. Chromatogr.*, 593 (1992) 253-258.

[MAN 93a] Manz A.; Harrison, D.J.; Verpoorte E.; Widmer, H.M.; in Brown, P.R.; Grushka, E. (eds.), *Advances in Chromatography*, Marcel Dekker Inc., New York, Vol. 33 (1993) 1-66.

[MAN 93b] Ref. [MAN 93a] p. 54.

[MAN 93c] Manz, A.; Verpoorte, E.; Effenhauser, C.S.; Burggraf, N.; Raymond, D.E.; Harrison, D.J.; Widmer, H.M.; *J. High Resolut. Chromatogr.*, 16 (1993) 433-436.

[MIK 79] Mikkers, F.E.P.; Everaerts, F.M.; Verheggen P.E.M.; *J. Chromatogr.*, 169 (1979) 11-20.

[MOS 92] Mosher, R.A; Saville, D.A.; Thormann, W.; *The Dynamics of Electrophoresis*, VCH Verlagsgesellschaft, Weinheim, Germany (1992).

[NEI 92a] Neiger, D.N.; *High Performance Capillary Electrophoresis - An Introduction*, Hewlett Packard Company, France (1992) 83.

[NEI 92b] Ref. [NEI 92a] p. 21.

[OCV 94] Ocvirk, G.; Verpoorte, E.; Manz, A.; Grasserbauer, M.; Widmer, H.M.; *Anal. Methods Instrum.*, 2 (1995) 74-82.

[ODA 94] Oda, R.P.; Spelsberg, T.C.; Landers, J.P.; *LC-GC*, 12 (1994) 50-51.

[RAM 88] Ramsteiner, K.A.; *J. Chromatogr.*, 456 (1988) 3-20.

[RAY 94a] Raymond, D.E.; Manz, A.; Widmer, H.M.; *Anal. Chem.*, 66 (1994) 2858-2865.

[RAY 94b] personal communication with Raymond, D.E., Corporate Analytical Research, Ciba Geigy Ltd., Basel, Switzerland (1994).

[REI 85] Reif, F.; *Statistische Physik und Theorie der Wärme*, de Gruyter, Berlin, Germany (1985) 666.

[RIC 65] Rice, C.L.; Whitehead, R.; *J. Phys. Chem.*, 69 (1965) 4017-4024.

[SCH 91] Schwer, C.; Kenndler, E.; *Anal. Chem.*, 63 (1991) 1802-1807.

[SCH 91b] Schär, M.; Börnsen, K.O.; Gassmann E.; *Rapid Commun. Mass Spectrom.*, 2 (1991) 319-326.

[SCH 92] Van der Schoot, B.; Jeanneret, S.; Van den Berg, A.; de Rooij, N.F.; *Sensors Actuators B*, 6 (1992) 57-60.

[SCH 93a] Van der Schoot, B.; Jeanneret, S.; Van den Berg, A.; de Rooij, N.F.; *Anal. Methods Instrum.*, 1 (1993) 38-42.

[SCH 93b] Van der Schoot, B.; Jeanneret, S.; Van den Berg, A.; de Rooij, N.F.; *Sensors Actuators B*, 13-14 (1993) 333-335.

[SCH 93c] Van der Schoot, B.; Jeanneret, S.; Van den Berg, A.; de Rooij, N.F.; *Sensors Actuators B*, 15-16 (1993) 211-213.

[SCH 95] Van der Schoot, B.; Verpoorte, E.M.J.; Jeanneret, S.; Manz, A.; de Rooij, N.F.; in Van den Berg, A.; Bergveld, P. (eds.), *Micro Total Analysis Systems*, The Netherlands (1995) 181-190.

[SEI 93] Seiler, K.; Harrison, D.J.; Manz, A.; *Anal. Chem.*, 65 (1993) 1481-1488.

[SEI 94a] Seiler, K.; Fan, Z.H.; Fluri, K.; Harrison, D.J.; *Anal. Chem.*, 66 (1994) 3485-3491.

[SEI 94b] Seiler, K.; Fluri, K.; Harrison, D.J.; *Mitt. Geb. Lebensmittelunters. Hyg.*, 85 (1994) 59-68.

[SHA 89] Shapiro, B.A.; Harrison, R.A.; Cane, R.D.; Kozlowsky-Templin, R.; *Clinical Application of Blood Gases*, Year Book Medical Publishers Inc., Chicago (1989) 379.

[SMO 03] Smoluchowski, M.M.; *Bulletin International de l'Académie des Sciences de Cracovie*, 8 (1903) 182-200.

[STA 93] *1. Statuskolloquium des Projektes Mikrosystemtechnik*, 23./24. September 1993, Kernforschungszentrum Karlsruhe, Germany, ISSN 0303-4003, 120-126.

[STE 24] Stern, O.; *Z. Elektrochem.*, 30 (1924) 508-516.

[STI 85] Stinshoff, K.E.; Freytag, J.W.; Laska, P.F.; Gill-Pazaris, L.; *Clinical Chemistry, Anal. Chem.*, 57 (1985) 114R-130R.

[TED 93] Tedesco, J.M.; Owen, H.; Pallister, D.M.; Morris, M.D.; *Anal.Chem.*, 65 (1993) 441A-449A.

[TSC 87] Tschulena, G.; Sensors for process control, *Physica Scripta*, T23 (Trends Phys., EPS-7), (1987, pub. 1988) 293-298.

[VER 93] Verpoorte, E.; Manz, A.; Widmer, H.M.; Van der Schoot, B.; de Rooij, N.F.; Digest of Technical Papers: The 7th International Conference on Solid-State Sensors and Actuators (*Transducers '93*), June 7-10, 1993; Yokohama, Japan; 939-942.

[VER 94a] Verpoorte, E.M.J.; Van der Schoot, B.H.; Jeanneret, S.; Manz, A.; Widmer, H.M.; de Rooij, N.F.; *J. Micromech. Microeng.*, 4 (1994) 246-256.

[VER94b] Verpoorte, E.; Van der Schoot, B.; Jeanneret, S.; Manz, A.; de Rooij, N.F.; in Mallouk, T.E.; Harrison, D.J. (eds.), ACS Symp. Ser. 561: *Interfacial Design and Chemical Sensing* (1994) 244-254.

[VER 94c] personal communication with Verpoorte, S.; Busch, M. and Malone, M., Corporate Analytical Research, Ciba Geigy Ltd., Basel, Switzerland (1994).

[WAL 89] Walcher, W.; *Praktikum der Physik*, Teubner Studienbücher Physik, Stuttgart, Germany (1989) 35.

[WED 82] Wedler, G.; *Lehrbuch der physikalischen Chemie*, Verlag Chemie, Weinheim, Germany (1982) 190-194.

[WEI 93] Weinberger, R.; *Practical Capillary Electrophoresis*, Academic Press, San Diego (1993).

[WID 83] Widmer, H.M.; *Trends Anal Chem.*, 2 (1983) 8-10.

[WID 93] Widmer, H.M.; *Anal. Methods Instrum.*, 1 (1993) 129-133.

[WIN 86] Winnacker A., *Physik von Maser und Laser*, B.I. Wissenschaftsverlag, Mannheim, Germany (1986).

[WOO 94] Wooley; A.T. Mathies, R.A.; *Proc. Natl. Acad. Sci.*, 91 (1994) 11348-11352.

[WU 93] Wu, C.-T.; Huang, T.-L.; Lee, C.S.; *Anal. Chem.*, 65 (1993) 568-571.

Acknowledgements

The work for this thesis was performed from March 1992 to March 1995 in the Corporate Analytical Research department, at Ciba-Geigy Ltd., Basle, Switzerland.

First of all I would like to thank Dr. A. Manz, Corporate Analytical Research, Ciba-Geigy Ltd., Basle, for giving me the opportunity to work on this future-oriented and very interesting topic, and for all the fruitful discussions and comments.

Thanks also is due to Prof. N.F. de Rooij, Institute de Microtechnique, Université de Neuchâtel, Switzerland, for the scientific supervision of this work.

The author wishes to thank Prof. H.M. Widmer, Corporate Analytical Research, Ciba-Geigy Ltd., for the opportunity to work in his department and for his support for this project.

Special thanks belongs to Dr. S. Verpoorte at Ciba-Geigy for reading the thesis and for her helpful discussions and contributions.

I would like to thank all my colleagues at Ciba-Geigy who actively helped me to carry out this work. A special thank belongs to Dr. C.S. Effenhauser, Ciba-Geigy, and Dr. D.E. Raymond, formerly of Ciba-Geigy, and now at Oak Ridge National Lab., Oak Ridge, TN, USA, for their stimulating discussions and helpful comments.

For his help and contributions in construction of the RI detection system, I would like to thank Dr. B. Krattiger, former co-worker at Ciba-Geigy.

Thanks goes to Mr. P.E. Jordi, Ciba-Geigy, and all his coworkers in the various technical support services. They often helped me in a very straightforward and unbureaucratic way.

I would like to thank Mr. R. Wildi, IMT Masken und Teilungen AG, Greifensee, Switzerland for his contribution to the manufacturing of the SCCE structures.

Finally, I would like to thank my parents for supporting me during my education at the university.

Curriculum Vitae

Name:	Norbert Burggraf
Address:	Maulbeerstrasse 37 CH-4058 Basel Switzerland
Date of birth:	January 28, 1965
Nationality:	German

Scientific education:

since March 1992	Ph.D. thesis in the Corporate Analytical Research department, Ciba-Geigy Ltd., Basel, Switzerland, in the field of capillary electrophoresis on planar glass structures. Supervisor: Prof. Nico F. de Rooij, Institute for Microtechnology, University of Neuchâtel.
March 1990 - June 1991	Diploma project at the Institute for Applied Physics, University of Heidelberg, Germany, with Prof. S. Hunklinger, topic: "Detection and correction of alignment errors of a system for direct writing microlithography on a rotating substrate"; grade: A

University:

Feb. 08, 1990	Physics diploma final examination, Ruprecht-Karls-University, Heidelberg; grade: B
Oct. 1986 - Sept. 1991	Diploma degree program in physics at the Ruprecht-Karls-University, Heidelberg
Sept. 29, 1986	Diploma intermediate examination, Justus Liebig University, Gießen, Germany; grade: B
Oct. 1984 - Sept. 1986	Diploma degree program in physics at the Justus Liebig University, Gießen

School:

June 19, 1984	University entrance qualification, Limburg
1975 - 1984	High school, "Tilemannschule", Limburg
1971 - 1975	Elementary school, Limburg-Offheim

date May 4, 1995 signature